

CHAPTER-5

BIOAVAILABILITY ENHANCEMENT OF FEBUXOSTAT

CHAPTER 5: BIOAVAILABILITY ENHANCEMENT OF FEBUXOSTAT

This chapter of the thesis has been aimed to the bioavailability enhancement of poorly water soluble drug Febuxostat. This chapter has been divided into two parts which are as following:

Part-1: Formulation of Febuxostat nanosuspension

Part-2: Formulation of Febuxostat inclusion complex with cyclodextrins

5.1 Materials:

FBX was kindly gifted by Lupin Pharmaceuticals Ltd., Aurangabad, Maharashtra, India. Marketed formulation "Febustat", (Febuxostat 40 mg, Abbott Healthcare Pvt. Ltd., Mumbai India) was purchased from local pharmacy.

Yttrium stabilized-Zirconium oxide beads were obtained as gift sample from Lupin Pharmaceuticals Ltd, Pune, India. Poloxamer 188 (Lutrol F68) and Poloxamer 407 (Lutrol F127) were kindly gifted by Dr. Reddy's Laboratories Ltd. Hyderabad, Andhra Pradesh, India. Sodium Lauryl Sulfate (SLS), Polyvinylpyrrolidone Kollidone® 30 (PVP K30), Tween 20 and Tween 80 were purchased from S.D. Fine Chemicals, Mumbai, India. Lactose, sucrose, trehalose and mannitol were purchased from Himedia, Mumbai, India. β -Cyclodextrin (β -CD) and Methyl- β -Cyclodextrin (M- β -CD) were purchased from Hi-media Laboratories Pvt. Ltd., Mumbai. Hydroxy propyl - β -Cyclodextrin (HP- β -CD) was obtained as a gift sample from Sun Pharma Advance Research Company, Vadodara. γ -Cyclodextrin (γ -CD) was procured as a gift sample from Roquette Pharma, U.S.A.

Acetonitrile (HPLC Grade) and Methanol (HPLC Grade) were procured from Merck Chemicals, Mumbai, India. Dimethylsulfoxide (HPLC grade), Triethylamine (TEA) (HPLC grade) Orthophosphoric acid (HPLC Grade), Glacial Acetic Acid (HPLC Grade) and Methyl tertiary butyl ether (MTBE) (HPLC Grade) were purchased from Spectrochem Chemicals (Mumbai, India). Potassium dihydrogen phosphate (AR grade), Sodium dihydrogen phosphate (AR grade), Ammonium acetate (AR grade), HCl (AR grade) and Sodium hydroxide (AR grade) were purchased from S.D. Fine Chemicals, Mumbai, India. Caco-2 cell lines were purchased from NCCS, Pune, India. Dulbecco's Modified Eagle's medium (DMEM), Fetal Bovine Serum (FBS), sodium pyruvate, sodium bicarbonate, penicillin-streptomycin solution, Trypsin-EDTA solution, Hank's balanced salt solution (HBSS) and phosphate buffered saline (PBS) were purchased from Himedia, Mumbai, India. Lucifer yellow and MTT (3-(4,5-dimethylthiazolyl-2)-2,5-diphenyltetrazolium bromide) dye were purchased from Sigma Aldrich INDIA, Bangluru, India. 12-well

Transwell inserts were purchased from Nunc, Denmark. 96-well plates were purchased from Coster, Corning, USA.

Purified HPLC grade water was obtained by filtering double distilled water through nylon filter paper 0.22 μm pore size and 47 mm diameter (Millipore, Bangalore, India).

5.2 Instruments:

1. Weighing balance (AX120, Shimadzu, Japan)
2. Bath Sonicator
3. High speed magnetic stirrer (Remi, MS500, Remi equipments Pvt. Ltd., Mumbai, India)
4. Centrifuge (3K 30 Sigma Laboratory Centrifuge, Osterode, Germany)
5. pH meter (LABINDIA Analyticals Instrument Pvt. Ltd., Mumbai, India)
6. Spinix MC-01 Vortex Shaker (Tarsons Products Pvt. Ltd. New Delhi, India)
7. Rotospin Test tube Rotator (Tarsons Products Pvt. Ltd. New Delhi, India)
8. Quartz Double Distillation Unit
9. Dissolution Test Apparatus-Basket type USP (VEEGO Instruments, Mumbai, India)
10. UV-visible Spectrophotometer (UV-1700, Shimadzu, Japan)
11. Spectrofluorimeter (RF-5301, Shimadzu, Japan)
12. High Performance Liquid Chromatography (Shimadzu, Japan)
13. Particle Size Analyzer (Malvern Zetasizer Nano ZS 90, Malvern Instruments, UK)
14. Laser Diffraction Particle Size Analyzer (Malvern Mastersizer-2000, UK)
15. Lyophilizer (Heto Dry Winner, Vaccubrand, Denmark)
16. Differential Scanning Calorimeter (DSC-60-A, Shimadzu, Japan)
17. X-ray Diffractometer (XRD, X-Pert-PRO, PANalytical, Netherland)
18. Bruker ALPHA FTIR Spectrometer (Bruker Optics, Germany)
19. Scanning Electron Microscope (SEM, JSM-6060, JEOL Ltd., Tokoyo, Japan)
20. Transmission Electron Microscope (TEM, PHILIPS, Technai 20, Japan)
21. Micro Plate Multi Detection Instrument (680-XR, Bio-Rad Laboratories, France)

5.3 Part-1: Formulation of Febuxostat Nanosuspension

5.3.1 Introduction

This part of the project was intended to formulate a stable NS of another water insoluble and low bioavailable drug, 'Febuxostat' (FBX), an urate lowering agent, in order to improve its oral bioavailability by enhancing its solubility and dissolution properties. As wet media milling technique was found very effective and user-friendly in the preparation of DAR-NS, hence here we had chosen the same approach for development of FBX nanosuspension (FBX-NS). Different types of surfactant and stabilizers which include Poloxamers, polysorbates, SLS and PVP K30 were attempted to achieve a stable FBX-NS with particle size in desired nanometric range. Various formulation parameters involved in preparation of FBX-NS were further optimized by multiple regression analysis (Factorial design of experiment). The optimized liquid NS was freeze dried to obtain physically and chemically stable solid NS. Sucrose, trehalose and mannitol were tried as cytoprotectant to prevent the agglomeration of drug particles during freeze drying. The mean particle size, polydispersity index (PDI) and zeta potential were investigated, prior and post to lyophilization of prepared NS. The freeze dried NS was further evaluated for FBX content, saturation solubility and *in-vitro* dissolution as per pharmacopoeial guidelines. The physical properties of lyophilized FBX-NS were investigated by Differential Scanning Calorimetry (DSC), X-ray Diffraction (XRD) Study, Scanning Electron Microscopy (SEM) and Transmission Electron Microscopy (TEM). Stability study of final formulation was performed at 4-8°C (refrigerator) and at 25°C (room temperature) for a period of six months. The chemical stability of FBX-NS was evaluated by assessing the percentage of FBX in the formulation. The physical stability FBX-NS was checked by analysing the particle size and zeta potential of same stored sample. *In vitro* cytotoxicity (MTT Assay) and *in vitro* gastrointestinal permeability studies of FBX-NS were performed using Caco-2 cell line model. *In vivo* pharmacokinetic study of FBX-NS was performed in rabbits to assess the oral bioavailability of optimized formulations and compared with standard API and marketed formulation (Febustat) of FBX.

5.3.2 Development of FBX-NS formulation

NS are composites of nanosized drug particles and stabilizing agent in an aqueous medium, widely prepared by wet media milling process¹⁻³. Zirconium oxide beads were used as milling media and water was used as an aqueous medium. NS was prepared by

transferring exactly weighed portion of stabilizer/surfactant in a 20 ml flat bottom A-grade glass vial previously containing 5 ml double distilled water and sonicated to dissolve the content. A weighed quantity of FBX was incorporated to the stabilizer solution and sonicated for 5 minutes to disperse the drug in the medium. Then magnetic stirring bar (22 x 8 mm) and weighed quantity of zirconium oxide beads were added in the dispersion and comminution was carried out on a high speed magnetic stirrer at 2000 rpm for a particular period of time. The outcome of this milling process was nanonization of FBX and thus producing the FBX-NS. In prepared NS, suitable cryoprotectant was added in definite ratio and stirred to solubilise. The resulting mixture was lyophilized (Heto Dry Winner, Vaccubrand, Denmark) to get the physically stable solid NS.

A plain drug suspension was also prepared by simply dispersing the FBX and surfactant/stabilizer in double distilled water at the same proportion as was used for the FBX-NS formulation. This FBX suspension was compared with FBX-NS for particle size of drug particles.

5.3.2.1 Preliminary optimization of formulation parameters

Prior to the formulation step, the possible parameters influencing the formation of nanosuspension and size of nanosuspension were identified and optimized. The effect of parameters was studied by varying one parameter at a time and keeping other constant so that selected parameter could be optimized. The parameters studied were type and ratio of milling beads, volume of milling beads and very importantly type of excipients (different surfactants/polymeric stabilizers were used). Each batch was repeated thrice (n=3) for confirmation of repeatability. The parameters were optimized to minimum mean particle size and PDI.

5.3.2.1.1 Type and ratio of milling beads

The effect of type of milling beads in formulation of NS was checked by using beads made up of Yttrium stabilized-Zirconium oxide and glass in two different size ranges (i.e. small and large). The diameters of small size beads were in the range of 0.4 to 0.5 mm whereas large size beads were in between 1.4 to 1.6 mm. Different ratios of beads varied from 0:100 to 100:0 for small: large size range beads were also tried to evaluate the effect of size of milling media on size reduction of FBX. Concentration of FBX (10% w/v), Poloxamer 188 concentration (1% w/v), volume of milling beads (100% w/v) and milling time at 4 hours were kept constant in this trial.

5.3.2.1.2 Volume of milling beads

The volume of milling beads was fixed by preparing trial batches with different volumes of small sized zirconium oxide milling beads at 80% w/v, 100% w/v and 120% w/v. FBX concentration (10% w/v), Poloxamer 188 concentration (1% w/v) and milling time at 4 hours were kept constant in this trial.

5.3.2.1.3 Selection of excipients

The choice of a surfactant i.e. stabilizer is specific to each drug candidate and each formulation procedure. In order to stabilize the nanosuspensions, the stabilizer (or mixture of stabilizers) should exhibit sufficient affinity for the particle surface^{4,5}. Different surfactants/polymeric stabilizers (Tween 20, Tween 80, poloxamer 188, poloxamer 407, PVP K30 and SLS) were tried to evaluate their effectiveness in particle size reduction and stabilization of NS. Concentration of all excipients was fixed at 1% w/v. FBX concentration (10% w/v), volume of small sized zirconium oxide beads (100% w/v) and milling time at 4 hours were kept constant in this trial.

5.3.2.2 Optimization of key parameters by Factorial Design

Identification and optimization of key process parameters that affect formulation response during development of any pharmaceutical formulation is an important step. While developing formulations, various formulation variables should be additionally optimized for their effectiveness, safety and usefulness. Factorial design of experiments are widely used for establishing approximate mathematical model in which the variables are screened by stepwise selection method according to statistical significance and final model would be used to predict the relationships between different variables and their levels⁶⁻⁸. A 3³ full factorial design was used to plan and perform the experiments. This approach allows the determination of influence of the different factors on the properties of nanosuspension, requiring a minimum numbers of experiments.

5.3.2.2.1 Selection of independent and dependent variables and structure of design

A three factorial three level 3³ randomized full factorial design was performed for optimization of FBX-NS formulation. As per the primary experiments, stabilizer concentration (X_1), drug concentration (X_2) and milling time (X_3) were selected as independent variables whereas particle size (PS) and saturation solubility (SS) were selected as dependent variables (responses). Experimental trials were performed at all

27 possible combinations with three replicates in complete randomized manner. Other factors such as type of stabilizer (poloxamer 188), type of milling beads (small sized ZrO₂ beads), volume of milling beads (100%w/v) and dispersing media (double distilled water, 5 ml) were kept constant for all the experiments.

A multilinear stepwise regression analysis was performed using Microsoft Excel software. The full models were used to plot two dimension contour plots for both PS and SS. All the statistical operations were carried out by Design Expert (version 8.0.7.1, statease, Inc. Minneapolis, USA). Table 5.1 and Table 5.2 summarize experimental batches studied, their factor combinations, and the translation of the coded levels to the experimental units employed during the study.

Table 5.1 Coded translation of formulation variables of 3³ full factorial design for FNX-NS.

	Independent Variables		Design Level		
	Uncoded	Coded	Low (-1)	Middle (0)	High (+1)
Poloxamer 188 Concentration (%w/v)		X ₁	0.5	1	1.5
FBX Concentration (%w/v)		X ₂	10	15	20
Milling Time (Hrs.)		X ₃	4	8	12

Table 5.2 Formulation of FBX-NS using 3³ factorial designs (coded values).

Batch No.	X ₁	X ₂	X ₃
B1	-1	-1	-1
B2	-1	-1	0
B3	-1	-1	+1
B4	-1	0	-1
B5	-1	0	0
B6	-1	0	+1
B7	-1	+1	-1
B8	-1	+1	0
B9	-1	+1	+1
B10	0	-1	-1
B11	0	-1	0
B12	0	-1	+1
B13	0	0	-1
B14	0	0	0
B15	0	0	+1
B16	0	+1	-1
B17	0	+1	0
B18	0	+1	+1
B19	+1	-1	-1
B20	+1	-1	0
B21	+1	-1	+1
B22	+1	0	-1
B23	+1	0	0
B24	+1	0	+1

B25	+1	+1	-1
B26	+1	+1	0
B27	+1	+1	+1

5.3.2.2.2 Optimization Data Analysis

Various RSM (Response Surface Methodology) computations for the current optimization study were performed employing Design Expert® software. Polynomial models including interaction and quadratic terms were generated for the response variable using multiple regression analysis (MRA) approach. The dependent response was measured for each trial and then either simple linear equation (Eq. 5.1), or interactive equation (Eq. 5.2) or quadratic model (Eq. 5.3) was fitted by carrying out MRA and F-statistic to identify statistically significant terms.

$$Y = b_0 + b_1X_1 + b_2X_2 + b_3X_3 \tag{Eq. 5.1}$$

$$Y = b_0 + b_1X_1 + b_2X_2 + b_3X_3 + b_{12}X_1X_2 + b_{13}X_1X_3 + b_{23}X_2X_3 + b_{123}X_1X_2X_3 \tag{Eq. 5.2}$$

$$Y = b_0 + b_1X_1 + b_2X_2 + b_3X_3 + b_{12}X_1X_2 + b_{13}X_1X_3 + b_{23}X_2X_3 + b_{11}X_1^2 + b_{22}X_2^2 + b_{33}X_3^2 + b_{123}X_1X_2X_3 \tag{Eq. 5.3}$$

Where b_0 is the intercept representing the arithmetic average of all quantitative outcomes of 27 runs; b_1, b_2, b_3 are linear coefficients; $b_{12}, b_{13}, b_{23}, b_{123}$ are the interaction coefficients; and b_{11}, b_{22}, b_{33} are quadratic coefficients computed from the observed experimental values of response Y ; and X_1, X_2 and X_3 are the coded levels of the independent variable(s). The terms X_1X_2, X_1X_3 and X_2X_3 represents the interaction terms whereas X_1^2, X_2^2 and X_3^2 quadratic terms, respectively. The main effects (X_1, X_2 and X_3) represent the average result of changing one factor at a time from its low to high value. The interaction terms ($X_1X_2X_3$) show how the response changes when three factors are simultaneously changed. The polynomial terms (X_1^2, X_2^2 and X_3^2) are included to investigate nonlinearity. The polynomial equation was used to draw conclusions after considering the magnitude of coefficients and the mathematical sign it carries, i.e., positive or negative. A positive sign signifies a synergistic effect, whereas a negative sign stands for an antagonistic effect⁹⁻¹¹.

Statistical validity of the polynomials was established on the basis of ANOVA provision in the Design Expert® 8 software. Level of significance was considered at $p < 0.05$. The best fitting mathematical model was selected based on the comparisons of several statistical parameters including the standard deviation (SD), multiple correlation coefficient or R-Square (R^2), adjusted multiple correlation coefficient (adjusted R^2),

predicted multiple correlation coefficient (predicted R^2) and the predicted residual sum of squares (PRESS), provided by the software. F-value and sequential p-value were also compared to select the best fitted model for analysis of responses. Among them, PRESS indicates how well the model fits the data, and for the chosen model it should be small relative to the other models under consideration¹⁰. A full model (FM) equation was established after putting the values of regression coefficients of responses PS (Y_1) and SS (Y_2) in the respective equation for selected polynomial model. Significance of the model was determined by applying analysis of variance (ANOVA) and significance of each coefficient was estimated by Student's 't' test and p-value. Non-significant terms ($p < 0.0500$) were neglected from the FM equation and a reduced model (RM) was generated to facilitate the optimization process. Also, the 3-D response surface graphs and the 2-D contour plots were plotted by keeping least significant independent variable constant and varying other two independent variables, to establish a relationship between dependent and independent variables using Design Expert® 8 software. F-statistic was applied on the results of ANOVA of FM and RM to check whether the non-significant terms can be omitted or not from the FM¹², using Design Expert® 8 and Microsoft Excel 2007. For simultaneous optimization of PS and SS, desirability was calculated using Design Expert® 8 software. A check point analysis was performed to confirm the utility of multiple regression analysis and established contour plots in the preparation of FBX-NS. Results of desirability criteria, check point analysis, and normalized error were considered to select the formulation with lowest PS and highest SS.

5.3.2.2.3 Contour Plots

Two dimensional contour plots were established between two independent variables (X_1 vs X_2 , X_1 vs X_3 and X_2 vs) at fixed level (either -1 or 0 or +1) of third independent variable ($X_1/ X_2/ X_3$) for responses Y_1 (PS) and Y_2 (SS) to explain the correlation between independent and dependent variables.

5.3.2.2.4 Response Surface Plots

Response surface plots were plotted to understand the main effect and the interaction effects of two variables by calculating the values taken by one factor where the other varies (from -1 to +1 for instance) with constraint of a given response value. The yield values for different levels of variables can also be predicted from the respective response surface plots.

5.3.2.2.5 Check Point Analysis

A check point analysis was performed to confirm the utility of the established contour plots and reduced polynomial equation in the preparation of FBX-NS. Values of independent variables (X_1 and X_2) were taken from three check points on contour plots plotted at fixed levels of -1, 0 and +1 of X_3 and the values of responses Y_1 (PS) and Y_2 (SS) were calculated by substituting the values in the reduced polynomial equation. FBX-NS was prepared experimentally by taking the amounts of the independent variables (X_1 and X_2). Each batch was prepared three times and mean values were determined. Difference in the predicted and mean values of experimentally obtained responses Y_1 and Y_2 was compared by using student's 't' test.

5.3.2.2.6 Desirability Criteria

For simultaneous optimization of responses Y_1 (PS) and Y_2 (SS), desirability function (multi-response optimization technique) was applied and total desirability was calculated using Design Expert® 8 software. The desirability lies between 0 and 1 and it represents the closeness of a response to its ideal value. Our desirability criteria included PS of less than 150 nm and maximum SS with minimum concentration of surfactant, high concentration of drug and low stirring time.

5.3.2.2.7 Normalized Error Determination

The quantitative relationship established by MRA was confirmed by evaluating experimentally prepared FBX-NS. PS and SS predicted from the MRA were compared with those generated from prepared batches of check point analysis using normalized error (NE).

5.3.2.3 Preparation of optimized FBX-NS

After screening the effect of independent variables on the responses, the levels of these variables that give the optimum response were determined. Optimization was performed to find out the levels of independent variables (X_1 , X_2 and X_3) that would yield a minimum value of PS and maximum value of SS using Design-Expert 8.0 software. For confirmation, fresh formulations were prepared in triplicate at the optimum levels of independent variables and the resultant FBX-NS were evaluated for responses and compared with the theoretical values.

5.3.2.4 Freeze drying of FBX-NS

The prepared FBX-NS formulation was freeze dried using lyophilizer (Heto Dry Winner, Vaccubrand, Denmark). Various cryoprotectants (i.e Sucrose, Trehalose dihydrate and

Mannitol) at different ratio to the total solid content of NS (i.e. 1:1% w/w, 1:2% w/w and 1:3% w/w) were tried. The selection of type and ratio of cryoprotectant was based on the minimum increment in particle size. The vials containing 5 ml of FBX-NS sample with respective amount of cryoprotectant were rapidly frozen at -70°C in deep freezer for 8 hours and lyophilized for 24 hours under vacuum condition.

5.3.3 Characterization of FBX-NS

5.3.3.1 Particle size determination

As per the procedure given in Section 4.3.3.1.

5.3.3.2 Zeta potential

As per the procedure given in Section 4.3.3.2.

5.3.3.3 Differential Scanning Calorimetry (DSC) Analysis

As per the procedure given in Section 4.3.3.3.

5.3.3.4 X-Ray Diffraction (XRD) Study

As per the procedure given in Section 4.3.3.4.

5.3.3.5 Morphological analysis by TEM and SEM

As per the procedure given in Section 4.3.3.5.

5.3.3.6 Percentage drug content in FBX-NS

Accurately weighed lyophilized FBX-NS powder (equivalent to 25 mg of FBX) was transferred in a 25 ml volumetric flask and 15 ml Methanol was added. Content was sonicated to dissolve and volume was made up to the mark with Methanol. The sample solution was centrifuged at 15,000 rpm for 10 minutes (Sigma centrifuge, Osterode, Germany) and supernatant was filtered with 0.22 µm pore size disposable filter (Millipore India, Bangalore). Filtrate was suitably diluted with diluent to get the sample concentration at 20 µg/ml. Standard solution of FBX (20 µg/ml) was also prepared and both the solutions were injected into the HPLC system (Shimadzu, Japan). (For instrumentation, chromatographic conditions and method refer Section 3.2.3) Each determination was performed in triplicate, chromatograms were recorded and mean % FBX content in the formulation and standard deviation was calculated.

5.3.3.7 Saturation solubility

The saturation solubility of standard FBX and FBX-NS formulation were determined by adding excess amount of material in a 15ml screw capped tube and 10 ml double distilled water was added. The resulting solutions were placed on mechanical shaker for 48 hours at 25°C. After equilibrium was reached, the dispersion was centrifuged at

15,000 rpm for 10 minutes (Sigma centrifuge, Osterode, Germany) to sediment the undissolved drug. Then supernatant was withdrawn and filtered with 0.22 μm pore size disposable filter (Millipore India, Bangalore). The content of dissolved FBX was analyzed by UV spectrophotometer (UV 1700, Shimadzu, Japan) at 315 nm after suitable dilution with methanol. Six replicates of each sample were measured and saturation solubility with SD was calculated.

5.3.3.8 *In vitro* dissolution study

In-vitro dissolution studies were carried out using hard gelatin capsules (Size 0) containing an amount of material (lyophilized FBX-NS or plain FBX) equivalent to 40 mg of FBX and marketed formulation (Febustat, Label claim-40mg) in different dissolution mediums (i.e. Distilled water, Phosphate Buffer pH-6.8, Acetate Buffer pH-4.5 and 0.1N HCl) using USP dissolution apparatus II (paddle method). The experiments were performed on 900mL media at $37^{\circ}\text{C}\pm 0.5^{\circ}\text{C}$ at a rotation speed of 75 rpm. At preselected time intervals, 5 mL samples were withdrawn, filtered immediately and replaced with 5 mL of pre-thermostated fresh dissolution medium. Quantitative determination was performed by UV spectrophotometer at 315 nm. Dissolution tests were performed in triplicate and graph of percent cumulative drug release vs time was plotted. Dissolution profiles were further evaluated on the basis of Dissolution efficiency (DE), Dissolution percentage at 5 min and 60 min (DP_5 and DP_{60}), time required to release 50% and 90% of drug (t_{50} and t_{90}), Mean dissolution time (MDT) and Area under curve (AUC). The DDSolver, an Excel add-in software package, which is designed to analyze data obtained from dissolution experiments was used to calculate different dissolution parameters¹³.

5.3.3.9 Stability Studies

Stability studies of lyophilized FBX-NS was carried out at $5^{\circ}\text{C}\pm 3^{\circ}\text{C}$ (refrigerator) and at room temperature (RT) for a period of 6 months. Periodically, samples were withdrawn at 1st, 3rd and 6th month and subjected to examined for chemical and physical stability. Chemical stability was determined by assessing the percentage content of FBX in stored formulations while physical stability was evaluated by measuring mean particle size (PS), PDI and zeta potential (ZP) of the same.

5.3.4 Cell Line Studies of FBX and it's formulations using Caco-2 cell line model

In-vitro cytotoxicity study and *in-vitro* permeability study of FBX and it's formulations, using caco2 cell lines, were carried out. Literature revealed that *in-vitro* cell lines studies

can be used as predictive tools for estimating the fate and activity of drug delivery system in the actual human body¹⁴⁻¹⁷.

5.3.4.1 Cell Culture

Same as described in Section 4.6.1.

5.3.4.2 *In vitro* Cell Cytotoxicity Studies (MTT Assay)

Experiment

MTT stock solution (1 mg/ml) was prepared by dissolving accurately weighed 10 mg of MTT reagent powder with 10 ml phosphate buffered saline (PBS) in an amber colored 10 ml volumetric flask. The stock solution was stored in dark place at 4°C till the further use.

The *in vitro* cytotoxicity of FBX-NS and plain FBX was evaluated for Caco-2 cells using MTT assay. The cells were cultured in 96-well plates (prelabelled as 4 hour, 24 hour and 48 hour) at a seeding density of 1.0×10^4 cells/well for 48 hours. Samples were dissolved in DMSO and different dilutions were made with DMEM culture medium so that the concentration of DMSO did not exceed more than 1% v/v in any diluted sample. Experiments were initiated by replacing the culture medium in each of 96 well of each plate with 100µl of sample solutions (0.1, 1, 10, 100, 250, 500 & 1000 µg/ml) and incubated at 37°C in ~85% relative humidity and ~5% CO₂ environment. After 4 hour of incubation, prelabelled 4 hour-96 well plate was removed from incubator into laminar flow hood area, sample solution was discarded and 100µl of MTT reagent (1 mg/ml) in phosphate buffered saline (PBS) was added aseptically. The plate was again incubated at 37°C in ~5% CO₂ environment for another 4 hours. At the end of incubation period, medium was removed carefully and intracellular formazan was solubilized with 100µl DMSO by agitating cells on orbital shaker for 15 mins. Absorbance was measured at 590 nm with a reference filter of 620 nm using Micro plate multi detection instrument (680-XR, Bio-Rad Laboratories, France). The medium treated cells were used as controls. Same procedure was followed for 24 hour and 48 hour plates.

Statistical analysis

All calculations, graph preparations and statistical analysis were performed using Microsoft Excel. Percentage of cell viability was calculated based on the absorbance measured relative to the absorbance of cells exposed to the negative control. To compare the sensitivity of cells to the FBX and its formulation, IC₅₀ values

(concentration of the drug that leads to 50% inhibition in cell proliferation) were calculated.

5.3.4.3 *In vitro* cell permeability assessment of FBX-NS

Experiment

Caco-2 cell passage 40-45 cultured in 12 well cell culture inserts (pore size-0.4 μ m, diameter-12/18 mm, area-1.13 cm², Product code 12565009, NUNC™, Roskilde, Denmark), were used for *in vitro* permeability assessment of FBX-NS, plain FBX and marketed formulation (Febustat, Label claim-40mg) after 21 days post seeding. Prior to the experiment, the inserts were washed twice and equilibrated for 30 mins with pre-warmed transport medium (Hank's balanced salt solution-HBSS containing 25 mM of HEPES, pH-7.4). Accurate quantity of samples were dispersed in transport medium to prepare the solutions having FBX concentration at 250 μ g/ml and sonicated. The integrity of the monolayers were checked by monitoring the permeability of paracellular leakage marker (Lucifer Yellow) across the monolayer. Quantification of Lucifer yellow was performed using a Spectrofluorimeter using excitation wavelength at 485 nm and emission wavelength at 530 nm. The cell monolayers were considered tight enough for the transport experiment enough when the apparent permeability coefficient (P_{app}) for Lucifer Yellow was less than 0.5×10^{-6} cm/s. All Transport studies were conducted aseptically at 37°C in an atmosphere of ~85% relative humidity and ~5% CO₂. The 150 μ l of transport buffer containing 250 μ g/ml test compounds was added to the apical side while the basolateral side of the inserts contained 1.5 ml of transport medium. After the incubation 30, 60, 120, 180, 240 and 480 mins, aliquot of 100 μ l was withdrawn from the receiver chamber and was immediately replenished with an equal volume of pre-warmed transport medium. The samples were stored at -20°C until analyzed. The concentration of the test compounds in the transport medium were estimated using developed RP-HPLC method as described in Section 3.2.4. The apical to basolateral permeability coefficients (P_{app} in cm/sec) for FBX-NS, plain FBX and marketed formulation were calculated using Microsoft Excel.

5.3.5 Pharmacokinetic evaluation of DAR-NS using *in vivo* animal model

In this study, pharmacokinetic behaviors of the prepared FBX-NS, plain FBX and marketed formulation were investigated to know the effect and advantages of nanosizing on oral bioavailability of FBX. The plots of drug plasma concentration vs time were plotted for FBX after oral administration of FBX-NS and compared it with plain

FBX and marketed formulation (Febustat). Non compartmental pharmacokinetic analysis was performed¹⁸. Various pharmacokinetic parameters were calculated using the computer based statistical package PKsolver add-in for microsoft excel¹⁹. The calculated parameters are Maximum plasma concentration (C_{max}), Time to maximum plasma concentration (T_{max}), Area under the plasma concentration-time curve from time zero to t (AUC_{0-t}), Elimination rate constant ($-K_{elimination}$), Elimination half life ($t_{1/2}$), Area under the plasma concentration-time curve from time zero to infinity ($AUC_{0-\infty}$), Area under momentum curve (AUMC), Mean residence time (MRT) and Relative bioavailability (%F)²⁰.

5.3.5.1 Animals

Same as described in Section 4.3.5.1.

5.3.5.2 Experimental: Dosing and sampling

Relative bioavailability of FBX-NS was evaluated by comparing the bioavailability of FBX-NS with bioavailabilities of plain FBX and marketed formulation.

The maximum dose of FBX that can be given to a adult human in a single day is 40 mg. So according to the section 4.3.5.2, the dose of FBX for rabbits was calculated to be 2.05 mg/kg. In this study, the FBX dose given to the rabbits is 3.70 mg/1.8 kg rabbit weight^{21,22}.

Animals were divided in three treatment groups and each group contained 3 rabbits. The animals were fasted over night prior to the experiment with free access of water. The FBX-NS, plain FBX and marketed formulation (equivalent to 3.70 mg of FBX) were filled in hard gelatin capsule (Capsugel®#size 5) and administered orally. Blood samples (1.0 ml) were collected through marginal ear vein using fresh sterilized disposable needles and syringes in heparinized tubes at 0, 0.25, 0.50, 0.75, 1.0, 1.5, 2, 3, 4, 6, 8, 12, 24 and 48 hours after administration. Collected blood samples were vortexed for 1 min and centrifuged at 20,000 rpm for 10 mins at 4°C (Ultra-centrifuge, 3K 30 Sigma Laboratory Centrifuge, Osterode, Germany). Separated plasma samples were withdrawn and stored at -20°C until further processing.

5.3.5.3 Instrumental and statistical analysis

Collected plasma samples were extracted and analyzed by using developed RP-HPLC method (Chapter 3, Section 3.2.5). The drug plasma concentration were determined from the calibration curve. Non-comprtmntal trapezoidal method was employed to calculate the area under the curve (AUC) of plasma concentration as a function of time

(t). All data were reported as mean \pm SD. The statistical significance of the differences between the groups was tested by one-way ANOVA followed by Bonferroni multiple comparison test.

5.3.6 Result and discussion

5.3.6.1 Development of FBX-NS formulation

5.3.6.1.1 Preliminary optimization of formulation parameters

5.3.6.1.1.1 Type and ratio of milling beads

In this trial batch, both glass and zirconium oxide beads were used at 100% w/v level to analyze the effect of material of beads on nanosizing of FBX by wet media milling. It was observed that beads made up of zirconium oxide were found more suitable for size reduction in comparison to glass beads, as minimum particle size of 268 ± 17 nm with PDI 0.105 ± 0.018 was obtained with zirconium oxide beads. Hence Yttrium stabilized zirconium oxide beads were selected for further experiments. The results of wet media milling with various types of beads are summarized in Table 5.3.

Table 5.3 Effect of beads type on MPS and PDI of FBX-NS.

Bead type	MPS \pm SD* (nm)	PDI \pm SD*
Small glass beads	554 \pm 29	0.418 \pm 0.062
Large glass beads	814 \pm 43	0.657 \pm 0.102
Small zirconium beads	268\pm17	0.105\pm0.018
Large zirconium beads	529 \pm 26	0.381 \pm 0.069

* Data are shown as Mean \pm SD, n=3.

The effect of mixed sizes of zirconium oxide on size reduction of FBX was studied by varying small : large zirconium beads varied from 0:100 to 100:0% w/v. Total volume of milling media was fixed at 100% w/v. Least particle size (259 ± 22 nm) was observed when small zirconium oxide beads were used at 100% w/v level whereas maximum particle size (538 ± 19 nm) was obtained when only large zirconium beads were used in milling process. It was also observed that particle size of FBX was increased as proportion of large zirconium beads was increased hence 100% w/v small zirconium oxide beads were selected for further studies. Results are tabulated in Table 5.4.

Table 5.4 Effect of ratio of beads on MPS and PDI of FBX-NS.

Ratio of beads (small : large)	MPS \pm SD* (nm)	PDI \pm SD*
0:100	538 \pm 19	0.416 \pm 0.052
25:75	502 \pm 47	0.388 \pm 0.045
50:50	394 \pm 28	0.325 \pm 0.019
75:25	316 \pm 23	0.267 \pm 0.037
100:0	259\pm22	0.112\pm0.015

* Data are shown as Mean±SD, n=3.

5.3.6.1.1.2 Volume of milling beads

Volume of milling media also plays an important role in size reduction of drug in media milling technique. Optimum volume of milling beads are required for maintaining stirring efficiency. Different volumes of beads (i.e. 80%, 100% and 120% w/v) were tried and observed that milling media at 100% w/v level offered minimum particle size and optimum stirring so 100% w/v of small zirconium oxide beads were selected for further optimization. Concentration of FBX (10% w/v), Poloxamer 188 concentration (1% w/v) and milling time at 4 hours were kept constant in this trial. Observations are tabulated in Table 5.5

Table 5.5 Effect of volume of milling media on MPS and PDI of FBX-NS.

Volume of beads (% w/v)	MPS±SD* (nm)	PDI±SD*
80	328±14	0.265±0.031
100	264±21	0.097±0.025
120	395±37	0.218±0.046

* Data are shown as Mean±SD, n=3.

5.3.6.1.1.3 Selection of excipients

The type and amount of stabilizer has a pronounced effect on the physical stability and *in-vivo* behaviour of nanosuspensions. Tween 20, Tween 80, poloxamer 188, poloxamer 407, PVP K30 and SLS were tried as stabilizers. Concentration of all excipients was fixed at 1% w/v. FBX concentration (10% w/v), volume of small sized zirconium oxide beads (100% w/v) and milling time at 4 hours were kept constant in this trial. Milling was carried out at room temperature. Results of preliminary experiment for selection of excipients are shown in Table 5.6 and Fig. 5.1.

Table 5.6 Effect of type of stabilizer on MPS and PDI of FBX-NS.

Stabilizer	MPS±SD* (nm)	PDI±SD*
Tween 20	429±27	0.328±0.017
Tween 80	456±23	0.306±0.028
Poloxamer 188	258±16	0.114±0.010
Poloxamer 407	386±19	0.254±0.018
PVP K30	404±15	0.213±0.027
SLS	682±29	0.542±0.032

* Data are shown as Mean±SD, n=3.

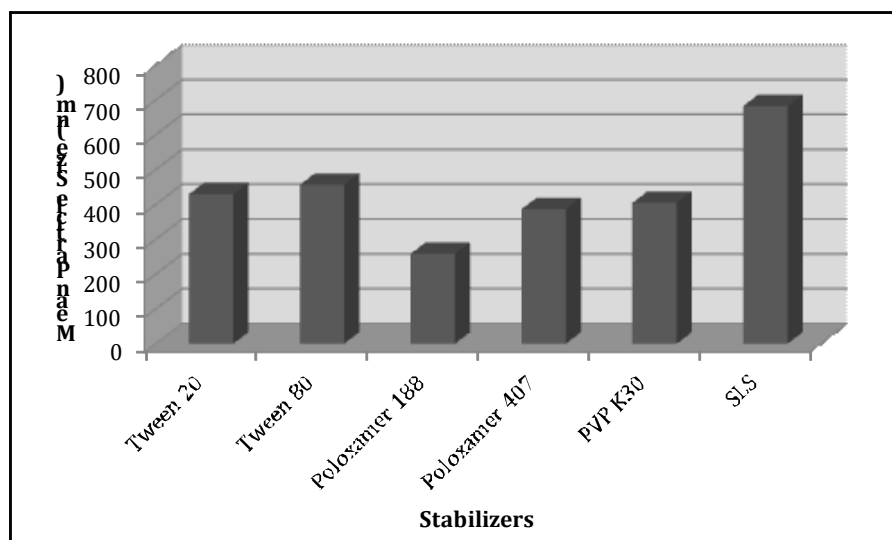


Fig. 5.1 Graphical representation of stabilizer's effect on mean particle size of FBX-NS. It could be observed that both the polysorbates, poloxamers and PVP K30 contributed proficiently in production of NSs with particle size less than 500nm but poloxamer 188 produced NS with least particle size at 258 ± 16 nm with very low PDI at 0.114 ± 0.01 , indicating narrow particle size distribution^{23,24}. Poloxamer 188 is a non-ionic surfactant in the form of white solid and has an average molecular weight of about 8400. It is prepared from a hydrophobe (propylene oxide blocks) with an average molecular weight of 1750 and its hydrophile (ethylene oxide blocks) comprises about 80% of the total molecular weight²⁵. Poloxamer 188 is approved by the FDA for various application routes ranging from 0.01% in emulsions for topical application up to 2.50% in suspensions for oral administration²⁶. Literature revealed that poloxamer 188 was found very efficient in stabilizing the pharmaceutical nanosuspensions^{2,27-32}.

It is evident that the mean particle size in FBX-NS, stabilized by poloxamer 188 was significantly lesser than those stabilized by other excipients. Therefore, poloxamer 188 was selected as a stabilizer for further optimization. Poloxamer 188 provided a proficient steric stabilization by forming a dynamic cloud of polymeric chains at the drug particle surface. It adsorb strongly onto the surface of hydrophobic nanoparticle via its hydrophobic poly(oxypropylene) centre blocks. This approach of adsorption leaves the hydrophilic polyoxyethylene side chains in a mobile state because they extend outwards from the particle surface. These side chains provide stability to the nanoparticle suspension by a repulsion effect through a steric mechanism of stabilization³³⁻³⁶.

It could be concluded that the type of stabilizer employed for preparation of NS has significant effect on the particle size and polydispersity value of NS and appeared to be

the main reason for efficient formation of nanoparticles and stabilization of the nanosuspension.

5.3.6.1.2 Optimization of key process parameters by Factorial Design

From the preliminary experiments, various basic process variables (i.e. type and ratio of milling beads, volume of milling beads, selection of excipient) essential for preparation of FBX-NS was optimized and fixed. Other important parameters (independent variables) such as stabilizer concentration (X_1), drug concentration (X_2) and milling time (X_3) were optimized by 3^3 factorial design using Design Expert® 8 software. Following formulation parameters were kept constant during factorial design experiments to study the effect of independent variables on mean particle size of FBX-NS and to avoid design complications.

Volume of dispersing media (i.e. water)	: 5 ml
Magnetic stirring bar (length×diameter)	: 22 mm × 8 mm
Stirring speed	: 2000 rpm
Type of milling media	: Yttrium stabilized Zirconium oxide beads
Size of milling media	: Small sized (0.4 mm to 0.5 mm diameter)
Volume of milling media	: 100 %w/v (i.e. 5 gm)
Type of stabilizer	: Poloxamer 188

By using three factorial three level 3^3 randomized full factorial design, 27 possible batches of FBX-NS were prepared with three replicates by media milling technique varying three independent variables, stabilizer concentration (X_1), drug concentration (X_2) and milling time (X_3). The coded values of independent variables (X_1 , X_2 and X_3) and observed, predicted and residual values of both the dependent variables PS (Y_1) and SS (Y_2) for the 27 combinations are enlisted in Table 5.7. The values of responses for 27 batches showed a wide variation from 110.9 nm to 631.9 nm and 98.5 µg/ml to 531.7 µg/ml for Y_1 and Y_2 , respectively. The ratio of maximum to minimum observed values for Y_1 and Y_2 was 5.7 and 5.4, respectively which are less than 10; therefore no transformation was required to the obtained values.

Table 5.7 Combinations of independent variables (X_1 , X_2 and X_3) and observed, predicted and residual values of responses Y_1 and Y_2 as per 3^3 full factorial design for formulation of FBX-NS.

Batch No.	Independent Variables (Coded)			Dependent Variables (Responses)					
				Observed Values		Predicted Values		Residual Values	
	X_1	X_2	X_3	Y_1^*	Y_2^*	Y_1	Y_2	Y_1	Y_2
B1	-1	-1	-1	516.4	129.4	497.5	107.5	18.9	21.9
B2	-1	-1	0	392.1	156.7	378.5	177.8	13.6	-21.1
B3	-1	-1	+1	367.7	172.1	366.4	167.1	1.3	5.0
B4	-1	0	-1	411.6	144.8	459.8	158.9	-48.2	-14.1
B5	-1	0	0	328.5	175.6	335.5	191.4	-7.0	-15.8
B6	-1	0	+1	309.2	201.3	318.2	229.3	-9.0	-28.0
B7	-1	+1	-1	631.9	98.5	617.4	74.2	14.5	24.3
B8	-1	+1	0	509.9	124.6	487.9	113.2	22.0	11.4
B9	-1	+1	+1	459.2	139.7	465.3	103.2	-6.1	36.5
B10	0	-1	-1	262.7	226.9	263.7	255.2	-1.0	-28.3
B11	0	-1	0	139.4	438.1	145.8	415.5	-6.4	22.6
B12	0	-1	+1	121.1	492.6	134.9	465.0	-13.8	27.7
B13	0	0	-1	229.2	264.5	228.1	298.5	1.1	-34.0
B14	0	0	0	124.8	501.7	108.7	477.2	16.1	24.5
B15	0	0	+1	114.7	524.6	96.3	507.9	18.4	16.7
B16	0	+1	-1	397.3	162.2	387.8	185.6	9.5	-23.4
B17	0	+1	0	240.4	254.8	267.0	284.8	-26.6	-30.0
B18	0	+1	+1	255.8	247.6	253.0	273.2	2.8	-25.6
B19	+1	-1	-1	249.6	253.8	250.3	248.7	-0.7	5.1
B20	+1	-1	0	129.4	469.1	133.6	469.1	-4.2	0.0
B21	+1	-1	+1	116.1	515.9	123.8	528.7	-7.7	-12.8
B22	+1	0	-1	214.8	284.6	216.9	293.9	-2.1	-9.3
B23	+1	0	0	117.2	520.4	102.4	480.8	14.8	39.6
B24	+1	0	+1	110.9	531.7	94.9	516.9	16.0	14.8
B25	+1	+1	-1	386.8	160.8	378.7	143.0	8.1	17.8
B26	+1	+1	0	244.2	252.3	266.5	256.4	-22.3	-4.1
B27	+1	+1	+1	259.3	238.1	261.2	259.1	-1.9	-21.0

X_1 : Stabilizer concentration (%w/v), X_2 : Drug concentration (%w/v), X_3 : Milling time (Hours), Y_1 : Particle size (nm) and Y_2 : Saturation solubility ($\mu\text{g/ml}$). *mean of three replicates, n=3.

Various statistical standards including SD, R-Squared values, predicted residual sum of square (PRESS), F-value and sequential p-value were evaluated to select the best fitted model for analysis of responses and are summarized in Table 5.8.. The model with low SD, higher R-Square value, lower PRESS value, higher F-value and p-values less than 0.05 was opted for further optimization. The given data clearly suggested the quadratic model for analysis of dependent variables, PS and SS. In quadratic model, the predicted R-Square 0.9705 and 0.9477 are in reasonable agreement with the adjusted R-Square of 0.9814 and 0.9349 for PS and SS, respectively. The higher R^2 values indicate an

excellent relationship among the selected independent variables. In brief, the preferred regression model proved its outstanding competency when compared to other models.

Table 5.8 Fit summary statistics of responses Y₁ and Y₂ as per 3³ full factorial design for formulation of FBX-NS.

Statistical Parameters	Source Model					
	Linear		2FI		Quadratic	
	Y ₁	Y ₂	Y ₁	Y ₂	Y ₁	Y ₂
SD	81.98	96.78	87.71	91.50	20.14	27.62
R-Square	0.7155	0.6342	0.7169	0.7157	0.9881	0.9684
Adjusted R-Square	0.6784	0.5865	0.6319	0.6304	0.9806	0.9477
Predicted R-Square	0.6122	0.5090	0.3910	0.4583	0.9705	0.9349
PRESS	210700	289100	330900	319000	18012	19470
F-value	11.28	13.29	8.44	8.39	132.42	24.37
p-Value Prob>F	<0.05	<0.05	<0.05	<0.05	<0.05	<0.05

A mathematical relationship was established in the form of a polynomial equation (full model) by putting values of regression coefficients (generated by Design Expert® 8) for measured responses PS (Y₁) and SS (Y₂), separately in Eq. 5.3. Full model (FM) equations for Y₁ and Y₂ are shown below as Eq. 5.4 and 5.5, respectively.

FM for PS.

$$Y_1 = 108.75 - 116.57X_1 + 60.57X_2 - 65.91X_3 + 5.87X_1X_2 + 4.91X_1X_3 - 1.49X_2X_3 + 110.22X_1^2 + 97.64X_2^2 + 53.47X_3^2 + 3.75X_1X_2X_3 \tag{Eq. 5.4}$$

FM for SS.

$$Y = 448.21 + 104.67X_1 - 65.33X_2 + 74.34X_3 - 41.02X_1X_2 + 37.18X_1X_3 - 30.55X_2X_3 - 92.03X_1^2 - 98.07X_2^2 - 55.42X_3^2 - 22.91X_1X_2X_3 \tag{Eq. 5.5}$$

To determine the significance of the model, ANOVA was applied. The results of ANOVA for Y₁ and Y₂ were summarized in Table 5.9. Using 5% significance level, a model is considered significant if the p-value (significance probability value) is less than 0.05. From the p-value presented in Table 5.9, it can be concluded that for responses Y₁ and Y₂, quadratic models were significant. As shown in the Table, the model F-values of 132.42 and 24.37 for PS and SS, respectively, also implies that the selected models were significant.

The significance of each coefficient of Eq. 5.4 and Eq. 5.5 were determined by Student's 't' test and p-value, which are enlisted in Table 5.9. The larger the magnitude of 't' value and smaller the p-value, the more significant is the corresponding coefficient^{37,38}. Small

values of the coefficients and p-value more than 0.0500 for the terms X_1X_2 , X_1X_3 , X_2X_3 and $X_1X_2X_3$ in Eq. 6.4 and $X_1X_2X_3$ in Eq. 5.5 for PS and SS respectively implied that all these terms were least contributing in the preparation of the FBX-NS by media milling method. The small values of coefficients were non-significant ($p < 0.0500$) and hence neglected from the FM (i.e. Eq. 5.4 & 5.5) to get the reduced model (RM) polynomial equations for PS and SS, respectively.

Reduced model (RM) equations for PS and SS are written below as Eq. 6.6 and Eq. 6.7, respectively.

RM for PS.

$$Y_1 = 108.75 - 116.57X_1 + 60.57X_2 - 65.91X_3 + 110.22X_1^2 + 97.64X_2^2 + 53.47X_3^2 \quad \text{Eq. 6.6}$$

RM for SS.

$$Y = 448.21 + 104.67X_1 - 65.33X_2 + 74.34X_3 - 41.02X_1X_2 + 37.18X_1X_3 - 30.55X_2X_3 - 92.03X_1^2 - 98.07X_2^2 - 55.42X_3^2 \quad \text{Eq. 6.7}$$

The results of ANOVA of the FM and RM second order polynomial equation of PS and SS are tabulated in Table 5.10. Since the F-calculated value is less than the F-tabulated value for both PS and SS, it was concluded that the neglected terms did not significantly contribute in the prediction of PS and SS¹². Hence, F-statistics of the results of ANOVA of full and reduced model justified the omission of non-significant terms of Eq. 5.4 and Eq. 5.5.

The goodness of fit of the selected model was checked by the squared correlation coefficient (R^2). In this case, the values of the correlation coefficients ($R^2 = 0.9881$ and 0.9684 for FM & 0.9865 and 0.9612 for RM, for PS and SS respectively) indicated that over 91% of the total variation were explained by the model. High R^2 values of the FM as compared to RM were due to large number of factors were included. More the number of factors more is the R^2 value³⁹. The values of adjusted R^2 (0.9806 and 0.9477 for FM & 0.9824 and 0.9411 for RM, for PS and SS respectively) were similar for FM and RM for both PS and SS, indicating the suitability of reducing the model. Moreover, the high values of the correlation coefficients ($R = 0.9940$ and 0.9752 for FM & 0.9932 and 0.9704 for RM, for PS and SS respectively) signifies an tremendous correlation between the independent variables⁴⁰. All the above considerations indicated an outstanding adequacy of the developed regression model^{37,38,40}.

Table 5.9 Results of model and coefficient estimation by ANOVA and Student's 't' test for responses Y₁ (PS) and Y₂ (SS) of FBX-NS.

Source	F-value		Coefficients		t-stat		p-value Prob>F	
	Y ₁	Y ₂	Y ₁	Y ₂	Y ₁	Y ₂	Y ₁	Y ₂
Model	132.42	24.37	-	-	-	-	<0.0001	<0.0001
Intercept	-	-	108.75	448.21	10.61	18.48	<0.0001	<0.0001
X₁	603.24	86.94	-116.57	104.67	-24.56	9.32	<0.0001	<0.0001
X₂	162.89	33.88	60.57	-65.33	12.76	-5.82	<0.0001	<0.0001
X₃	192.84	43.86	-65.91	74.34	-13.89	6.62	<0.0001	<0.0001
X₁X₂	1.02	8.90	5.87	-41.02	13.41	-4.73	0.3279	0.0088
X₁X₃	0.71	7.31	4.91	37.18	11.88	-5.04	0.4109	0.0156
X₂X₃	0.07	4.94	-1.49	-30.55	6.50	-2.85	0.8007	0.0410
X₁²	179.79	22.41	110.22	-92.03	1.01	-2.98	<0.0001	0.0002
X₂²	141.08	25.44	97.64	-98.07	0.84	2.70	<0.0001	0.0001
X₃²	42.31	8.12	53.47	-55.42	-0.26	-2.22	<0.0001	0.0116
X₁X₂X₃	0.28	1.85	3.75	-22.91	0.53	-1.36	0.6056	0.1924

Table 5.10 Analysis of Variance (ANOVA) of full and reduced models for PS and SS of FBX-NS.

Source	Model	df	SS	MSS	F	R	R ²	Adj. R ²
For Y₁								
Regression	FM	10	536896.57	53689.66	132.42	0.9940	0.9881	0.9806
	RM	6	536055.25	89342.54	243.82	0.9932	0.9865	0.9824
Residual	FM	16	6487.09	405.44				
	RM	20	7328.40	366.42				
For Y₂								
Regression	FM	10	552617.80	55261.78	24.37	0.9752	0.9684	0.9477
	RM	9	548417.9	60935.33	25.59	0.9704	0.9612	0.9411
Residual	FM	16	36288.29	2268.02				
	RM	17	40488.16	2381.66				

Where; df: degree of freedom, SS: sum of square, MSS: mean sum of square, R: correlation coefficient, R²: squared correlation coefficient and Adj. R²: adjusted correlation coefficient.

For Y₁,

$$SS(RM)_{Y_1} - SS(FM)_{Y_1} = 7328.40 - 6487.09 = 841.31$$

Number of parameters omitted=04

MSS of error (FM)=405.44

$$\begin{aligned} F\text{-calculated } (Y_1) &= [SS(RM)_{Y_1} - SS(FM)_{Y_1}] / \text{No. of parameters omitted} / \text{MSS of error (FM)} \\ &= (841.31) / (04) / (405.44) \\ &= 0.5188 \end{aligned}$$

F-tabulated (Y₁)= 3.0069 (α=0.05, v₁=4 and v₂=16)

For Y₂,

$$SS(RM)_{Y_2} - SS(FM)_{Y_2} = 40488.16 - 36288.29 = 4199.87$$

Number of parameters omitted=01

MSS of error (FM)=2268.02

$$\begin{aligned} F\text{-calculated } (Y_2) &= [SS(RM)_{Y_2} - SS(FM)_{Y_2}] / \text{No. of parameters omitted} / MSS \text{ of error (FM)} \\ &= (4199.87) / (01) / (2268.02) \\ &= 1.8518 \end{aligned}$$

$$F\text{-tabulated } (Y_2) = 3.6337 \quad (\alpha=0.05, \nu_1=2 \text{ and } \nu_2=16)$$

5.3.6.1.2.1 Contour Plots

Two-dimensional contour plots were established between X_1 vs X_2 , X_1 vs X_3 and X_2 vs X_3 at fixed level (0) of third variable for PS (Fig. 5.2) and SS (Fig. 5.3), which are very useful to study the interaction effects of two factors on the responses at one time. It can be observed that PS and SS were highly dependent on stabilizer concentration (X_1), drug concentration (X_2) and milling time (X_3). Fig. 5.2(a) showed that PS was at its upper limit with maximum level of X_2 and minimum of X_1 whereas PS was dropped with increase in X_1 and decrease in X_2 . Fig. 5.2(b), when X_1 and X_3 were in between 0 to +1 levels, PS was found to be minimum. However, the contour of X_2 and X_3 (Fig. 5.2(c)) showed higher PS with increase in X_2 and lower PS with increase in X_3 . Fig. 5.2(c), also described that PS < 200nm could be achieved with -1 to +0.50 of X_3 and -0.50 to +1 level of X_2 . Highest SS was observed at 0.00 to +1 level of X_1 and -1 to 0.00 level of X_2 (Fig. 5.3(a)). Fig. 5.3(b) illustrated that desired SS (i.e. >450 $\mu\text{g/ml}$) could be achieved by keeping X_1 and X_3 in between 0 to +1. Whereas Fig. 5.3(c) depicted that SS increased by lowering the X_2 and raising the X_3 . It was concluded from the expression of contours that middle concentration of drug with middle concentration of stabilizer concentration with high milling time was required for desired PS (<200nm) and SS (>400 $\mu\text{g/ml}$) in preparation of optimized FBX-NS.

5.3.6.1.2.2 Response Surface Plots

Response surface plots play an important role in optimization of independent variables and are very helpful to understand the interaction effects of variables, at any given time. 3D-response surface plots were obtained between between X_1 vs X_2 , X_1 vs X_3 and X_2 vs X_3 at fixed level (0) of third variable as shown in Fig. 5.4 and Fig. 5.5 for both PS and SS respectively. By analysing the Fig. 5.4 and 5.5, we can say, that all the three independent variables (X_1 -surfactant concentration, X_2 -drug concentration and X_3 -milling time) showed their significant effect on PS and SS of the NS when varied alone as well as simultaneous. Fig. 5.4(a) showed the decrease in PS with decrease in X_2 from +1 to -1 and increase in X_1 from -1 to +1 but not much difference in PS was observed when increasing X_1 from 0 to +1. Response surface plot between X_1 and X_3 [Fig. 5.4(b)]

described that desired PS could be achieved with simultaneous increase in X_1 and X_3 from 0 to +1. Fig. 5.4(c) illustrated that PS decreased with decrease in X_2 from +1 to -1 and simultaneously increase in X_3 from -1 to +1. 3D-plots for SS between X_1 and X_2 [Fig. 5.5(a)] showed that optimum SS could be achieved in the range of 0 to +1 for X_1 and 0 to -1 for X_2 whereas Fig. 5.5(b) represented that SS could be maximized with higher levels of X_1 and X_3 . Fig. 5.5(c) also depicted that SS can be increased with decrease in X_2 from +1 to -1 and increase in X_3 from -1 to +1.

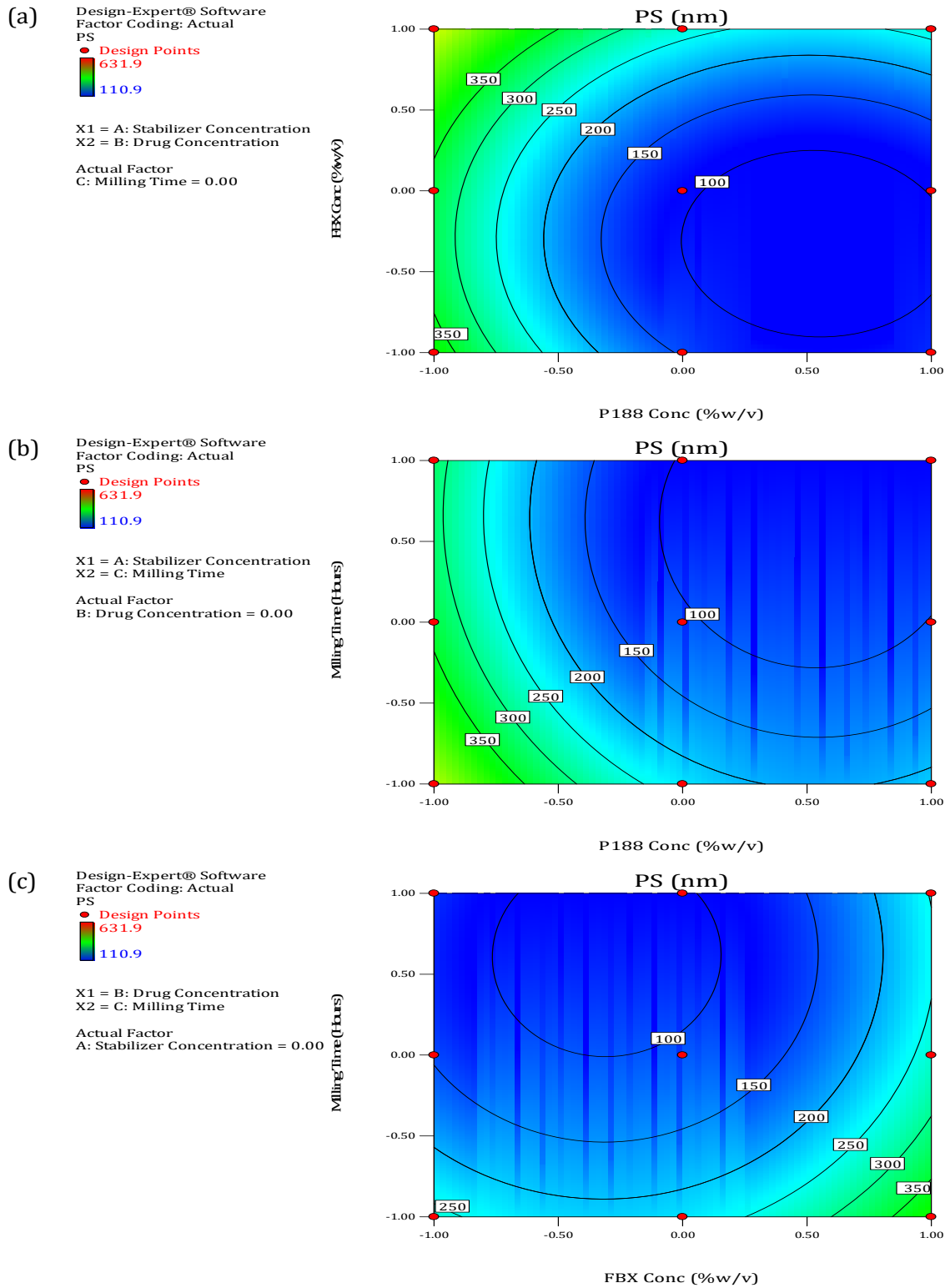


Fig. 5.2 Contour plots showing effect of (a) X_1 vs X_2 (at 0 level of X_3), (b) X_1 vs X_3 (at 0 level of X_2) and (c) X_2 vs X_3 (at 0 level of X_1) on PS of FBX-NS.

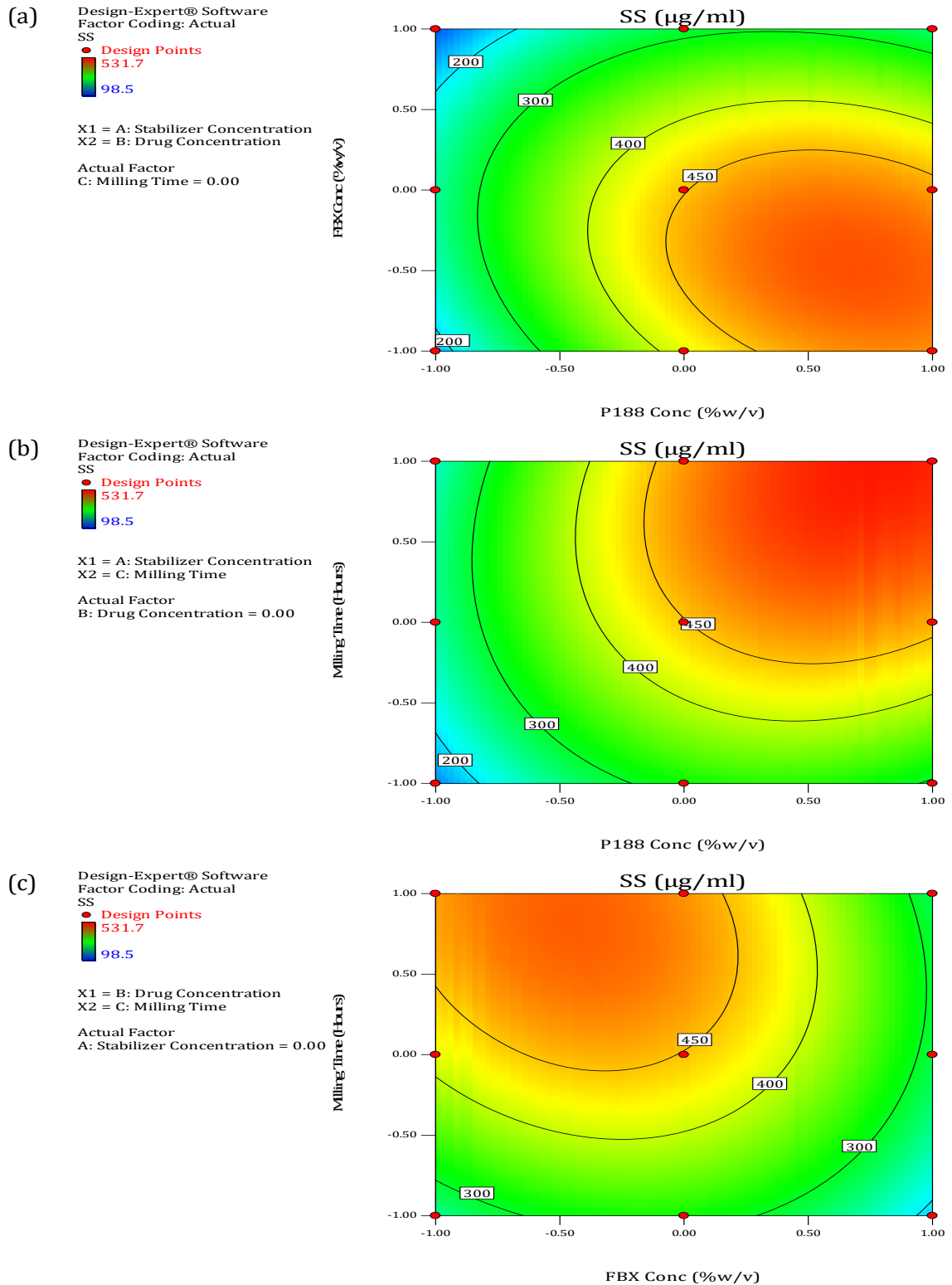


Fig. 5.3 Contour plots showing effect of (a) X_1 vs X_2 (at 0 level of X_3), (b) X_1 vs X_3 (at 0 level of X_2) and (c) X_2 vs X_3 (at 0 level of X_1) on SS of FBX-NS.

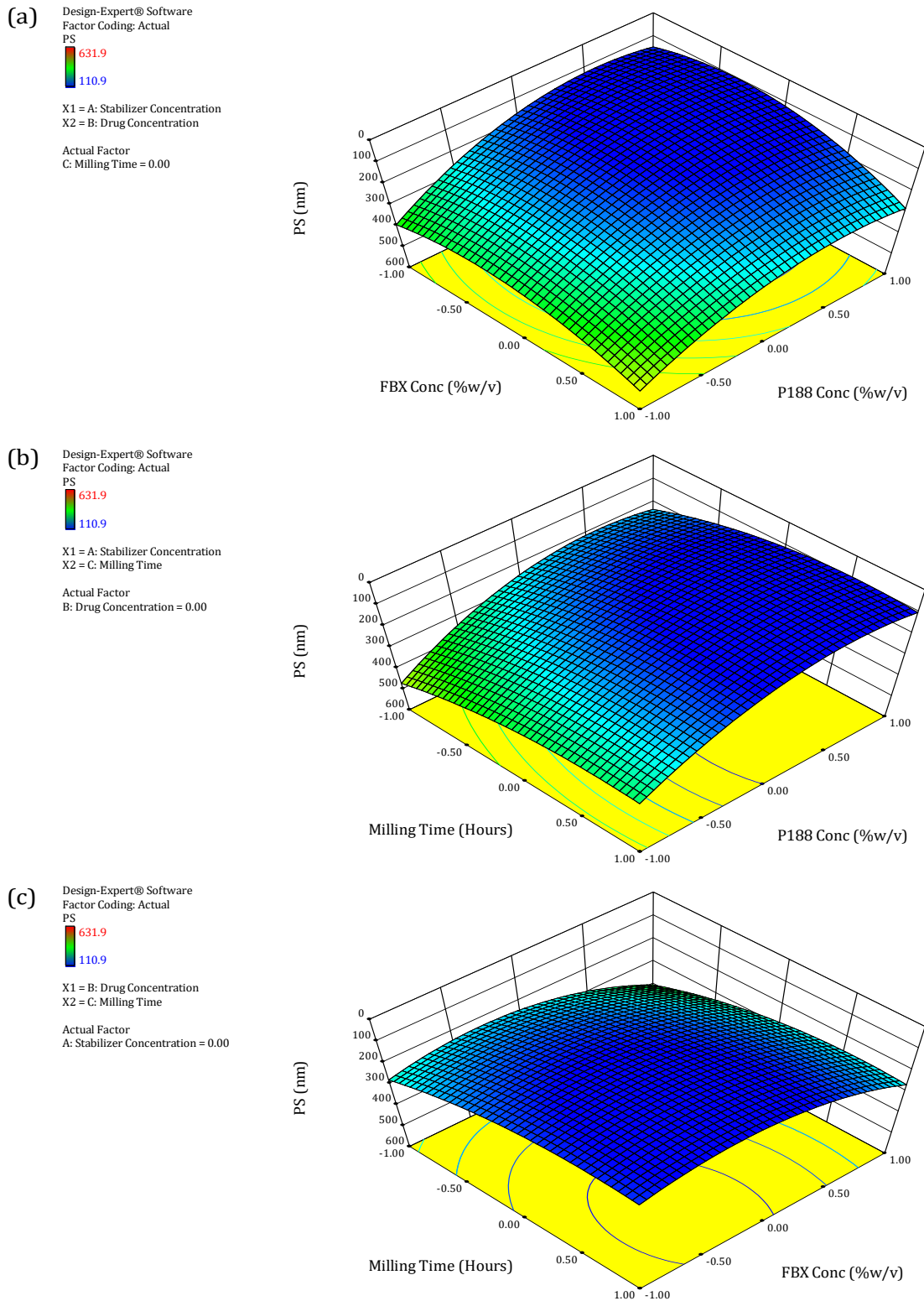


Fig. 5.4 Response surface plots showing effect of (a) X_1 vs X_2 (at 0 level of X_3), (b) X_1 vs X_3 (at 0 level of X_2) and (c) X_2 vs X_3 (at 0 level of X_1) on PS of FBX-NS.

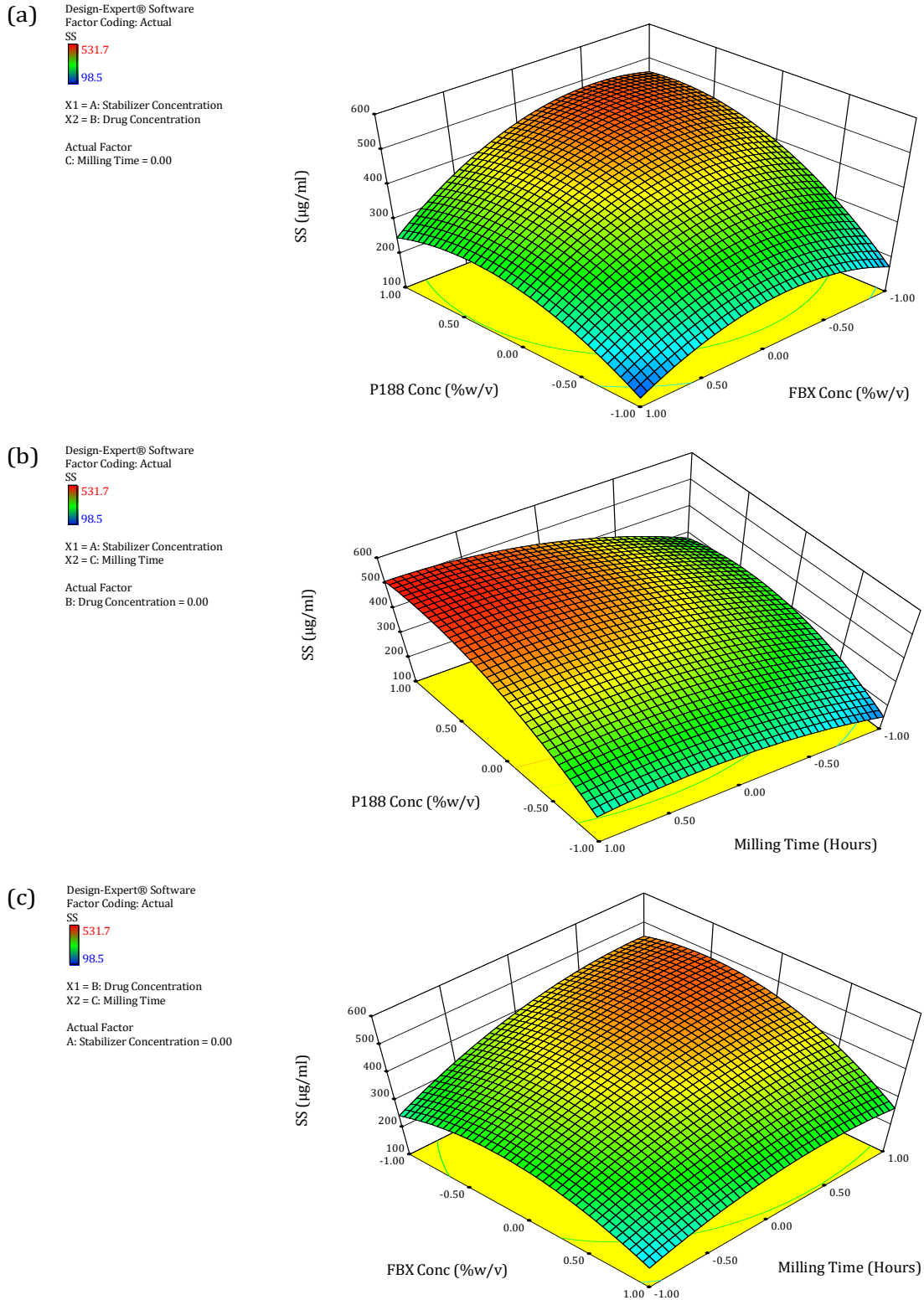


Fig. 5.5 Response surface plots showing effect of (a) X_1 vs X_2 (at 0 level of X_3), (b) X_1 vs X_3 (at 0 level of X_2) and (c) X_2 vs X_3 (at 0 level of X_1) on SS of FBX-NS.

5.3.6.1.2.3 Check Point Analysis and Normalized Error Determination

Check point analysis was carried out by preparing three FBX-NSs batches. PS and SS were determined and results were represented in Table 5.11. Results for PS and SS showed that the measured responses were more accurately predicted by regression analysis which was supported by Lower NE values (0.0536 and 0.0352 for PS and SS of FBX-NS respectively). Data analysis using Student's t-test showed that there was no statistically significant difference ($p < 0.05$) between experimentally attained values and predicted values by MRA.

Table 5.11 Check point analysis, Student's t-test analysis and NE determination of PS and SS of FBX-NS.

Batch No.	X ₁	X ₂	X ₃	PS		SS	
				Obs. (Avg)	Pred.	Obs. (Avg)	Pred.
1	0.48 (62mg)	-0.27 (682.5mg)	-1 (4 hrs)	192.6	185.4	326.1	334.3
2	-0.34 (41.5mg)	-0.09 (727.5mg)	0 (8 hrs)	150.8	156.2	415.5	406.2
3	-0.01 (49.75mg)	-1 (500mg)	1 (12 hrs)	137.7	135.8	468.2	463.4
t_{calculated}				0.7678		0.7438	
t_{tabulated}				2.9199		2.9199	
Normalized Error (NE)				0.0536		0.0352	

5.3.6.1.2.4 Desirability Criteria

Design Expert® 8 software was employed to obtain optimum formulation parameters meeting with our desirability criteria. Our desirability criteria included PS of less than 150 nm and maximum SS with minimum concentration of surfactant, high concentration of drug and low stirring time. From the previous results, the optimum levels of X₁, X₂ and X₃ were selected by multiple regression analysis. Since PS and SS were taken into account simultaneously, the optimum levels suggested by software were 0.0 (50mg), 0.34 (835mg) and -0.02 (7.92 Hour) for X₁, X₂ and X₃, respectively. The theoretical values of PS and SS were 142.3 nm and 415.8 µg/ml, respectively. The calculated desirability factor for offered formulation was 0.921 which is about to 1.0, hence confirmed the applicability and suitability of design of experiment model.

5.3.6.1.3 Preparation of optimized FBX-NS

FBX-NS was prepared by media milling technique. Weighed and transferred 50 mg of poloxamer 188 (i.e. 1% w/v) in a 20 ml flat bottom A-grade glass vial. 5 ml double

distilled water was added in the vial and sonicated to dissolve the content. Subsequently, 835 mg of FBX (i.e. 16.7% w/v) was incorporated to the stabilizer solution and sonicated for 5 minutes to disperse the drug in the medium. Then magnetic stirring bar (22 x 8 mm) and 5 gm of zirconium oxide beads were added in the dispersion and comminution was carried out on a high speed magnetic stirrer at 2000 rpm for about 8.0 hours at room temperature. The diameter of zirconium oxide beads was in the range of 0.4 to 0.5 mm. After completion of comminution, NS was separated from milling beads by decanting the suspension, followed by washing of beads with double distilled water. The prepared FBX-NS was stored in a sealed glass vial at room temperature till the further processing.

The practical values of PS and SS were found to be $139.7 \pm 4.2 \text{ nm}$ and $421.1 \pm 6.8 \mu\text{g/ml}$, respectively, which were in close agreement with the theoretical values.

5.3.6.1.4 Freeze drying of FBX-NS

Freeze drying of prepared FBX-NS was performed with different cryoprotectants to prevent the agglomeration of particles during the process⁴¹. The dried lyophilized powder form of the NS enhanced its stability during storage. Different cryoprotectants such as Sucrose, Trehalose dihydrate and Mannitol were tried in different ratios to the solid content of NS (i.e. 1:1% w/w, 1:2% w/w and 1:3% w/w) and PS were estimated as shown in Table 5.12. The PS of FBX-NS before freeze drying was $139.7 \pm 4.2 \text{ nm}$. Dry fluffy powder was obtained in batches 1,2,4,7 and 8 whereas hard cake formation was found in batches 3,5,6 and 9. It was observed that dry powders were easily redispersed in 5ml distilled water on manual shaking for 1-2 mins but hard cakes need to be sonicated for more than 10 mins to reconstitute in the same conditions. The ratio of PS (after freeze drying, PS_{FD} and initial, PS_{initial}) was found to be lowest (i.e. 1.07) for trehalose at 1:1 ratio, indicating its suitability in maintaining particle size of FBX-NS after freeze drying. This formulation was considered for further studies.

Table 6.12 Effect of cryoprotectants and their concentration on PS of freeze dried FBX-NS after redispersion in distilled water.

Batch No.	Cryoprotectant	Ratio	Avg. PS in nm (PS _{FD}) [#]	PS _{FD} /PS _{initial}
1	Trehalose	1:1	149.6±7.3	1.07*
2		1:2	199.4±11.5	1.43*
3		1:3	252.6±9.8	1.81
4	Mannitol	1:1	189.9±12.2	1.36*
5		1:2	278.2±18.4	1.99
6		1:3	345.4±13.6	2.47
7	Sucrose	1:1	170.3±8.5	1.22*
8		1:2	238.9±10.7	1.71*
9		1:3	298.4±17.2	2.14

Initial PS of FBX-NS (PS_{initial}) = 139.7±4.2nm

[#] Data are shown as Mean±SD, n=3.

* showed good redispersibility on manual shaking.

5.3.6.2 Characterization of FBX-NS

5.3.6.2.1 Particle size determination

FBX-NS formulation was optimized and successfully prepared by wet media milling, achieving the average particle size of 149.6±7.3nm with PDI value of 0.103±0.011 (Fig. 5.6). The PDI measures the width of distribution. The PDI value of FBX-NS was below 0.2 indicating a narrow size distribution of the prepared nanosuspension. It can be observed that there was no significant difference in particle size before and after freeze drying indicating the suitability of freeze drying process. The particle size of plain FBX was evaluated by Malvern Mastersizer 2000 and it was found to be 26.95±1.04 μm (PDI= 0.447) (Fig. 5.7). Thus there was significant reduction in particle size of FBX from micron to nano range by nanosizing.

5.3.6.2.2 Zeta potential

Zeta potential of prepared nanosuspension was evaluated to get the information about surface properties of nanoparticles. The average zeta potential of FBX-NS was found to be -43.8±2.8 mV (Fig. 5.8). It is considered that for a nanosuspension exhibiting good physical stability (stabilized by electrostatic repulsion), a minimum zeta potential of ±30 mV is required.

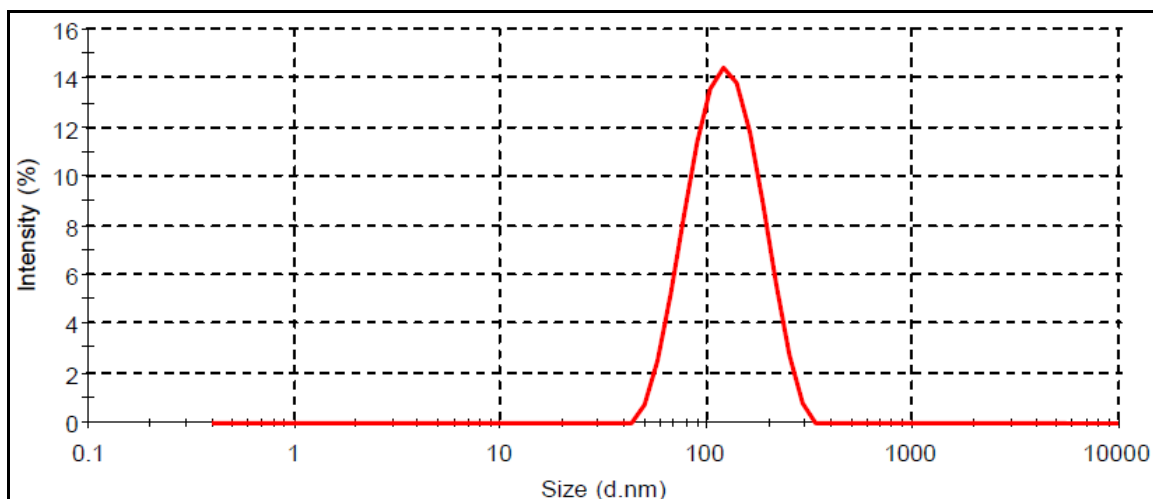


Fig. 5.6 Particle size distribution of FBX-NS by Malvern Zetasizer.

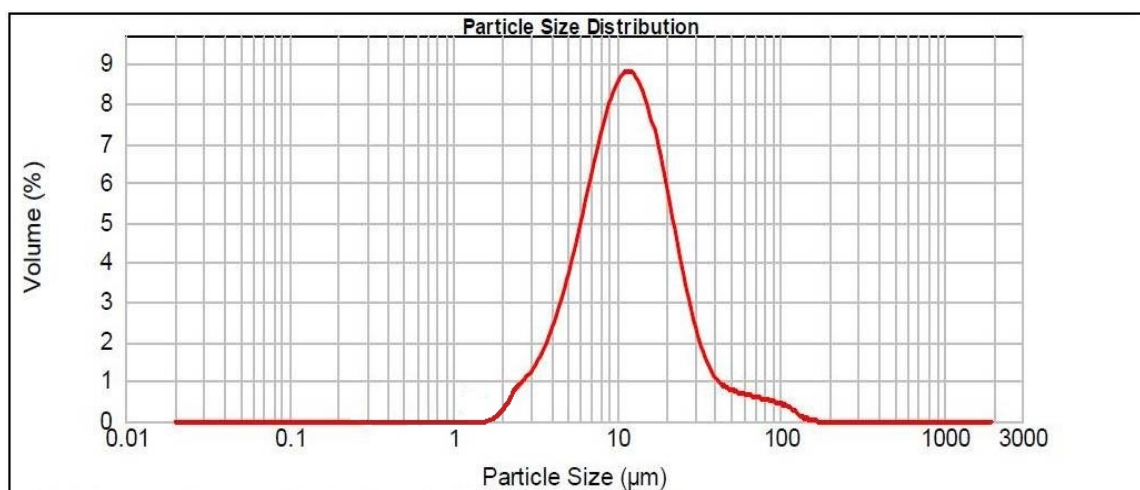


Fig. 5.7 Particle size distribution of Plain FBX by Malvern Mastersizer.

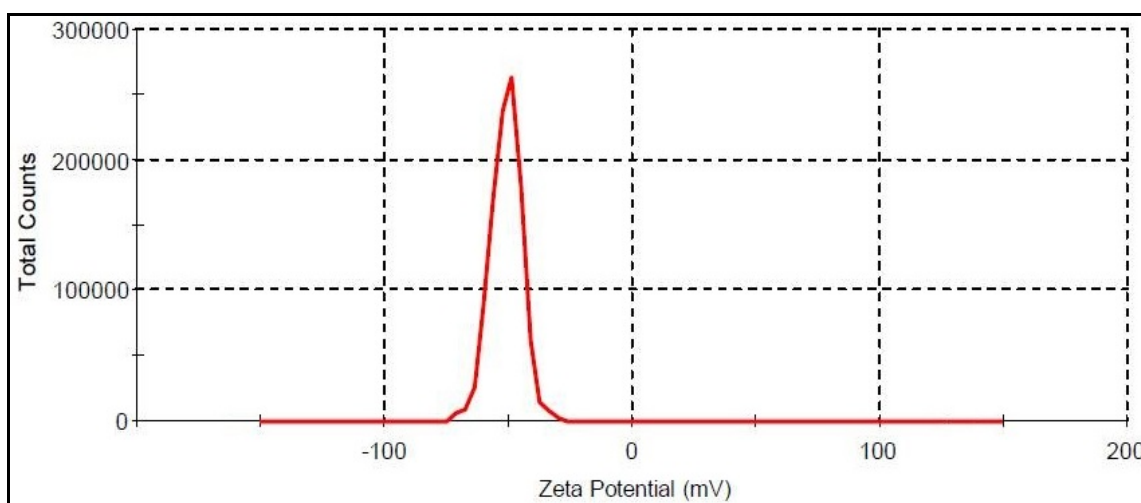


Fig 5.8 Zeta potential report of FBX-NS by Malvern Zetasizer.

5.3.6.2.3 Differential Scanning Calorimetry (DSC) Analysis

Under the physicochemical characterization, DSC analysis of plain FBX, poloxamer 188, trehalose, physical mixture for FBX-NS and freeze dried FBX-NS was carried out. DSC thermogram of bulk FBX showed sharp endothermic peak at 209.4°C corresponding to its melting point which indicate the crystalline nature of drug. DSC thermogram of poloxamer 188 exhibited an endothermic peak at 50.1°C while trehalose showed a melting peak at 99.8°C. Three endothermic peaks were observed in PM corresponding to the individual components of FBX-NS from 100°C to 300°C. Three low intense and broad peaks were detected in the thermogram of FBX-NS. The very initial small bulge probably due to the melting of poloxamer 188, whereas second low intense peak corresponded to Trehalose. And the third melting peak at 208.2°C was due to the FBX. The occurrence of broader peaks in FBX-NS thermogram were probably due to the depression of the melting points of materials in form of small crystals as explained by the Gibbs-Thomson equation. Gibbs–Thomson equation⁴². Additionally, the reduction in sharpness of corresponding peaks also supports the reduction in crystallinity of material in matrix⁴³. The thermograms of studied materials are represented in Fig. 5.9.

5.3.6.2.4 X-Ray Diffraction (XRD) Study

XRD study was carried out to investigate the physical state of FBX in pure form, in physical mixture and most importantly in formulation i.e. NS which is influencing the dissolution and stability behaviour of compound. This study also predict the effect of wet media milling on the physical state of FBX. XRD patterns has ben used to analyze the potential changes in the iner structure of FBX crystals. The results clearly indicated the significant reduction in crystallinity of FBX as compared to plain drug (Fig. 5.10). All the major peaks which are associated with pure drug were disappeared in case of FNX-NS except the peaks at 7.2 2θ and 12.8 2θ, but the intensities of both were reduced significantly, indicating reduction in crystallinity. However, the reduction in the relative intensities of FNX-NS peaks as compared to pure FBX peaks might be attributed to small particle size (nanometer range), high specific surface area and presence of excipients on the surface of FBX nanoparticles^{44,45}. The results were in line with those of DSC studies, which also indicated decrease in crystallinity due to nanosizing.

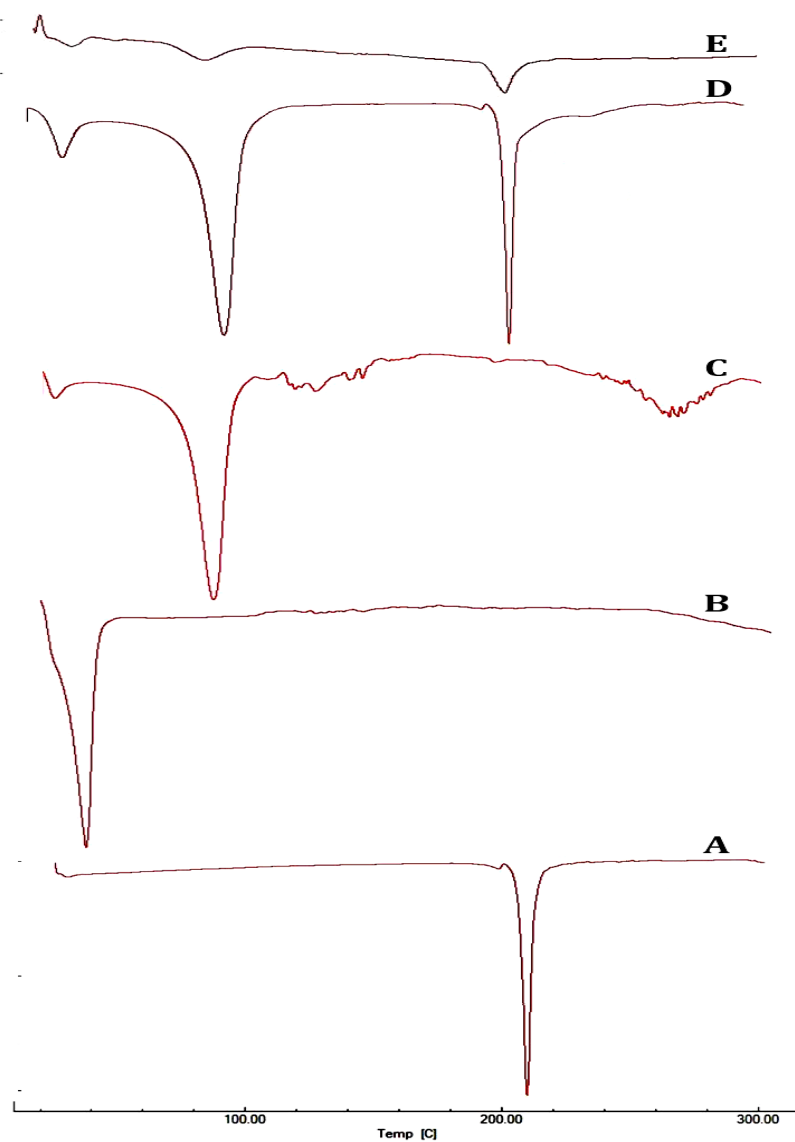


Fig. 5.9 DSC thermograms of (A) Plain FBX, (B) Poloxamer 188, (C) Trehalose, (D) Physical Mixture for FBX-NS (PM) and (E) Freeze dried FBX-NS.

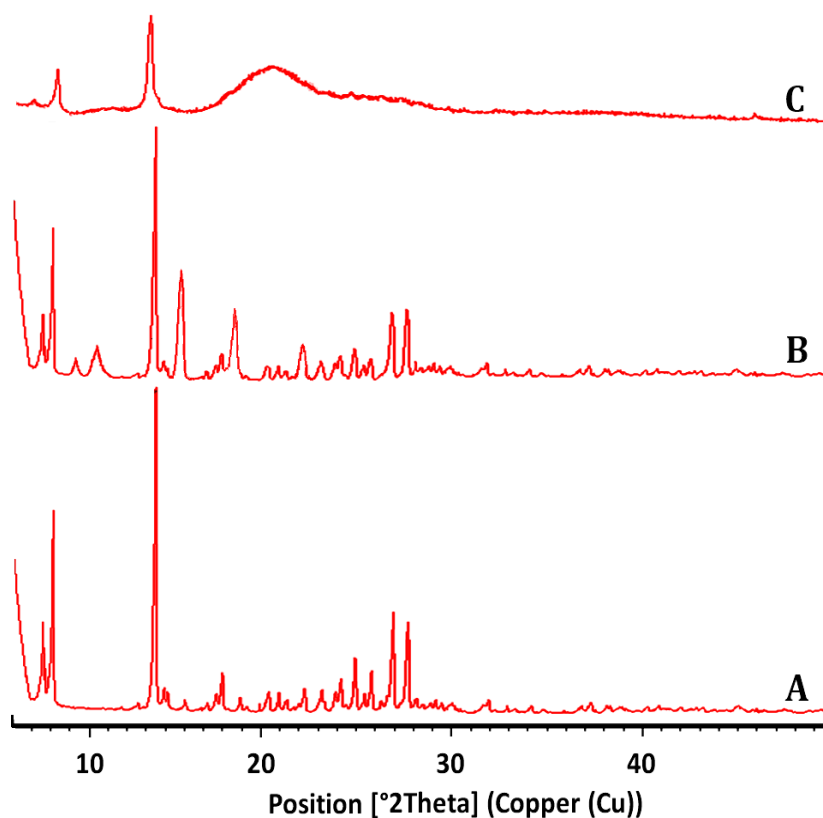


Fig. 5.10 XRD spectra of (A) Plain FBX, (B) Physical Mixture for FBX-NS (PM) and (C) Freeze dried FBX-NS.

5.3.6.2.5 Morphological analysis by SEM and TEM

Analysis by SEM has been performed to evaluate the morphology of drug particles in bulk drug and nano-formulations. It was observed in SEM images that there were distinct differences in morphologies of raw FBX and FBX-NS. SEM image of plain FBX exhibited discrete needle shaped crystals (Fig. 5.11). By evaluating the SEM image of FBX-NS (Fig. 5.12), it can be predicted that media milling of FBX in presence of stabilizer (poloxamer 188) led to a change in morphology of drug particles and decrease in particle size from micron to nanometric range with relatively narrow size distribution. TEM image of FBX-NS demonstrate that the nanoformulation could be easily redispersed in water without forming any large aggregates. TEM image revealed that the particles of FBX were discrete, non-aggregated, homogeneously dispersed but irregular in shape and were in accordance with particle size obtained by DLS method (Fig. 5.13).

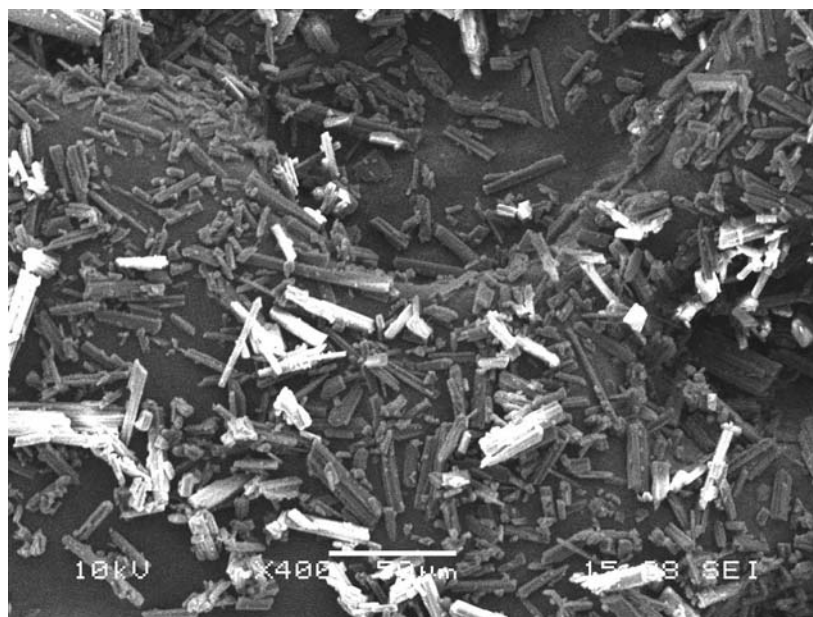


Fig. 5.11 SEM image of plain FBX.

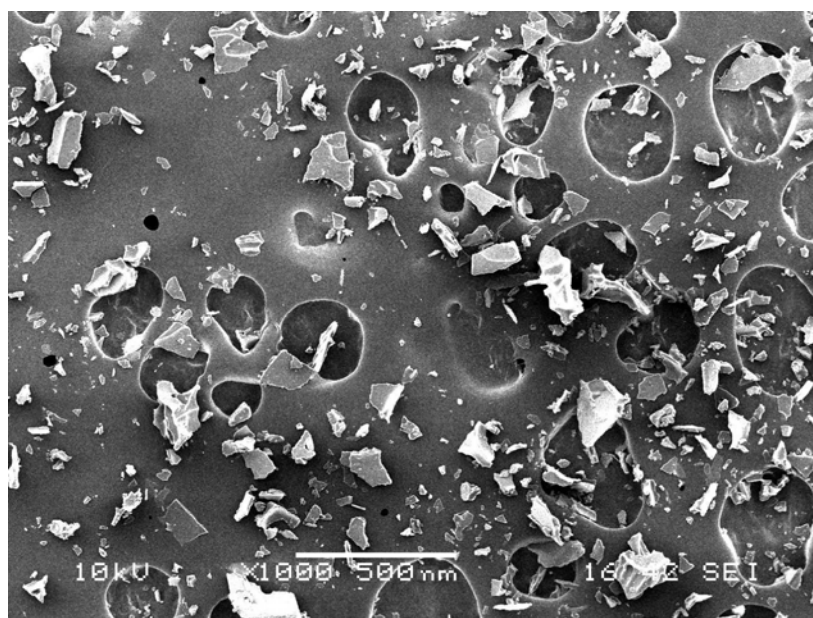


Fig. 5.12 SEM image of FBX-NS.

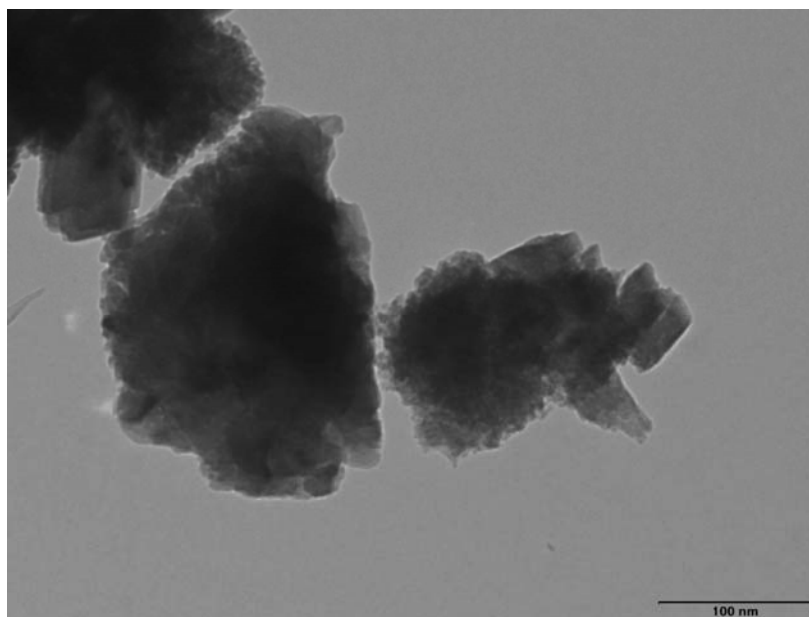


Fig. 5.13 TEM image of FBX-NS.

5.3.6.2.6 Percentage drug content in FBX-NS

Percentage drug content in FBX-NS was found to be $99.24 \pm 1.02\%$, indicating the suitability of media milling method for preparation of nanosuspension.

5.3.6.2.7 Saturation solubility

Poorly water soluble drugs are normally accompanied with poor dissolution and low absorption in body. Enhancement in saturation solubility is the most successful and interesting way to outline this issue. Among many classical approaches, nanotechnology or more precisely, formulation of nanosuspension is very easy, economical and effective technique. To get an idea about efficiency of nanosuspension, estimation of saturation solubility is an important parameter.

In this study the saturation solubility of plain FBX was compared with freeze dried FBX-NS. The saturation solubility of plain FBX was found to be $4.45 \pm 0.23 \mu\text{g/ml}$ which is very low whereas FBX-NS showed enhanced saturation solubility of FBX $416.18 \pm 1.69 \mu\text{g/ml}$. It can be observed that FBX-NS enhanced the saturation solubility of FBX by about 93.5 folds than plain FBX, attributed to nanosizing of FBX particles.

5.3.6.2.8 *In vitro* dissolution study

The *in-vitro* dissolution studies of capsules containing plain FBX (FBX-P), marketed formulation (FBX-M) and freeze dried FBX nanosuspension (FBX-NS) were carried out in phosphate buffer pH-6.8, acetate buffer pH-4.5, 0.1N HCl and water and results have been described in Table 5.13 and graphically represented in Fig 5.14. The drug release was markedly increased in the FBX-NS as more than 50% of FBX was dissolved

in first 5 mins, as compared to 6.1-11.4% and 1.4-5.4% from FBX-M and FBX-P, respectively. FBX-P and FBX-M did not achieve complete dissolution in any of the selected media over the test period of 120 mins, which may be due to large crystal size of drug present in FBX-P and FBX-M. However, FBX-NS showed 69-99.5% drug dissolved with significantly enhanced dissolution rate over the time period of 120 mins, in all the selected dissolution mediums.

Table 5.13: Statistical representation of % Cumulative drug release versus sampling time of FBX-P, FBX-M and freeze dried FBX-NS in phosphate buffer pH-6.8 (PB), acetate buffer pH-4.5 (AB), 0.1N HCl and water.

Time (min) ⇒	0	5	10	15	30	45	60	120
% Cumulative release from Phosphate Buffer, pH-6.8*								
FBX-NS	0.0	90.4±0.3	95.5±0.5	97.2±0.1	98.6±0.2	99.7±0.2	99.9±0.6	99.5±0.4
FBX-M	0.0	11.4±0.6	20.2±0.4	28.6±0.3	49.1±0.4	58.8±0.2	65.3±0.1	72.9±0.4
FBX-P	0.0	5.4±0.1	11.8±0.2	17.5±0.1	31.1±0.5	42.8±0.4	48.1±0.2	55.4±0.3
% Cumulative release from Acetate Buffer, pH-4.5*								
FBX-NS	0.0	36.2±0.7	52.4±0.2	60.2±0.5	68.3±0.4	72.9±0.2	75.6±0.8	77.1±0.2
FBX-M	0.0	7.2±0.5	11.4±0.7	13.9±0.2	20.9±0.8	24.1±0.5	26.4±0.1	27.9±0.4
FBX-P	0.0	2.1±0.4	3.8±0.2	4.7±0.3	6.8±0.2	9.1±0.6	10.6±0.5	11.2±0.2
% Cumulative release from 0.1N HCl*								
FBX-NS	0.0	24.2±0.5	40.3±0.9	47.4±0.8	59.2±0.3	64.9±0.5	67.4±0.9	69.6±0.7
FBX-M	0.0	6.1±0.2	8.3±0.5	10.4±0.5	14.2±0.4	18.6±0.8	20.9±1.1	21.6±0.7
FBX-P	0.0	1.4±0.5	2.9±0.2	3.8±0.5	5.2±0.4	7.9±0.8	8.5±0.7	9.6±0.5
% Cumulative release from water*								
FBX-NS	0.0	82.3±0.9	88.9±0.7	91.4±1.3	95.2±0.8	96.9±0.8	97.5±0.6	98.1±0.3
FBX-M	0.0	9.3±0.5	16.7±0.4	22.6±0.8	37.2±0.2	46.4±0.3	52.8±0.6	64.5±0.1
FBX-P	0.0	3.8±0.3	9.2±0.2	13.5±0.6	27.2±0.4	36.1±0.4	40.3±0.8	45.5±0.7

* Data are shown as Mean±SD, n=3.

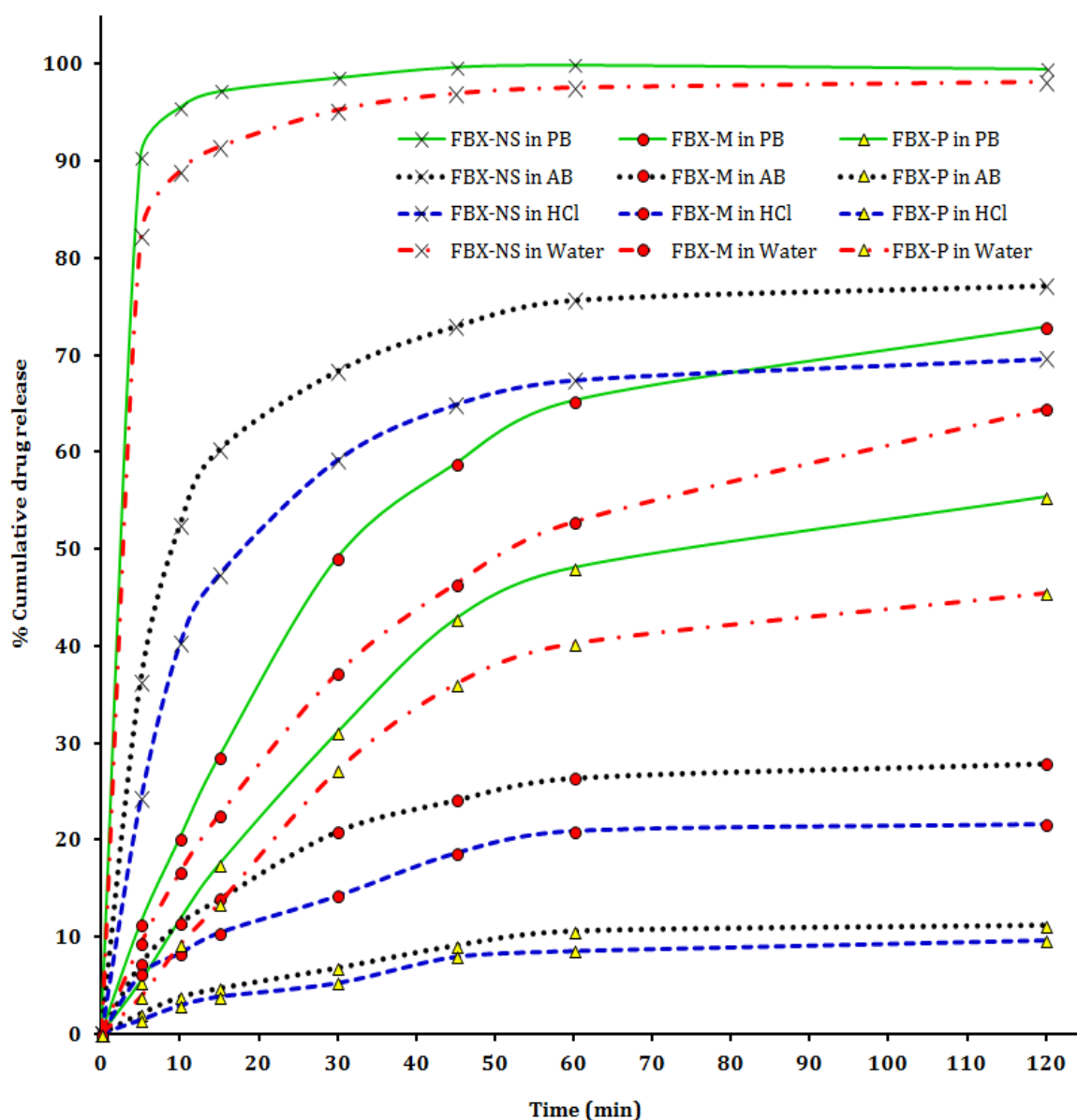


Fig. 5.14 Graphical representation of % Cumulative drug release versus sampling time of FBX-P FBX-M and freeze dried FBX-NS in phosphate buffer pH-6.8 (PB), acetate buffer pH-4.5 (AB), 0.1N HCl and water.

Various dissolution parameters were calculated using DDSolver, an excel add-in program and reported in Table 5.14. The Dissolution efficiency (DE), Dissolution percentage at 5 min and 60 min (DP₅ and DP₆₀) and Area under curve (AUC) values were increased in the following order: FBX-P<FBX-M<FBX-NS; while time required to release 50% of drug (t₅₀) and mean dissolution time (MDT) were increased in vice versa i.e. FBX-P>FBX-M>FBX-NS. The t₅₀ for FBX-NS was strongly reduced to 2-5 mins compared to FBX-M and FBX-P in all the dissolution mediums. FBX-NS achieved high

dissolution (i.e. >98%) in phosphate buffer and water along with 80-85% dissolution in rest of two mediums over the period of 60mins. This improved dissolution rate can be due to the larger surface to volume ratio of nanoparticles available for dissolution and decrease in diffusion layer thickness in comparison to microcrystals (Noyes-Whitney Equation)⁴⁶. The presence of surfactant in nanosuspension also play a noteworthy role in enhancement of dissolution of drug by increasing the surface wettability of compound⁴⁷. It has also been claimed that the surface of finely devided solids may be less regularly crystalline and more amorphous than that of well-grown crystals⁴⁸.

Thus, it can be said that prepared FBX-NS have superior characteristics to plain FBX and marketed formulation, indicating a major prospect to enhance the bioavailability of such drugs by nanosuspensions for oral administration where solubility and dissolution are rate limiting factors in bioavailability in the body. Nanotechnology is therefore more effective in increasing dissolution velocity and offers economical process and formulation.

Table 5.14 Comparison of various dissolution parameters of FBX-P, FBX-M and freeze dried FBX-NS in phosphate buffer pH-6.8 (PB), acetate buffer pH-4.5 (AB), 0.1N HCl and water.

	DE	DP ₅	DP ₆₀	t ₅₀	t ₉₀	MDT	AUC
In Phosphate Buffer, pH-6.8*							
FBX-NS	0.97±0.05	90.4±0.3	99.9±0.6	1.5±0.2	5.1±0.1	3.3±0.1	11607±55
FBX-M	0.56±0.07	11.4±0.6	65.3±0.1	37.5±0.7	>60	28.1±0.4	6698±38
FBX-P	0.40±0.02	5.4±0.1	48.1±0.2	>60	>60	32.7±0.3	4835±36
In Acetate Buffer, pH-4.2*							
FBX-NS	0.69±0.06	36.2±0.7	75.6±0.8	14.4±0.3	>60	12.2±0.2	8311±50
FBX-M	0.23±0.01	7.2±0.5	26.4±0.1	>60	>60	22.0±0.3	2734±27
FBX-P	0.09±0.03	2.1±0.4	10.6±0.5	>60	>60	26.4±0.1	1048±31
In 0.1N HCl*							
FBX-NS	0.61±0.02	24.2±0.5	67.4±0.9	25.3±0.5	>60	15.5±0.1	7273±42
FBX-M	0.17±0.04	6.1±0.2	20.9±1.1	>60	>60	22.8±0.6	2099±47
FBX-P	0.07±0.01	1.4±0.5	8.5±0.7	>60	>60	30.1±0.3	862±25
In water*							
FBX-NS	0.94±0.02	82.3±0.9	97.5±0.6	2.3±0.3	13.6±0.3	5.3±0.5	11250±75
FBX-M	0.46±0.03	9.3±0.5	52.8±0.6	55.7±0.9	>60	31.5±0.5	5525±61
FBX-P	0.34±0.05	3.8±0.3	40.3±0.8	>60	>60	34.3±0.3	4025±32

* Data are shown as Mean±SD, n=3. DE: Dissolution efficiency, DP₅: Dissolution percentage at 5 min, DP₆₀: Dissolution percentage at 60 min, t₅₀: time required to release 50% of drug (min), t₉₀: time required to release 90% of drug (min), MDT: Mean dissolution time (min), AUC: Area under curve.

5.3.6.2.9 Stability studies

The stability of FBX-NS was monitored and evaluated for physical stability (i.e. PS, PDI and zeta potential) and chemical stability (i.e. percentage drug content), carried out for 6 months at different time intervals (i.e. 1st, 2nd, 3rd and 6th month) stored at 5°C±3°C and at room temperature. It was observed that there was no significant difference in the PS, PDI, ZP and % FBX content remained more than 98% at both conditions for 6 months (Table 5.15 and Table 5.16) so it can be concluded that formulation is physically and chemically stable for a period of 6 months and indicating its suitability for storage at both the conditions.

Table 5.15 Physical stability (i.e. PS, PDI and ZP) of FBX-NS at different time intervals stored at 5°C±3°C and room temperature.

Sr. No.	Time	At 5°C±3°C*			At Room Temperature*		
		PS (nm)	PDI	ZP (mV)	PS (nm)	PDI	ZP (mV)
1	Initial	149.6±7.3	0.103±0.011	-43.8±2.8	149.6±7.3	0.103±0.011	-43.8±2.8
2	1 st Month	150.7±2.5	0.117±0.009	-44.3±3.6	153.2±4.4	0.112±0.015	-43.9±3.8
3	2 nd Month	151.2±3.9	0.108±0.008	-43.9±2.4	150.9±2.6	0.107±0.006	-44.7±2.1
4	3 rd Month	150.1±4.2	0.114±0.012	-44.1±3.1	150.3±5.2	0.115±0.004	-44.2±2.9
5	6 th Month	152.4±2.1	0.121±0.007	-44.8±3.7	152.7±6.1	0.109±0.009	-44.4±3.2

* Data are shown as Mean±SD, n=3.

Table 5.16 Chemical stability (i.e. percentage drug content) of FBX-NS at different time intervals stored at 5°C±3°C and room temperature.

Sr. No.	Time	At 5°C±3°C*	At Room Temperature*
		% content of FBX in FBX-NS	% content of FBX in FBX-NS
1	Initial	99.24±1.02	99.24±1.02
2	1 st Month	99.89±0.98	99.03±0.91
3	2 nd Month	99.52±1.25	98.96±0.67
4	3 rd Month	99.16±1.23	99.41±1.16
5	6 th Month	99.66±1.07	98.79±0.43

* Data are shown as Mean±SD, n=3.

5.3.6.3 Cell Line Studies using Caco-2 cell line model

5.3.6.3.1 *In vitro* Cell Cytotoxicity Studies (MTT Assay)

Cytotoxicity study of FBX-NS and FBX-P was accomplished in Caco2 cells by mitochondrial activity (MTT assay) to assess the safety/tolerability of prepared formulation on viability of cells. As Caco2 cells were used as absorption model, the biocompatibility and tolerability assessment of FBX-P and FBX-NS on absorption barrier was necessary. At initial 4 hr and 24 hr, the % cell viability is more than 80% at the 500 µg/ml concentration of FBX-P and FBX-NS. Hence for permeability studies, the drug and formulation concentration was fixed at 250 µg/ml. It can be observed that the FBX-NS

showed very less cytotoxicity than the plain FBX upto 48 hours at all the concentrations. (Table 5.17) This confirms the biocompatibility of FBX-NS and explains that composition of nanosuspension did not contribute to toxicity of Caco2 cells⁴⁹. At initial 4 hours, 24 hours and 48 hours, FBX-NS was found to have less cytotoxicity with more than 80% cell viability as compared to FBX-P at all the concentrations except upto 48 hours condition. This could be attributed to protective effect of poloxamer 188⁵⁰. Literature revealed that poloxamer 188 own some wonderful properties that can affect the cell physiology. Poloxamer 188, as a supplement in cell culture medium, it saved cells from starvation death and protected them against high ion concentration or trace metal ions⁵¹. Secondly Poloxamer 188 inhibits the P-gp-function and thereby enhance the intestinal absorption of various drugs⁵². The stabilizer also decreased the rate of cell death from shear stress in flow cytometric chambers due to interaction of Poloxamer 188 with the cell membrane resulting in a decreased fluidity of the plasma membrane^{53,54}.

Cytotoxicity graphs at 4 hours, 24 hours and 48 hours were constructed (Fig. 5.15, 5.16 and 5.17) and IC₅₀ values were calculated for FBX-P and FBX-NS (Table 5.18). The higher IC₅₀ values for FBX-NS than FBX-P at all the incubation time conditions concluded to lack of cytotoxicity due to formulation of a biocompatible nanosuspension.

Table 5.17 In vitro cytotoxicity studies of FBX-P and FBX-NS in Caco2 cell lines at 4 hours, 24 hours and 48 hours.

Conc. (µg/ml)	%Cell Viability at 4 Hrs.*		%Cell Viability at 24 Hrs.*		%Cell Viability at 48 Hrs.*	
	FBX-P	FBX-NS	FBX-P	FBX-NS	FBX-P	FBX-NS
0.1	99.78±0.21	99.91±0.52	98.21±0.54	99.02±0.42	93.42±0.90	96.29±0.27
1	99.12±0.36	99.54±0.29	98.23±0.27	98.65±0.87	92.71±0.61	95.12±0.61
10	98.85±0.74	99.24±0.57	97.96±0.42	98.14±0.58	91.25±0.35	94.23±0.52
100	95.23±0.51	98.75±0.26	93.24±0.42	97.51±0.69	89.56±0.56	93.25±0.76
250	91.42±0.35	97.21±0.62	88.67±0.33	95.63±0.28	83.28±0.82	90.14±0.66
500	88.42±0.72	95.19±0.37	84.23±0.39	93.28±0.34	80.56±0.37	88.96±0.48
1000	85.26±0.63	91.68±0.19	81.69±0.76	90.10±0.57	75.63±0.59	86.75±0.53

* Data are shown as Mean±SD, n=3.

Table 5.18 IC₅₀ values of FBX-P and FBX-NS in Caco2 cell lines at 4 hours, 24 hours and 48 hours.

Conditions	IC ₅₀ Values (µg/ml)*	
	FBX-P	FBX-NS
At 4 hours	3301.52±96.21	6186.63±77.84
At 24 hours	2664.43±25.78	5497.84±52.36
At 48 hours	2359.77±48.63	5050.46±70.62

* Data are shown as Mean±SD, n=3.

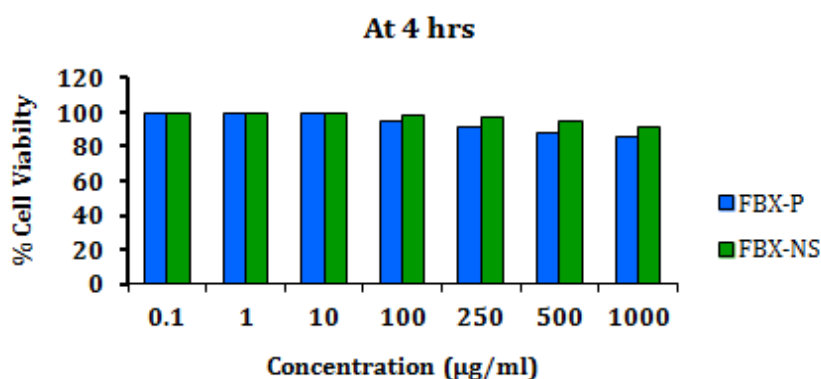


Fig. 5.15 In vitro cytotoxicity studies of FBX-P and FBX-NS in Caco2 cell lines at 4 hours.

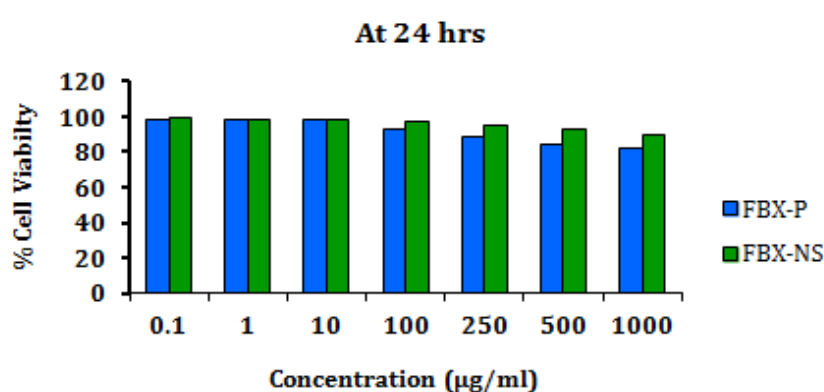


Fig. 5.16 In vitro cytotoxicity studies of FBX-P and FBX-NS in Caco2 cell lines at 24 hours.

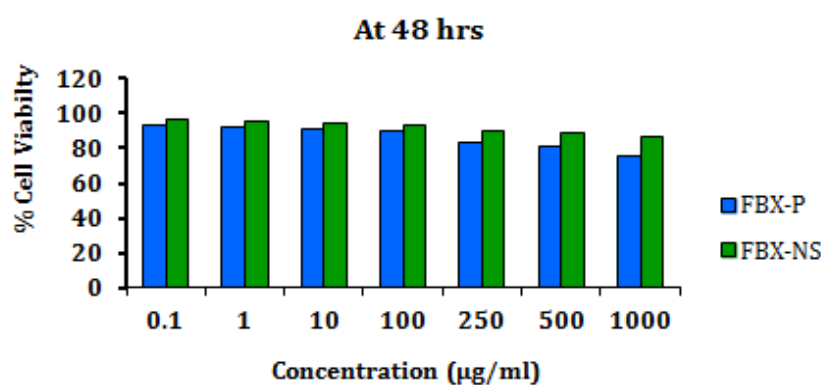


Fig. 5.17 In vitro cytotoxicity studies of FBX-P and FBX-NS in Caco2 cell lines at 48 hours.

5.3.6.3.2 *In vitro* cell permeability assessment of FBX-NS

Caco-2 monolayer model is an informative and interesting method for *in vitro* assessment of gastrointestinal permeability of drug as these cells spontaneously differentiate morphologically and functionally to yield monolayers that mimic the human intestinal epithelium⁵⁰. Caco-2 cells provide a prediction of the human absorption of the drug

which show active uptake or efflux or pass through the membrane via paracellular route. Additionally, because use of this model can decrease the number of animals needed for experimental studies. In this study, *in vitro* permeability assessment of FBX-NS, plain FBX (FBX-P) and marketed formulation (FBX-M) was done by calculating apparent permeability coefficient (P_{app}) from apical to basolateral. Transepithelial permeability of FBX was measured at concentration of 250 μ g/ml, as negligible toxicity towards Caco-2 cells was found at this concentration during MTT assay of the same. The average P_{app} for Lucifer yellow with Caco-2 cells was found $(0.87\pm 0.07) \times 10^{-6}$ cm/sec, confirmed the integrity of monolayers and suitability of monolayers for further experiment. The P_{app} for FBX-P and FBX-M were calculated and found to be $(10.15\pm 0.68) \times 10^{-6}$ cm/sec and $(12.19\pm 0.57) \times 10^{-6}$ cm/sec respectively while the P_{app} for FBX-NS was observed at $(50.16\pm 0.72) \times 10^{-6}$ cm/sec which is about 4.94 fold and 4.11 fold higher than the FBX-P and FBX-M, respectively (Table 5.19). The found results were very much satisfactory and matching with the aim of the project. It can be concluded that the higher P_{app} for FBX-NS was because of small particle size of FBX in nanosuspension additionally the hydrophilic and lipophilic nature of poloxamer-188 present in the formulation. Poloxamer 188 inhibits the P-gp-function and thereby enhance the intestinal absorption of various drugs⁵². Whereas the permeability coefficient of FBX can be attributed to hydrophobicity and low permeation ($\log P$ 3.5-3.8) of drug. If the P_{app} value of a compound is less than 1×10^{-6} cm/sec, in between $1-10 \times 10^{-6}$ cm/sec, and more than 10×10^{-6} cm/sec can be classified as poorly (0-20%), moderately (20-70%) and well (70-100%) absorbed compounds, respectively^{15,55}.

Table 5.19 Apparent permeability coefficient (P_{app}) from apical to basolateral for FBX-P, FBX-M and FBX-NS using Caco-2 cells model.

Drug/Formulation	Apparent permeability coefficient (P_{app}) \pm SD (10^{-6} cm/sec)*
FBX-P	10.15 \pm 0.68
FBX-M	12.19 \pm 0.57
FBX-NS	50.16 \pm 0.72

* Data are shown as Mean \pm SD, n=3.

5.3.6.4 Pharmacokinetic evaluation of FBX-NS using *in vivo* animal model

Over the last 40 years, Pharmacokinetics has emerged as an integral part of drug development, especially when identifying a drug's biological properties. The general definition of pharmacokinetics broadly embraces *absorption, distribution, metabolism (biotransformation) and excretion* (ADME). In pharmacokinetics, route of drug

administration has great impact on ADME process. The most important property of any orally administered dosage form, intended to treat a systemic condition, is the ability to deliver the active ingredient to the bloodstream in an amount sufficient to cause the desired response. This property of a dosage form has historically been identified as physiologic availability, biologic availability or *bioavailability*. Bioavailability captures two essential features, namely how fast the drug enters the systemic circulation (rate of absorption) and how much of the nominal strength enter in the body (extent of absorption). Hence as per the clinical, academic and regulatory aspects, the bioavailability assessment of a newly developed formulation is very much necessary.

In this section of chapter, the *in-vivo* animal study is discussed which was performed to evaluate the oral bioavailability and other pharmacokinetic parameters of prepared formulation (FBX-NS) with respect to plain drug (FBX-P) and commercial formulation (FBX-M). The mean drug plasma concentration versus time after oral administration of FBX-P, FBX-M and FBX-NS are reported in Table 5.20 whereas Fig 5.19 illustrate the same graphically. The pharmacokinetic parameters for all the three orally administered forms of FBX were determined using PKsolver add-in in microsoft excel¹⁹. Non-compartmental analysis of plasma with linear trapezoidal method after extravascular administration in rabbits was performed and obtained parameters are represented in Table 5.21. Drug plasma concentration profile of FBX-NS showed significant improvement in drug absorption compared to FBX-P and FBX-M. Area under concentration-time curve (AUC_{0-t}) of FBX was found $218.26 \pm 4.86 \mu\text{g} \cdot \text{h}/\text{ml}$ for FBX-NS which was 2.59 fold and 2.16 fold higher with that of FBX-P ($84.30 \pm 1.35 \mu\text{g} \cdot \text{h}/\text{ml}$) and FBX-M ($101.14 \pm 4.12 \mu\text{g} \cdot \text{h}/\text{ml}$), respectively. The area under moment curve ($AUMC_{\text{total}}$) showed significantly higher value for FBX-NS ($1769.39 \pm 21.35 \mu\text{g} \cdot \text{h}^2/\text{ml}$), compared to FBX-P ($760.75 \pm 9.24 \mu\text{g} \cdot \text{h}^2/\text{ml}$) and FBX-M ($1076.82 \pm 9.85 \mu\text{g} \cdot \text{h}^2/\text{ml}$). The maximum peak plasma concentration (C_{max}) of FBX-NS was about 2.99 fold and 2.59 fold greater than that of FBX-P and FBX-M, respectively. The enhancement in AUC and C_{max} of FBX-NS compared to FBX-P and FBX-M could be due to the quick absorption of drug molecule by gastrointestinal wall due to the reduced particle size and increased surface area followed by significantly improved dissolution rate and increase in adhesion surface area between nanoparticle and intestinal epithelium of villi which provides a direct contact with the absorbing membrane of the gut wall⁵⁶. Time to reach maximum plasma concentration (T_{max}) for FBX-NS, FBX-M and FBX-P was found to be 0.5, 1.0 and

1.0 hour, respectively. Mean residence time (MRT) for FBX-NS was decreased by 1.11 and 1.17 fold when compared to FBX-P and FBX-M, respectively. The shortest T_{max} and MRT for FBX-NS may be due to fastest dissolution rate and the highest T_{max} of FBX-P could be attributed to crystalline nature of drug¹.

When half life ($t_{1/2}$) of FBX-NS was compared with FBX-P and FBX-M, the $t_{1/2}$ for FBX-NS (12.59 ± 0.62 h) was not found much different than that of FBX-P (14.58 ± 0.29 h) and FBX-M (16.32 ± 0.18 h). The elimination rate constant ($K_{elimination}$) for FBX-P, FBX-M and FBX-NS were found to be 0.05 ± 0.01 h⁻¹, 0.04 ± 0.01 h⁻¹ and 0.06 ± 0.01 h⁻¹, respectively. No significant difference in $t_{1/2}$ and $K_{elimination}$ of all three was observed which indicated that their elimination was comparable.

Relative bioavailability or bioequivalence is the most important criteria for comparing the bioavailabilities of different formulations of same drug. The relative bioavailability (F) of FBX-NS and FBX-M were found to be 258.91% and 134.21%, respectively, with respect to FBX-P. Thus there was 2.59 and 1.93 fold increase in bioavailability of FBX from FBX-NS with respect to FBX-P and FBX-M, respectively.

The higher bioavailability of FBX from FBX-NS compared to FBX-P and FBX-M, attributed to its greater dissolution rate, increased wettability and reduced particle size with increased surface area and reduced diffusion layer thickness⁴⁷. This was in agreement with the *in-vitro* dissolution studies. In addition, nanoparticles could stay a longer time in the gastrointestinal tract due to the adhesive property^{57,58}. The reduction of drug dose is not only favourable economically but also is desirable in decreasing its side effects especially when administered in multiple dosage regimens.

Table 5.20 Statistical representation of FBX plasma profile for FBX-P, FBX-M and FBX-NS in Albino rabbits following oral administration.

Time (Hour)	FBX mean plasma concentration \pm SD*		
	FBX-P ($\mu\text{g/ml}$)	FBX-M ($\mu\text{g/ml}$)	FBX-NS ($\mu\text{g/ml}$)
0.0	0	0	0
0.25	3.42 \pm 0.11	5.11 \pm 0.17	18.66 \pm 0.24
0.5	6.29 \pm 0.35	9.65 \pm 0.14	48.71 \pm 0.46
0.75	9.54 \pm 0.28	12.51 \pm 0.37	40.52 \pm 0.41
1.0	16.25 \pm 0.51	18.76 \pm 0.25	36.38 \pm 0.62
1.5	14.21 \pm 0.29	16.98 \pm 0.61	30.75 \pm 0.26
2.0	11.54 \pm 0.42	13.42 \pm 0.41	26.76 \pm 0.29
3.0	8.28 \pm 0.24	10.65 \pm 0.48	19.89 \pm 0.31
4.0	6.15 \pm 0.27	8.79 \pm 0.36	14.67 \pm 0.28
6.0	4.16 \pm 0.20	6.39 \pm 0.31	10.58 \pm 0.49
8.0	3.11 \pm 0.18	4.78 \pm 0.46	8.12 \pm 0.17
12.0	0.95 \pm 0.21	1.12 \pm 0.19	3.15 \pm 0.23
24.0	0.62 \pm 0.17	0.81 \pm 0.09	1.19 \pm 0.14
48.0	0.31 \pm 0.12	0.52 \pm 0.13	0.68 \pm 0.11

* Data are shown as Mean \pm SD, n=3.

Table 5.21 Pharmacokinetic parameters after oral administration of FBX-P, FBX-M and FBX-NS in Albino rabbits.

Pharmacokinetic parameters*	FBX-P	FBX-M	FBX-NS
C _{max} ($\mu\text{g/ml}$)	16.25 \pm 0.51	18.76 \pm 0.25	48.71 \pm 0.46 ^{†#}
T _{max} (h)	1	1	0.5 ^{†#}
AUC _{0-t} ($\mu\text{g}\cdot\text{h/ml}$)	84.30 \pm 1.35	113.14 \pm 4.12	218.26 \pm 4.86 ^{†#}
AUC _{0-∞} ($\mu\text{g}\cdot\text{h/ml}$)	94.37 \pm 2.14	138.02 \pm 6.18	226.17 \pm 5.32 ^{†#}
AUMC _{total} ($\mu\text{g}\cdot\text{h}^2/\text{ml}$)	760.75 \pm 9.24	1076.82 \pm 9.85	1769.39 \pm 21.35 ^{†#}
MRT (h)	9.02 \pm 0.22	9.52 \pm 0.39	8.11 \pm 0.98 ^{†#}
T _{1/2} (h)	14.58 \pm 0.29	16.32 \pm 0.18	12.59 \pm 0.62 ^{†#}
K _{elimination} (h ⁻¹)	0.05 \pm 0.01	0.04 \pm 0.01	0.06 \pm 0.01 ^{†#}
F (%) w.r.t FBX-P	100	134.21	258.91 ^{†#}

* Data are shown as Mean \pm SD, n=3, [†]P<0.05 compared with FBX-P, [#]P<0.05 compared with FBX-M.

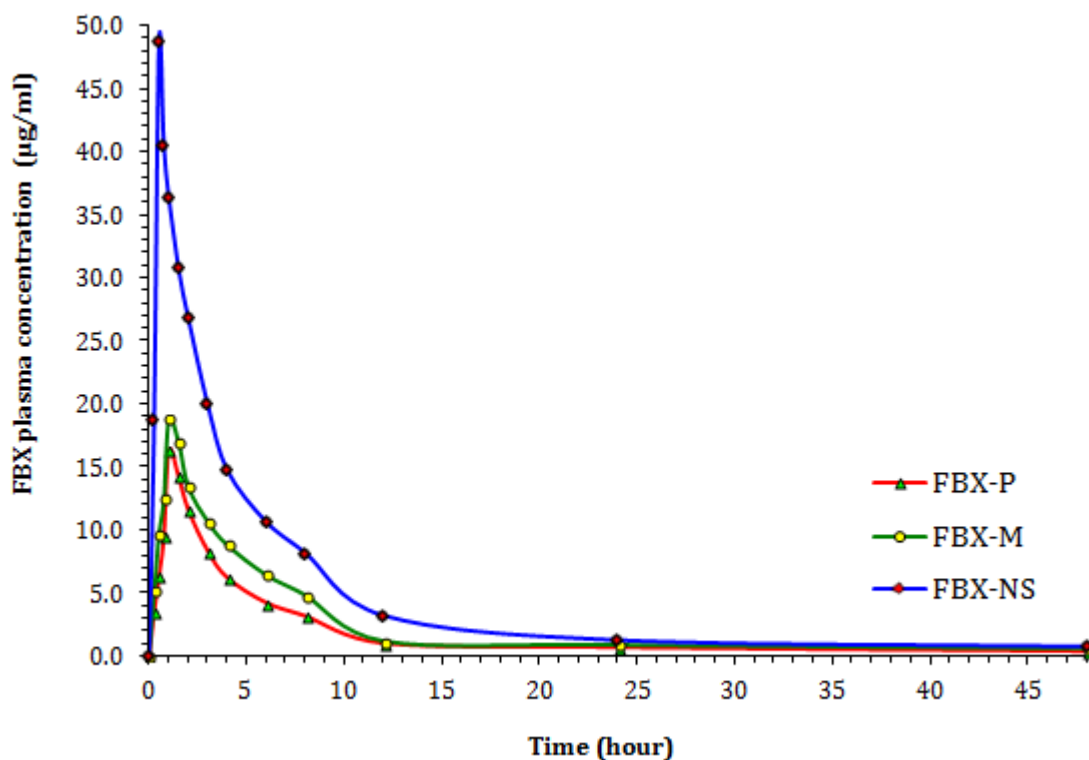


Fig. 5.18 Graphical representation of FBX plasma profile for FBX-P, FBX-M and FBX-NS in Albino rabbits following oral administration.

5.3.7 Conclusion

The purpose of this study was to develop an orally administrable nanosuspension of poorly water soluble drug with enhanced bioavailability. The nanosuspension formulation with smaller particle size, can be effectively produced with wet media milling technique. To overcome particle growth during long term storage of nanosuspension, freeze drying was carried out with suitable cryoprotectant, in order to assess the feasibility of transferring aqueous nanosuspension in a dry product. Nanosuspension might give additional effect by allowing reduction in either the dose or its dosing frequency of administration. Moreover, a nanosuspension may also reduce the risk of undesired adverse effect related to the initial peak plasma peak, without losing the high overall exposure³⁶.

This chapter of thesis includes the optimization, development and formulation of an efficient and stable, solid nanosuspension of BCS Class-2 drug, 'Febuxostat', followed by physicochemical characterization, stability studies, *in-vitro* release kinetics, cytotoxicity and GI permeability study using Caco-2 cell lines and finally bioavailability study using *in-vivo* animal model.

FBX-NS was prepared by media milling method using Zirconium oxide beads. Preliminary optimization of formation parameters was done systematically and critical variables were selected. The significant parameters such as drug concentration, stabilizer concentration and milling time were optimized by factorial design. Study revealed that the particle size can be greatly influenced by these factors. The optimized formulation contained 16.7% w/v of FBX, 1% w/v poloxamer 188 and 100% milling media in 5 ml double distilled water and comminution was carried out for about 8 hours at room temperature. Completely dried and fluffy powder was obtained by successful freeze drying of prepared FBX-NS with cryoprotectant, trehalose. The lyophilized powder was completely and easily re-dispersed in water. Efficient particle size ($149.6 \pm 7.3 \text{ nm}$) with low PDI (0.103 ± 0.011) of lyophilized FBX-NS was achieved using suitable excipients that provide physical stabilization (zeta potential $-43.8 \pm 2.8 \text{ mV}$) (steric and electrostatic) and improved saturation solubility ($416.18 \pm 1.69 \text{ } \mu\text{g/ml}$) of water insoluble FBX in FBX-NS.

DSC and XRD studies revealed that crystallinity of FBX in FBX-NS is reduced significantly after nanonization leads to better dissolution properties and sustained stability of the drug during its shelf life compared to pure FBX. The SEM images confirmed that the media milling process in presence of poloxamer 188 was effective in converting large aggregates of irregular shaped crystals of bulk FBX into submicron to nanometric range with relatively narrow size distribution. TEM image revealed that the particles of FBX were discrete, non-aggregated, homogeneously dispersed but irregular in shape and were in accordance with particle size obtained by DLS method.

Drug content of FBX-NS was found to be $99.24 \pm 1.02\%$ which again proved the suitability of method for particle size reduction. The dissolution profiles of FBX-P, FBX-M and FBX-NS were checked in phosphate buffer pH-6.8, acetate buffer pH-4.5, 0.1N HCl and water over the test period of 120 mins. FBX-NS was found superior to FBX-P and FBX-M in terms of % cumulative release of FBX, dissolution efficiency and mean dissolution time. FBX-NS achieved high dissolution (i.e. $>98\%$) in phosphate buffer and water along with 80-85% dissolution in rest of two mediums over the period of 60mins. The prepared FBX-NS was found physically and chemically stable over a time period of 6 months.

In vitro Cell Cytotoxicity Studies (MTT Assay) confirmed the biocompatibility and tolerability of FBX-NS and explains that composition of nanosuspension did not

contribute to toxicity of Caco2 cells, although the cytotoxicity of prepared NS was reduced due to the presence of biocompatible stabilizer Poloxamer 188 in the formulation. *In vitro* assessment of permeability using Caco-2 cell line model demonstrated that FBX-NS was successfully enhanced the permeability of FBX by 4.94 and 4.11 fold to FBX-P and FBX-M respectively. *In vivo* assessment demonstrated that FBX-NS exhibited better pharmacokinetic properties compared to FBX-P and FBX-M. The relative oral bioavailability of FBX from FBX-NS in Albino rabbits resulted from NS was found 2.59 and 1.93 fold greater than FBX-P and FBX-M, respectively. Thus it can be concluded that nanosuspension of FBX with poloxamer 188 produced by wet media milling technique has confirmed its efficiency in sense of increased saturation solubility, improved dissolution rate, enhanced permeability and bioavailability of poorly water soluble drug.

4.3.8 References

- 1 Sigfridsson, K., Forssén, S., Holländer, P., Skantze, U. & de Verdier, J. A formulation comparison, using a solution and different nanosuspensions of a poorly soluble compound. *Eur J Pharm Biopharm.* **67**, 540-547 (2007).
- 2 Van Eerdenbrugh, B. *et al.* Characterization of physico-chemical properties and pharmaceutical performance of sucrose co-freeze-dried solid nanoparticulate powders of the anti-HIV agent loviride prepared by media milling. *Int J Pharm.* **338**, 198-206 (2007).
- 3 Ahuja, B. K., Jena, S. K., Paidi, S. K., Bagri, S. & Suresh, S. Formulation, optimization and in vitro-in vivo evaluation of febuxostat nanosuspension. *Int J Pharm* **478**, 540-552 (2015).
- 4 Kocbek, P., Baumgartner, S. & Kristl, J. Preparation and evaluation of nanosuspensions for enhancing the dissolution of poorly soluble drugs. *Int J Pharm* **312**, 179-186 (2006).
- 5 Ambrus, R. *et al.* Investigation of preparation parameters to improve the dissolution of poorly water-soluble meloxicam. *Int J Pharm* **381**, 153-159 (2009).
- 6 Miller, A. J. Selection of Subsets of Regression Variables. *J R Stat Soc Ser A-G* **147**, 389-425, (1984).
- 7 Wagner, J. M. & Shimshak, D. G. Stepwise selection of variables in data envelopment analysis: Procedures and managerial perspectives. *Eur J Oper Res* **180**, 57-67 (2007).
- 8 Kumar, A. & Sawant, K. K. Application of multiple regression analysis in optimization of anastrozole-loaded PLGA nanoparticles. *J Microencapsul* **31**, 105-114 (2014).
- 9 Gupta, P., Hung, C. & Lam, F. Factorial design based optimization of the formulation of albumin microspheres containing adriamycin. *J Microencapsul* **6**, 147-160 (1989).
- 10 Huang, Y.-B., Tsai, Y.-H., Lee, S.-H., Chang, J.-S. & Wu, P.-C. Optimization of pH-independent release of nifedipine hydrochloride extended-release matrix tablets using response surface methodology. *Int J Pharm.* **289**, 87-95 (2005).
- 11 Zhang, X. *et al.* Formulation optimization of dihydroartemisinin nanostructured lipid carrier using response surface methodology. *Powder technology* **197**, 120-128 (2010).
- 12 Bolton S & Bon C. *Pharmaceutical statistics: practical and clinical applications*. third edn, (Marcel Dekker Inc, 1997).
- 13 Zhang, Y. *et al.* DDSolver: An Add-In Program for Modeling and Comparison of Drug Dissolution Profiles. *The AAPS Journal* **12**, 263-271 (2010).
- 14 Tavelin, S. *et al.* Prediction of the oral absorption of low-permeability drugs using small intestine-like 2/4/A1 cell monolayers. *Pharm Res* **20**, 397-405 (2003).
- 15 Artursson, P. & Karlsson, J. Correlation between oral drug absorption in humans and apparent drug

- permeability coefficients in human intestinal epithelial (Caco-2) cells. *Biochem Biophys Res Commun.* **175**, 880-885 (1991).
- 16 Elsby, R., Surry, D., Smith, V. & Gray, A. Validation and application of Caco-2 assays for the in vitro evaluation of development candidate drugs as substrates or inhibitors of P-glycoprotein to support regulatory submissions. *Xenobiotica* **38**, 1140-1164 (2008).
 - 17 Matsson, P. *et al.* Exploring the role of different drug transport routes in permeability screening. *J Med Chem.* **48**, 604-613 (2005).
 - 18 Shin, S.-C., Bum, J.-P. & Choi, J.-S. Enhanced bioavailability by buccal administration of triamcinolone acetonide from the bioadhesive gels in rabbits. *Int J Pharm.* **209**, 37-43 (2000).
 - 19 Zhang, Y., Huo, M., Zhou, J. & Xie, S. PKSolver: An add-in program for pharmacokinetic and pharmacodynamic data analysis in Microsoft Excel. *Comput Meth Prog Biomed* **99**, 306-314 (2010).
 - 20 Liversidge, G. G. & Cundy, K. C. Particle size reduction for improvement of oral bioavailability of hydrophobic drugs: I. Absolute oral bioavailability of nanocrystalline danazol in beagle dogs. *Int J Pharm.* **125**, 91-97 (1995).
 - 21 Center for Drug Evaluation and Research-Center for Biologics Evaluation and Research. (U.S. Food and Drug Administration, Rockville, Maryland, USA, 2002).
 - 22 Reagan-Shaw S, Nihal M & Ahmad N. Dose translation from animal to human studies revisited. *The FASEB Journal*Life Sciences Forum* **22**, 659-661 (2007).
 - 23 Ali, H. S. M., York, P. & Blagden, N. Preparation of hydrocortisone nanosuspension through a bottom-up nanoprecipitation technique using microfluidic reactors. *Int J Pharm* **375**, 107-113 (2009).
 - 24 Patravale, V. B., Date, A. A. & Kulkarni, R. M. Nanosuspensions: a promising drug delivery strategy. *J Pharm Pharmacol* **56**, 827-840 (2004).
 - 25 Schmolka, I. R. Physical Basis for Poloxamer Interactions. *Annals of the New York Academy of Sciences* **720**, 92-97 (1994).
 - 26 <http://www.accessdata.fda.gov/scripts/cder/iig/getiigWEB.cfm>.
 - 27 Van Eerdenbrugh, B., Van den Mooter, G. & Augustijns, P. Top-down production of drug nanocrystals: Nanosuspension stabilization, miniaturization and transformation into solid products. *Int J Pharm* **364**, 64-75 (2008).
 - 28 Ganta, S., Paxton, J. W., Baguley, B. C. & Garg, S. Formulation and pharmacokinetic evaluation of an asulacrine nanocrystalline suspension for intravenous delivery. *Int J Pharm* **367**, 179-186 (2009).
 - 29 Mishra, P. R., Shaal, L. A., Müller, R. H. & Keck, C. M. Production and characterization of Hesperetin nanosuspensions for dermal delivery. *Int J Pharm* **371**, 182-189 (2009).
 - 30 Liu, P. *et al.* Nanosuspensions of poorly soluble drugs: Preparation and development by wet milling. *Int J Pharm* **411**, 215-222 (2011).
 - 31 Silva, L. D. *et al.* Elucidating the influence of praziquantel nanosuspensions on the in vivo metabolism of *Taenia crassiceps cysticerci*. *Acta Tropica* **161**, 100-105 (2016).
 - 32 Pireddu, R. *et al.* Diclofenac acid nanocrystals as an effective strategy to reduce in vivo skin inflammation by improving dermal drug bioavailability. *Coll Surf B: Biointerfaces* **143**, 64-70 (2016).
 - 33 Storm, G., Belliot, S. O., Daemen, T. & Lasic, D. D. Surface modification of nanoparticles to oppose uptake by the mononuclear phagocyte system. *Adv Drug Del Rev* **17**, 31-48 (1995).
 - 34 Moghimi, S. M., Muir, I. S., Illum, L., Davis, S. S. & Kolb-Bachofen, V. Coating particles with a block copolymer (poloxamine-908) suppresses opsonization but permits the activity of dysopsonins in the serum. *Biochimica et biophysica acta* **1179**, 157-165 (1993).
 - 35 Li, J.-T. & Caldwell, K. D. Plasma protein interactions with Pluronic™-treated colloids. *Colloids and Surfaces B: Biointerfaces* **7**, 9-22 (1996).
 - 36 Ganta, S. *Development and Evaluation of Nanoparticulate Drug Delivery Systems for Anticancer Drugs* PhD thesis, The University of Auckland, (2008).
 - 37 Adinarayana, K. & Ellaiah, P. Response surface optimization of the critical medium components for the production of alkaline protease by a newly isolated *Bacillus* sp. *J Pharm Pharma Sci* **5**, 272-278 (2002).
 - 38 Joyce, R. M. Experiment optimization in chemistry and chemical engineering, S. Akhnazarova and V.

- Kafarov, Mir Publishers, Moscow and Chicago, 1982, 312 pp. *J Polymer Sci: Poly Lett Edition* **22**, 372-372 (1984).
- 39 Montgomery, D. C. USING FRACTIONAL FACTORIAL DESIGNS FOR ROBUST PROCESS DEVELOPMENT. *Quality Engineering* **3**, 193-205 (1990).
- 40 George E P Box, J. S. H., William G Hunter *Statistics for Experimenters: Design, Innovation, and Discovery, 2nd Edition*. (John Wiley and Sons, 1978).
- 41 Abdelwahed, W., Degobert, G., Stainmesse, S. & Fessi, H. Freeze-drying of nanoparticles: formulation, process and storage considerations. *Adv Drug Deli Rev* **58**, 1688-1713 (2006).
- 42 Jackson, C. L. & McKenna, G. B. The melting behavior of organic materials confined in porous solids. *The J Chem Phy* **93**, 9002-9011 (1990).
- 43 Kumar, P., Mohan, C., KanamSrinivasan Uma Shankar, M. & Gulati, M. Physiochemical Characterization and Release Rate Studies of Solid Dispersions of Ketoconazole with Pluronic F127 and PVP K-30. *Iranian J Pharm Res : IJPR* **10**, 685-694 (2011).
- 44 Wang, Y. *et al.* Development and in vitro evaluation of deacety mycoepoxydiene nanosuspension. *Colloids and Surfaces B: Biointerfaces* **83**, 189-197 (2011).
- 45 Dodiya, S. S., Chavhan, S. S., Sawant, K. K. & Korde, A. G. Solid lipid nanoparticles and nanosuspension formulation of Saquinavir: preparation, characterization, pharmacokinetics and biodistribution studies. *J Microencap* **28**, 515-527 (2011).
- 46 Mosharraf, M. & Nyström, C. The effect of particle size and shape on the surface specific dissolution rate of microsized practically insoluble drugs. *Int J Pharm* **122**, 35-47 (1995).
- 47 Hintz, R. J. & Johnson, K. C. The effect of particle size distribution on dissolution rate and oral absorption. *Int J Pharm* **51**, 9-17 (1989).
- 48 Mukerjee, P. Thermodynamic aspects of solubility of small particles. *J Pharm Sci* **61**, 478-479 (1972).
- 49 Semete, B. *et al.* In vivo evaluation of the biodistribution and safety of PLGA nanoparticles as drug delivery systems. *Nanomed: Nanotech, Bio Med* **6**, 662-671 (2010).
- 50 Vera, K. *The impact of the interplay between nonionics and the cell membrane on the nanoparticle-cell association and stability of Caco-2 cells* PhD thesis, University of Vienna, (2010).
- 51 Hellung-Larsen, P., Assaad, F., Pankratova, S., Saietz, B. L. & Skovgaard, L. T. Effects of Pluronic F-68 on Tetrahymena cells: protection against chemical and physical stress and prolongation of survival under toxic conditions. *J Biotech* **76**, 185-195 (2000).
- 52 Batrakova, E. V., Han, H. Y., Alakhov, V., Miller, D. W. & Kabanov, A. V. Effects of pluronic block copolymers on drug absorption in Caco-2 cell monolayers. *Pharm Res* **15**, 850-855 (1998).
- 53 al-Rubeai, M., Emery, A. N., Chalder, S. & Goldman, M. H. A flow cytometric study of hydrodynamic damage to mammalian cells. *J Biotech* **31**, 161-177 (1993).
- 54 Ramirez, O. T. & Mutharasan, R. The role of the plasma membrane fluidity on the shear sensitivity of hybridomas grown under hydrodynamic stress. *Biotech Bioengg* **36**, 911-920 (1990).
- 55 Yee, S. In vitro permeability across Caco-2 cells (colonic) can predict in vivo (small intestinal) absorption in man--fact or myth. *Pharm Res* **14**, 763-766 (1997).
- 56 Xia, D. *et al.* Preparation of stable nitrendipine nanosuspensions using the precipitation-ultrasonication method for enhancement of dissolution and oral bioavailability. *Eur J Pharm Sci* **40**, 325-334 (2010).
- 57 Jinno, J.-i. *et al.* Effect of particle size reduction on dissolution and oral absorption of a poorly water-soluble drug, cilostazol, in beagle dogs. *J Control Release* **111**, 56-64 (2006).
- 58 Shegokar, R. & Muller, R. H. Nanocrystals: industrially feasible multifunctional formulation technology for poorly soluble actives. *Int J Pharm* **399**, 129-139 (2010).

5.4 Part-2: Formulation of Febuxostat inclusion complex with cyclodextrins

5.4.1 Introduction

The objective of this study was to develop and prepare a stable and efficient inclusion complex of poorly water soluble drug Febuxostat (FBX) with cyclodextrin and derivatives to enhance the solubility, dissolution and bioavailability of FBX. During development, the phase solubility study was carried out in order to investigate the effect of β -cyclodextrin, 2-hydroxypropyl- β - cyclodextrin, Methyl- β - cyclodextrin and γ -cyclodextrin on the solubility of FBX was studied in buffer solutions (pH-1.2 and pH-6.8) and water. The stability constants between FBX and cyclodextrins were calculated from the obtained phase solubility diagrams. The extent of inclusion of FBX in various cyclodextrins was evaluated by inclusion efficiency study. The Febuxostat/cyclodextrin inclusion complexes were prepared by physical mixing, kneading method and freeze drying method. The physicochemical characterization of prepared inclusion complexes was performed by Differential Scanning Calorimetry (DSC), X-ray Diffraction (XRD) and Fourier Transform Infrared (FTIR) spectroscopy. Dissolution studies were carried out in Distilled water, Phosphate Buffer pH-6.8, Acetate Buffer pH-4.5 and 0.1N HCl. The % content of FBX in FBX inclusion complexes was checked. Stability studies of prepared inclusion complexes were carried out at $5^{\circ}\text{C}\pm 3^{\circ}\text{C}$ (refrigerator) and at room temperature (RT) for a period of 6 months. *In-vitro* Cell Cytotoxicity Studies (MTT Assay) and *in-vitro* permeability assessment of FBX and its inclusion complex were performed using Caco-2 cell line model. Pharmacokinetic study was performed to evaluate the bioavailability and other pharmacokinetic parameters of FBX and its inclusion complex *in-vivo* animal model.

5.4.2 Preparation of Febuxostat inclusion complexes

The Cyclodextrins (CDs) used for the preparation of inclusion complexes were β -CD, HP- β -CD, M- β -CD and γ -CD. The FBX-CDs inclusion complexes were prepared in 1:1, 1:2 and 1:3 molar ratios by using two different methods (1) Kneading method and (2) Freeze drying method and compared with the Physical mixtures of CDs and FBX in the respective molar ratios.

5.4.2.1 Physical Mixture

The physical mixture was prepared by mixing of pulverized powder of FBX and selected CDs (β -CD, HP- β -CD, M- β -CD and γ -CD) in 1:1, 1:2 and 1:3 drug-CD molar ratios individually. The specified quantities of FBX and CD were accurately weighed

individually according to the molar ratio and transferred in a glass vial and sealed. The vial was shaken vigorously to mix the content completely. The mixture then passed through sieve (mesh # 100) and stored in dessicator containing activated silica gel until further evaluation.

5.4.2.2 Kneading Method

Inclusion complexes of FBX with various cyclodextrins (i.e. γ -CD, β -CD, HP- β -CD and M- β -CD) in different molar ratios like 1:1, 1:2 and 1:3 were prepared using Kneading method. First of all, a specified and accurately weighed quantity of cyclodextrin as per the pre-decided molar ratio was added to the mortar and small quantity of water was added while triturating to get slurry like consistency. Then accurately weighed quantity of FBX was slowly incorporated in the small parts into the slurry with continuous trituration. Trituration was continued for 1 hour. The viscosity of the mixture increased indicating the formation of the complex. Finally the mixture was dried in an oven at 45°C until dry. The mixture was ground to get a fine powder and passed through sieve (mesh # 100). All the prepared inclusion complexes were stored in dessicator containing activated silica until further evaluation.

5.4.2.3 Freeze drying method

Inclusion complexes of FBX with various cyclodextrins (i.e. γ -CD, β -CD, HP- β -CD and M- β -CD) in different molar ratios like 1:1, 1:2 and 1:3 were prepared using freeze drying method. In this method, the specified quantity of cyclodextrin (as per the FBX:CD molar ratio) was transferred in a glass vial containing 10 ml of distilled water and sonicated to dissolve. Then the corresponding quantity of FBX was added and stirred at a high speed magnetic stirrer for 24 hrs at 25°C. Afterwards, the mixture was centrifuged at 5000 rpm for 15mins and clear solution was separated. The obtained solution was freeze-dried immediately after preparation. The acquired solution was filled into glass vials and frozen at -70°C for 24 hr using an ultra cold deep freezer; later the samples were freeze-dried using a Lyophilizer (Heto Dry Winner, Germany) for 24 hr to yield dry powder.

5.4.3 Selection of Inclusion Complex

The best suitable carrier (i.e. CD) and FBX:CD molar ratio were selected on the basis of phase solubility experiment and inclusion efficiency.

5.4.3.1 Phase solubility Study

An excess amount of plain FBX (60mg) was introduced into several 15ml stoppered glass tubes and 5ml of aqueous vehicle of containing successively different concentrations (5-30mM/L) of the CDs (i.e. β -CD, HP- β -CD, M- β -CD and γ -CD) were added separately. The tubes were shaken for 48 hours at 80cycles/min at room temperature using Rotospin Test tube Rotator (Tarsons Products Pvt. Ltd. New Delhi, India). At equilibrium after 48 hours, aliquots were withdrawn, filtered with 0.45 μ m Nylon filters and suitably diluted, if needed. Concentrations of FBX in solutions were determined using UV spectrophotometer (UV-1700, Shimadzu, Japan) at 315nm (Refer Section 3.2.2). The phase solubility studies were further also carried out in HCl pH-1.2 and Phosphate buffer pH-6.8 instead of water.

The phase-solubility profiles were then constructed between the concentrations of FBX (at Y-axis) and different mM concentrations of CDs (i.e. β -CD, HP- β -CD, M- β -CD and γ -CD) at X-axis. The stability constants (K_s) were calculated and types of phase solubility graphs were predicted.

5.4.3.2 Inclusion efficiency estimation

All Freeze dried inclusion complexes, kneaded mixtures and physical mixtures of FBX with cyclodextrins (i.e. β -CD, HP- β -CD, M- β -CD and γ -CD) prepared in the selected molar ratios of FBX:CD (1:1, 1:2 and 1:3) were weighed accurately (50 mg) and transferred in 50 ml volumetric flasks individually. Added 30 mL of methanol, mixed thoroughly and sonicated for 10 min to dissolve the content at ambient temperature. The volume was made up to mark with methanol and resulting solution was suitably diluted with methanol for further analysis. Concentration of FBX in solutions was determined using UV spectrophotometer (UV-1700, Shimadzu, Japan) at 315nm (Refer Section 3.2.2). Inclusion efficiency was calculated.

5.4.4 Characterization of selected Inclusion complex

The Physical mixture, Kneaded mixture and Freeze dried solid of selected inclusion complex in defined molar ratio were further characterized for FTIR Spectroscopy, DSC Study and XRD analysis. The final product was analyzed for % drug content. The inclusion complex was subjected to *in-vitro* dissolution study and compared with marketed formulation (Febustat, Label claim-40mg) and plain FBX. Stability studies of lyophilized inclusion complex was performed. Comparative *in-vitro* cytotoxicity study (MTT Assay) and *in-vitro* permeability study of freeze dried inclusion complex and plain

FBX were carried out using Caco-2 cell lines. Finally, relative bioavailability of finalized inclusion complex was evaluated by comparing with bioavailabilities of plain FBX and marketed formulation.

5.4.4.1 FTIR Spectroscopy

The FTIR spectra for plain FBX, pure HP- β -CD, physical mixture of FBX:HP- β -CD, Kneaded mixture of FBX:HP- β -CD and freeze dried inclusion complexes of FBX:HP- β -CD in defined molar ratio were obtained using a Bruker ALPHA FT-IR spectrometer equipped with DTGS detector and OPUS/Mentor software (Bruker Optics, Germany). The samples were prepared in KBr disc (2 mg sample in 200 mg KBr). Data were collected over a spectral region from 4000 cm^{-1} to 600 cm^{-1} with resolution 4 cm^{-1} and 100 scans.

5.4.4.2 Differential Scanning Calorimetric (DSC) Analysis

The plain FBX, pure HP- β -CD, physical mixture of FBX:HP- β -CD, Kneaded mixture of FBX:HP- β -CD and freeze dried inclusion complexes of FBX:HP- β -CD in selected molar ratio were investigated for their thermal properties, physical state and recognition of inclusion complex using Differential Scanning Calorimeter (DSC 60-A, Shimadzu, Japan). When the drug molecules were encapsulated in CD cavity, their melting, boiling or sublimation points generally shifted to a different temperatures which indicate some interaction between host and guest molecule². Accurately weighed samples (4-7 mg) were placed in hermetically sealed aluminium pans and empty pan was used as a reference. Heating scans by heat runs for each sample was set from 30 $^{\circ}\text{C}$ to 300 $^{\circ}\text{C}$ at 10 $^{\circ}\text{C min}^{-1}$ in a nitrogen atmosphere.

5.4.4.3 Powder X-Ray Diffraction (XRD) Study

The XRD spectra of plain FBX, pure HP- β -CD, physical mixture of FBX:HP- β -CD, Kneaded mixture of FBX:HP- β -CD and freeze dried inclusion complexes of FBX:HP- β -CD in selected molar ratio were obtained using X-Ray Diffractometer (X-Pert-PRO, PANalytical, Netherland). The samples were mounted on a sample holder and XRD patterns were recorded in the range of $3^{\circ} < 2\theta < 50^{\circ}$ at the speed of 5 $^{\circ} \text{min}^{-1}$.

5.4.4.4 Percentage drug content in lyophilized inclusion complex

Accurately weighed lyophilized powder of FBX:HP- β -CD inclusion complex in selected molar ratio (equivalent to 25 mg of FBX) was transferred in a 25 ml volumetric flask and 15 ml methanol was added. Content was sonicated to dissolve and volume was made up to the mark with methanol. The sample solution was centrifuged at 15,000 rpm for 10

minutes (Sigma centrifuge, Osterode, Germany) and supernatant was filtered with 0.22 μm pore size disposable filter (Millipore India, Bangalore). Filtrate was suitably diluted with diluent to get the sample concentration at 20 $\mu\text{g}/\text{ml}$. Standard solution of FBX (20 $\mu\text{g}/\text{ml}$) was also prepared and both the solutions were injected into the HPLC system (Shimadzu, Japan). (For instrumentation, chromatographic conditions and method refer Section 3.2.3) Each determination was performed in triplicate, chromatograms were recorded and average % content of FBX in the formulation and standard deviation was calculated.

5.4.4.5 *In vitro* dissolution study

In vitro release studies of lyophilized powder of FBX:HP- β -CD inclusion complex in selected molar ratio, marketed formulation (Febustat, Label claim-40mg) and plain FBX were carried out in different dissolution mediums (i.e. Distilled water, Phosphate Buffer pH-6.8, Acetate Buffer pH-4.5 and 0.1N HCl) using USP dissolution apparatus II (paddle method).

Dissolution studies were carried out using clear hard gelatin capsules (Size 0) filled with an accurately weighed quantity of lyophilized FBX:HP- β -CD inclusion complex or plain FBX (FBX-P) (equivalent to 40 mg of FBX). The experiments were performed on 900mL media at $37^{\circ}\text{C}\pm 0.5^{\circ}\text{C}$ at a rotation speed of 75 rpm. At preselected time intervals, 5 mL samples were withdrawn, filtered immediately and replaced with 5 mL of pre-thermostated fresh dissolution medium. Quantitative determination was performed by UV spectrophotometer at 315 nm. Dissolution tests were performed in triplicate and graph of percent cumulative drug release vs time was plotted. Dissolution profiles were further evaluated on the basis of Dissolution efficiency (DE), Dissolution percentage at 5 min and 60 min (DP_5 and DP_{60}), time required to release 50% and 90% of drug (t_{50} and t_{90}), Correlation coefficient (r^2), Mean dissolution time (MDT) and Area under curve (AUC). The DDSolver, an Excel add-in software package, which is designed to analyze data obtained from dissolution experiments was used to calculate different dissolution parameters³.

5.4.4.6 Stability Studies

Stability studies of lyophilized FBX:HP- β -CD inclusion complex in selected molar ratio was carried out at $5^{\circ}\text{C}\pm 3^{\circ}\text{C}$ (refrigerator) and at room temperature (RT) for a period of 6 months. Periodically, samples were withdrawn at 1st, 3rd and 6th month and subjected to examine for chemical stability. Chemical stability was checked by assessing the

percentage content of FBX in stored formulations.

5.4.5 Cell Line Studies of FBX and its Inclusion complex with HP- β -CD using Caco-2 cell line model

In the present research scenario, *in-vitro* cytotoxicity study and permeability assessment using Caco-2 cell line, are essential experiment for the drug development and discovery. Caco-2 cell lines have been extensively used for such types of experiments due to their wide acceptability and applicability. In this section, we studied the cytotoxicity and intestinal permeability of developed FBX: HP- β -CD inclusion complex and plain FBX, using Caco-2 cell lines as best fitted model.

5.4.5.1 Cell Culture

Same as described in Section 4.6.1.

5.4.5.2 *In vitro* Cell Cytotoxicity Studies (MTT Assay)

Experiment

MTT stock solution (1 mg/ml) was prepared by dissolving accurately weighed 10 mg of MTT reagent powder with 10 ml phosphate buffered saline (PBS) in an amber colored 10 ml volumetric flask. The stock solution was stored in dark place at 4°C till the further use.

The *in vitro* cytotoxicity of lyophilized FBX:HP- β -CD inclusion complex and plain FBX was evaluated for Caco-2 cells using MTT assay. The cells were cultured in 96-well plates (prelabelled as 4 hour, 24 hour and 48 hour) at a seeding density of 1.0×10^4 cells/well for 48 hours. Samples were dissolved in DMSO and different dilutions were made with DMEM culture medium so that the concentration of DMSO did not exceed more than 1% v/v in any diluted sample. Experiments were initiated by replacing the culture medium in each of 96 well of each plate with 100 μ l of sample solutions (0.1, 1, 10, 100, 250, 500 & 1000 μ g/ml) and incubated at 37°C in ~85% relative humidity and ~5% CO₂ environment. After 4 hour of incubation, prelabelled 4 hour-96 well plate was removed from incubator into laminar flow hood area, sample solution was discarded and 100 μ l of MTT reagent (1 mg/ml) in phosphate buffered saline (PBS) was added aseptically. The plate was again incubated at 37°C in ~5% CO₂ environment for another 4 hours. At the end of incubation period, medium was removed carefully and intracellular formazan was solubilized with 100 μ l DMSO by agitating cells on orbital shaker for 15 mins. Absorbance was measured at 590 nm with a reference filter of 620 nm using Micro plate multi detection instrument (680-XR, Bio-Rad Laboratories,

France). The medium treated cells were used as controls. Same procedure was followed for 24 hour and 48 hour plates.

Statistical analysis

All calculations, graph preparations and statistical analysis were performed using Microsoft Excel. Percentage of cell viability was calculated based on the absorbance measured relative to the absorbance of cells exposed to the negative control. To compare the sensitivity of cells to the FBX and its formulation, IC₅₀ values (concentration of the drug that leads to 50% inhibition in cell proliferation) were calculated.

5.4.5.3 *In vitro* assessment of permeability using Caco-2 cell line model

Among the various techniques available for the prediction of intestinal permeability, the Caco-2 cell lines has been widely used and referred as identical model of the intestinal barrier^{4,5}. These human cells are capable to grow into differentiated monolayers with well established tight junctions and brush border membrane as well as to express several membrane transporters and metabolizing enzymes, allowing the measurement of functional permeability (both passive diffusion and active transport)^{6,7}. As a result, this assay is widely accepted by both the pharmaceutical industry and regulatory bodies as the permeability determined using Caco-2 cell lines associates well with oral absorption in humans⁸⁻¹⁰.

Experiment

Caco-2 cell passage 40-45 cultured in 12 well cell culture inserts (pore size-0.4 μ m, diameter-12/18 mm, area-1.13 cm², Product code 12565009, NUNC™, Roskilde, Denmark), were used for *in vitro* permeability assessment of lyophilized FBX:HP- β -CD inclusion complex and plain FBX after 21 days post seeding. Prior to the experiment, the inserts were washed twice and equilibrated for 30 mins with pre-warmed transport medium (Hank's balanced salt solution-HBSS containing 25 mM of HEPES, pH-7.4). Samples were dissolved in DMSO and diluted with transport medium so that the concentration of DMSO did not exceed more than 1% v/v in any diluted sample (250 μ g/ml). The integrity of the monolayers were checked by monitoring the permeability of paracellular leakage marker (Lucifer Yellow) across the monolayer. Quantification of Lucifer yellow was performed using a Spectrofluorimeter using excitation wavelength at 485 nm and emission wavelength at 530 nm. The cell monolayers were considered tight enough for the transport experiment enough when the apparent permeability

coefficient (P_{app}) for Lucifer Yellow was less than 0.5×10^{-6} cm/s. All Transport studies were conducted aseptically at 37°C in an atmosphere of $\sim 85\%$ relative humidity and $\sim 5\%$ CO_2 . The $150 \mu\text{l}$ of transport buffer containing $250 \mu\text{g/ml}$ test compounds was added to the apical side while the basolateral side of the inserts contained 1.5 ml of transport medium. After the incubation 30, 60, 120, 180, 240 and 480 mins, aliquot of $100 \mu\text{l}$ was withdrawn from the receiver chamber and was immediately replenished with an equal volume of pre-warmed transport medium. The samples were stored at -20°C until analyzed. The concentration of the test compounds in the transport medium were analyzed using developed RP-HPLC method as described in Section 3.1.4. The apical to basolateral permeability coefficient (P_{app} in cm/sec) was calculated according to following equation:

$$P_{app} = \frac{dQ/dt}{A \times C_0 \times 60}$$

where, dQ/dt (flux) is the amount of drug transported across the monolayer from apical to basolateral compartment as a function of time (mg/min), A is the monolayer membrane surface area (cm^2) and C_0 is the initial concentration of drug on the apical compartment (mg/ml).

5.4.6 Pharmacokinetic evaluation of lyophilized FBX:HP- β -CD inclusion complex using *in vivo* animal model

In this study, pharmacokinetic behaviors of the prepared lyophilized FBX:HP- β -CD inclusion complex, plain FBX and marketed formulation were investigated to know the effect of complexation of FBX with HP- β -CD on oral bioavailability of FBX. The plots of drug plasma concentration vs time were plotted for FBX after oral administration of lyophilized inclusion complex and compared it with plain FBX and marketed formulation (Febustat). Non compartmental pharmacokinetic analysis was performed¹¹. Various pharmacokinetic parameters were calculated using the computer based statistical package PKsolver add-in for microsoft excel¹². The calculated parameters are Maximum plasma concentration (C_{max}), Time to achieve maximum plasma concentration (T_{max}), Area under the plasma concentration-time curve from time zero to t (AUC_{0-t}), Elimination rate constant ($-K_{elimination}$), Elimination half life ($t_{1/2}$), Area under the plasma concentration-time curve from time zero to infinity ($\text{AUC}_{0-\infty}$), Area under momentum curve (AUMC), Mean residence time (MRT) and Relative bioavailability (%F)¹³.

5.4.6.1 Animals:

Same as described in Section 4.3.5.1.

5.4.6.2 Experimental: Dosing and sampling

Relative bioavailability of lyophilized FBX:HP- β -CD inclusion complex was evaluated by comparing with bioavailabilities of plain FBX and marketed formulation.

The maximum dose of FBX that can be given to a adult human in a single day is 40 mg. So according to the section 4.3.5.2 , the dose of FBX for rabbits was calculated to be 2.05 mg/kg. In this study, the FBX dose given to the rabbits is 3.70 mg/1.8 kg rabbit weight^{14,15}.

Animals were divided in three treatment groups and each group contained 3 rabbits. The animals were fasted over night prior to the experiment with free access of water. The FBX-NS, plain FBX and marketed formulation (equivalent to 3.70 mg of FBX) were filled in hard gelatin capsule (Capsugel®#size 5) and administered orally. Blood samples (1.0 ml) were collected through marginal ear vein using fresh sterilized disposable needles and syringes in heparinized tubes at 0, 0.25, 0.50, 0.75, 1.0, 1.5, 2, 3, 4, 6, 8, 12, 24 and 48 hours after administration. Collected blood samples were vortexed for 1 min and centrifuged at 20,000 rpm for 10 mins at 4°C (Ultra-centrifuge, 3K 30 Sigma Laboratory Centrifuge, Osterode, Germany). Separated plasma samples were withdrawn and stored at -20°C until further processing.

5.4.6.3 Instrumental and statistical analysis

Collected plasma samples were extracted and analyzed by using developed RP-HPLC method (Chapter 3, Section 3.2.5). The drug plasma concentrations were determined from the calibration curve. Non-compartmental trapezoidal method was employed to calculate the area under the curve (AUC) of plasma concentration as a function of time (t). All data were reported as mean \pm SD. The statistical significance of the differences between the groups was tested by one-way ANOVA followed by Bonferroni multiple comparison test.

5.4.7 Result and Discussion

5.4.7.1 Selection of Inclusion complex

5.4.7.1.1 Phase solubility Analysis

Phase solubility analysis has been the very important and initial requirement for optimizing the development process of an inclusion complex of a drug as it allows the assessment of affinity between CD and drug molecule in aqueous phase. Phase solubility

study provides the stability constant for drug-cyclodextrin inclusion complex as well as it also present the insight into stoichiometry of the complex at equilibrium¹⁶.

The phase-solubility profiles were constructed between the apparent equilibrium concentrations of FBX (at Y-axis) and defined concentrations of CDs (i.e. β -CD, HP- β -CD, M- β -CD and γ -CD) at X-axis in water, phosphate buffer pH-6.8 and HCl pH-1.2 as shown in the Fig 5.19, 5.20 and 5.21 respectively. The slopes, intercepts, R^2 and calculated stability constants (K_s) were tabulated and types of phase solubility graphs were predicted (Table 5.22).

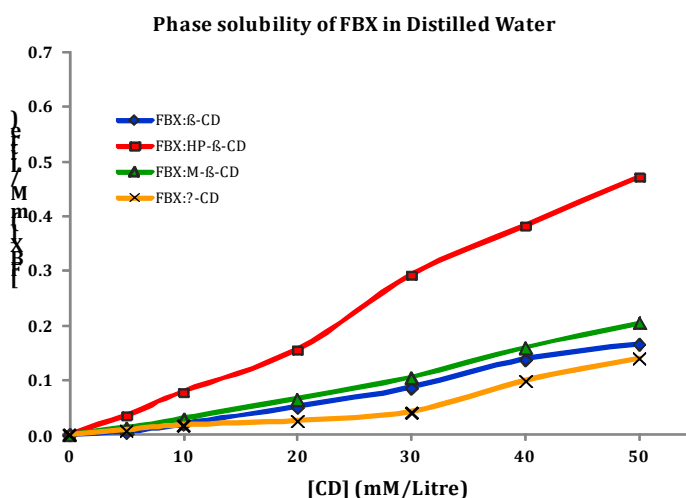


Fig. 5.19 Phase solubility studies of FBX with CDs in distilled water.

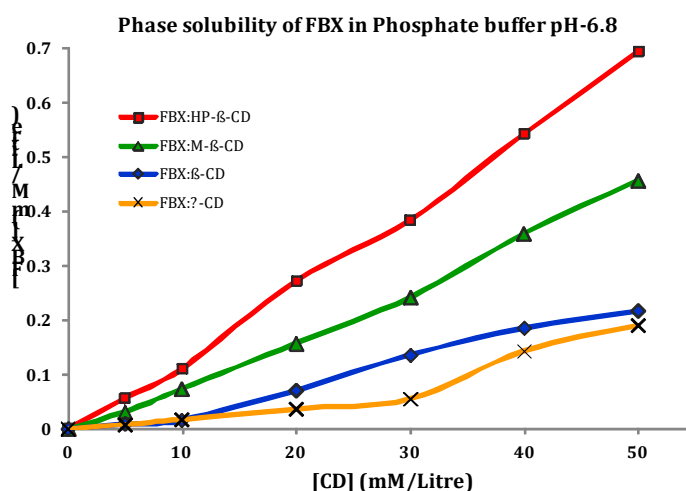


Fig. 5.20 Phase solubility studies of FBX with CDs in Phosphate Buffer pH6.8.

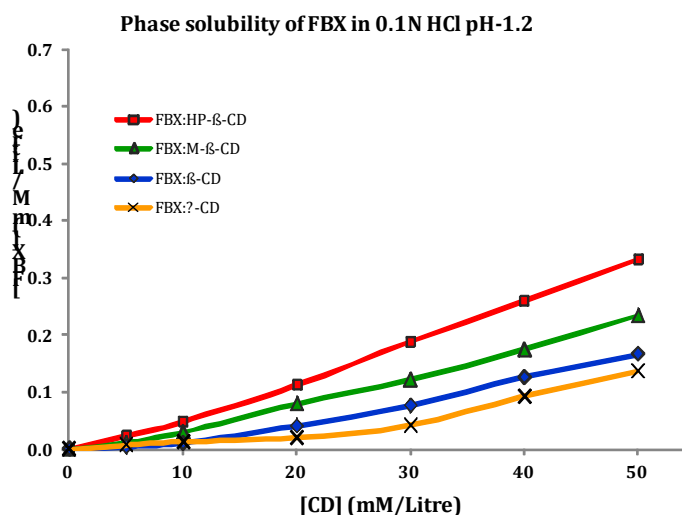


Fig. 5.21 Phase solubility studies of FBX with CDs in 0.1N HCl pH-1.2.

Table 5.22 Comparison of slopes, intercepts, R^2 and K_S of phase solubility studies in water, phosphate buffer pH-6.8 and HCl pH-1.2 for FBX with CDs.

Drug:CD	Slope	Intercept	R^2	K_S (M^{-1})	Type of Graph
In Distilled Water*					
FBX: HP-β-CD	0.009±0.003	0.013±0.001	0.994±0.006	736.5±12.3	A_L -Type
FBX: M-β-CD	0.004±0.001	0.010±0.002	0.991±0.007	439.4±6.8	A_L -Type
FBX: β-CD	0.004±0.001	0.011±0.003	0.986±0.009	308.1±5.7	A_L -Type
FBX: γ-CD	0.002±0.001	0.012±0.002	0.906±0.012	193.7±7.7	A_L -Type
In Phosphate Buffer, pH-6.8*					
FBX: HP-β-CD	0.014±0.001	0.014±0.001	0.998±0.007	985.7±9.2	A_L -Type
FBX: M-β-CD	0.009±0.002	0.016±0.001	0.995±0.003	592.2±14.5	A_L -Type
FBX: β-CD	0.005±0.001	0.015±0.001	0.983±0.008	323.4±7.1	A_L -Type
FBX: γ-CD	0.004±0.001	0.019±0.002	0.909±0.004	194.4±5.7	A_L -Type
In HCl pH-1.2*					
FBX: HP-β-CD	0.007±0.001	0.012±0.002	0.996±0.008	543.9±6.5	A_L -Type
FBX: M-β-CD	0.005±0.001	0.011±0.002	0.992±0.006	403.6±5.8	A_L -Type
FBX: β-CD	0.003±0.001	0.016±0.002	0.972±0.005	220.1±7.6	A_L -Type
FBX: γ-CD	0.003±0.001	0.014±0.001	0.903±0.009	188.9±10.3	A_L -Type

* Data are shown as Mean±SD, n=3

The results indicated that the low solubility of FBX was increased linearly with all the CDs in all the mediums and the value of K_S for inclusion complex increased in the order of (FBX:HP-β-CD)>(FBX:M-β-CD)>(FBX:β-CD)>(FBX:γ-CD). The smaller values of K_S (less than 200 M^{-1}) indicate a weak interaction between drug and CD, while larger values of K_S (more than 1000 M^{-1}) are symptomatic of an incompatible drug release from the inclusion complex¹⁷. The inclusion of FBX with HP-β-CD showed highest value of K_S compared to other FBX:CD complexes which indicated that FBX form sufficiently stable and efficient inclusion complex with HP-β-CD. It was also observed that K_S values

were found highest in phosphate buffer pH-6.8. This may be due to acidic nature of FBX which was completely unionized at this pH and lead to formation of a stable complex with HP- β -CD. The pH value has significant influence on the interaction mode between drug and CDs, indicating the different affinity of acidic, neutral and basic drugs for the inclusion complex formation and additionally the increase in drug ionization at particular pH resulted in decrease of the complex stability constant^{18,19}. The linear increase in solubility of FBX with increase in CDs concentration gave rise to A_L -type phase solubility diagram at different pH values. The R^2 values were also increased in the order of (FBX:HP- β -CD)>(FBX:M- β -CD)>(FBX: β -CD)>(FBX: γ -CD). On the basis of phase solubility study, it can be concluded that FBX:HP- β -CD formed most stable inclusion complex with highest solubility, among the four.

5.4.7.1.2 Inclusion efficiency estimation

Inclusion efficiencies of all Freeze dried inclusion complexes, kneaded mixtures and physical mixtures of FBX with cyclodextrins (i.e. β -CD, HP- β -CD, M- β -CD and γ -CD) in the selected molar ratios of FBX:CD (1:1, 1:2 and 1:3) were determined and results were presented in Table 5.23. The results clearly showed that the %IE of FBX: HP- β -CD inclusion complex at all the molar ratios were found higher for physical mixture (61.25-63.08%), kneaded mixture (75.69-77.32%) and freeze dried inclusion complex (98.95-99.78%) than the other inclusion complexes prepared by respective mode of preparation. It indicated that FBX was uniformly distributed in FBX:HP- β -CD inclusion complex at all molar ratios while others did not show satisfactory drug incorporation. Results also showed that there are minor differences in the inclusion efficiencies of FBX:HP- β -CD at all the three molar ratios in physical mixtures, kneaded mixture and freeze dried inclusion complex, respectively which described that FBX:HP- β -CD in the molar ratio of 1:1 is sufficient to produce an efficient inclusion complex.

Table 5.23 Inclusion efficiency values of all Freeze dried inclusion complexes, kneaded mixtures and physical mixtures of FBX with cyclodextrins (β -CD, HP- β -CD, M- β -CD and γ -CD) in 1:1, 1:2 and 1:3 molar ratios of FBX:CD.

FBX:CD	% Inclusion Efficiency (% IE)*		
	Molar ratio (1:1)	Molar ratio (1:2)	Molar ratio (1:3)
Physical Mixtures			
FBX: HP- β -CD	62.66 \pm 2.54	61.25 \pm 3.14	63.08 \pm 2.35
FBX: M- β -CD	42.35 \pm 1.82	44.85 \pm 1.86	41.96 \pm 2.32
FBX: β -CD	29.23 \pm 3.24	28.36 \pm 2.53	30.96 \pm 1.42
FBX: γ -CD	22.34 \pm 1.72	21.66 \pm 2.09	22.98 \pm 1.54
Kneaded Mixtures			
FBX: HP- β -CD	76.89 \pm 3.68	77.32 \pm 3.12	75.69 \pm 3.21
FBX: M- β -CD	59.31 \pm 2.07	57.29 \pm 1.86	58.37 \pm 1.53
FBX: β -CD	36.85 \pm 2.75	35.57 \pm 1.38	39.24 \pm 1.01
FBX: γ -CD	30.56 \pm 1.63	31.69 \pm 2.01	35.26 \pm 2.60
Freeze dried inclusion complex			
FBX: HP- β -CD	99.78 \pm 3.08	99.95 \pm 3.12	99.06 \pm 1.05
FBX: M- β -CD	80.12 \pm 2.71	79.54 \pm 2.34	81.21 \pm 2.32
FBX: β -CD	59.28 \pm 3.85	60.29 \pm 1.36	60.56 \pm 0.98
FBX: γ -CD	49.63 \pm 1.96	48.82 \pm 2.52	50.75 \pm 1.56

* Data are shown as Mean \pm SD, n=3

Based on the results obtained from phase solubility studies and inclusion efficiency estimation, FBX: HP- β -CD in the molar ratio of 1:1 was selected as best suitable inclusion complex for further studies due to its superior solubilizing capacity and greater inclusion efficiency. Moreover, earlier reports suggest that the modified β -cyclodextrins (HP- β -CD) have enormous applicability in development of solid oral dosage forms due to their higher complexation efficiency and lower cytotoxicity than the β -cyclodextrin²⁰⁻²³.

5.4.7.2 Characterization of selected Inclusion complex

5.4.7.2.1 FTIR Spectroscopy

The FTIR Spectroscopy of Plain FBX, pure HP- β -CD, physical mixture, kneaded mixture and freeze dried inclusion complex for FBX: HP- β -CD::(1:1)M was carried out and result had been represented in Fig. 5.22.

The IR studies of FBX exhibited peaks at 3449.63 cm^{-1} and 3122.19 cm^{-1} were due to alcohol/phenol O-H stretching whereas peaks at 2653.74 cm^{-1} and 2547.89 cm^{-1} were due to carboxylic acid O-H stretch. Peaks observed at 2963.97 cm^{-1} , 2939.46 cm^{-1} and 2876.52 cm^{-1} were pointing towards alkyl C-H stretch. Peak observed at 2231.57 cm^{-1} was due to nitrile $\text{C}\equiv\text{N}$ stretch. Peaks at 1678.26 cm^{-1} , 1605.91 cm^{-1} and 1276.79 cm^{-1}

were due to aryl carboxylic acid C=O stretching, C=C stretching of ring and C-O-C stretching of ether group, respectively. Aromatic bending was observed from 763.90 cm^{-1} . These bands confirmed the structure of FBX. However, the FTIR spectra of HP- β -CD showed a large and broad band at 3381.51 cm^{-1} corresponding to absorption by hydrogen bonded O-H groups.

The IR spectrum of physical mixture of FBX:HP- β -CD::1:1M had shown peaks at 1677.39 cm^{-1} , 1605.62 cm^{-1} and 1276.50 cm^{-1} were due to C=O stretching of carboxylic group, C=C stretching of ring and C-O-C stretching of ether group, respectively. The intense appearance and little shifting of these peaks indicate weak interaction between drug and excipient.

The IR spectrum of kneaded mixture of FBX:HP- β -CD::1:1M had shown peaks at 1677.97 cm^{-1} , 1606.28 cm^{-1} and 1278.05 cm^{-1} were due to C=O stretching of carboxylic group, C=C stretching of ring and C-O-C stretching of ether group, respectively. The intense appearance and little shifting of these peaks indicate weak interaction between drug and excipients but more than the physical mixture. Whereas in the IR spectrum of freeze dried inclusion complex of FBX:HP- β -CD::1:1M, all the characteristic peaks of FBX disappeared which indicate a good inclusion and interaction of FBX within the cavity of HP- β -CD at the selected molar ratio. Moreover this study also proved the efficiency of selected method of preparation.

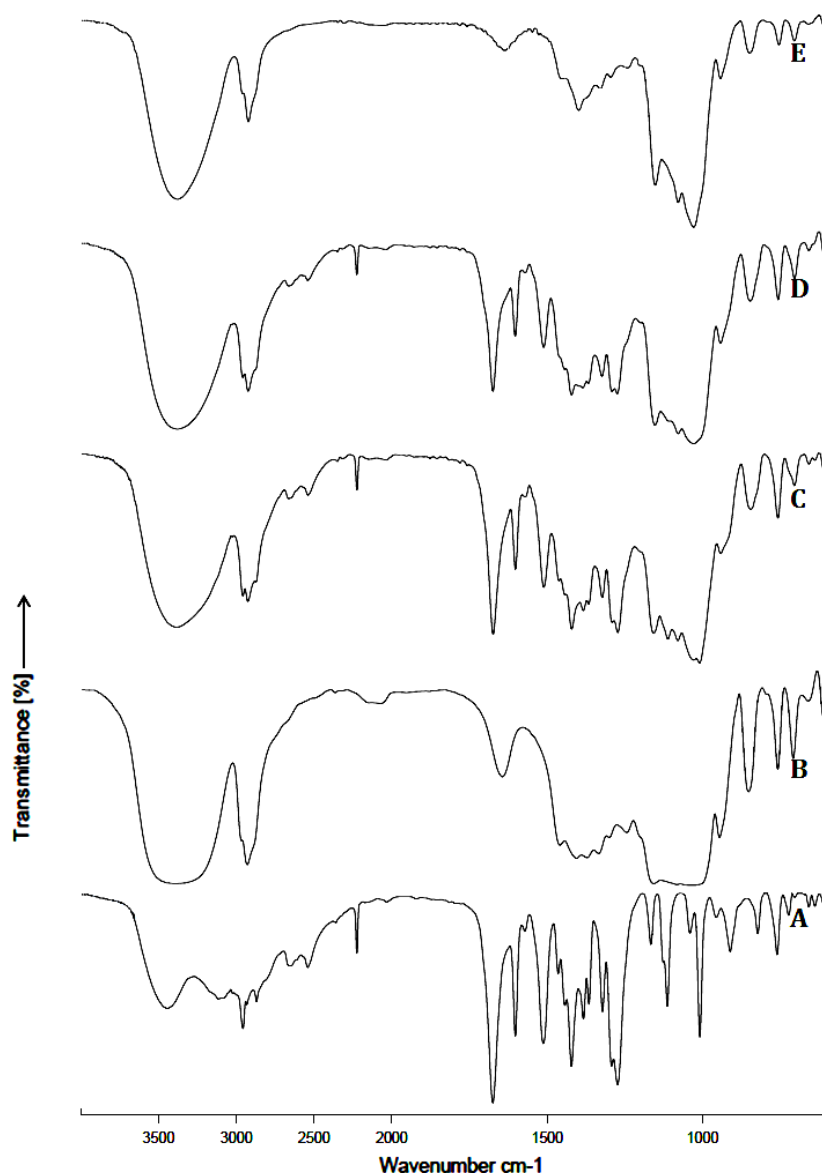


Fig. 5.22 IR spectrums of (A) Plain FBX, (B) HP-β-CD, (C) Physical Mixture for FBX: HP-β-CD::(1:1)M, (D) Kneaded Mixture for FBX: HP-β-CD::(1:1)M and (E) Freeze dried inclusion complex of FBX: HP-β-CD::(1:1)M.

5.4.7.2.2 Differential Scanning Calorimetric (DSC) Analysis

The thermal analysis of plain FBX, pure HP-β-CD, physical mixture, kneaded mixture and freeze dried inclusion complex for FBX: HP-β-CD::(1:1)M was performed using Differential Scanning Calorimetry (DSC) in order to confirm the formation of solid inclusion complexes (Fig. 5.23). When guest molecules are incorporated in the cyclodextrin cavity or in the crystal lattice, their melting, boiling and sublimation points usually shifted to a different temperature or disappear within the temperature range, where the cyclodextrin lattice is decomposed.

The DSC thermogram of FBX showed a sharp endothermic peak for at 209.4°C corresponding to its melting point. The DSC thermogram of HP-β-CD exhibited a broad endothermic peak at 88.7°C which corresponded to the loss of hydration water of the material. The HP-β-CD decomposed at the temperature of 300°C hence not showing any melting peak of HP-β-CD in between 30°C to 300°C.

In the DSC thermogram of physical mixture and kneaded mixture of FBX:HP-β-CD::1:1 molar ratio showed two endothermic peaks, corresponding to HP-β-CD and FBX indicated that inclusion of drug within CD cavity was not sufficiently achieved. The occurrence of FBX peak also reflected the existence of few FBX crystals in the preparations.

The DSC thermogram of freeze dried inclusion complex of FBX:HP-β-CD::1:1M had shown an endothermic peak for HP-β-CD but the disappearance of characteristic endothermic peak due to FBX with this system, clearly indicated the formation of true inclusion complex. The absence of FBX peak might also be attributed to the amorphous form of the drug in the complex formation. On the basis of results, it can be concluded that preparation of inclusion complex followed by freeze drying was the best suitable method for formation of inclusion complex of FBX.

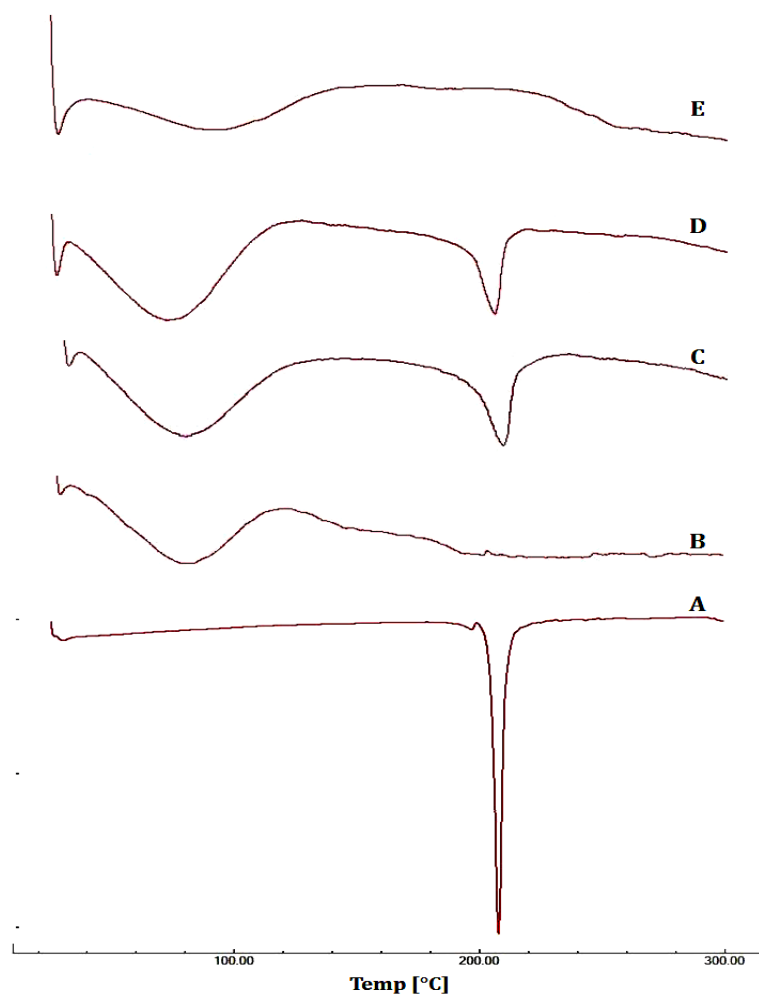


Fig. 5.23 DSC thermograms of (A) Plain FBX, (B) HP-β-CD, (C) Physical Mixture for FBX: HP-β-CD::(1:1)M, (D) Kneaded Mixture for FBX: HP-β-CD::(1:1)M and (E) Freeze dried inclusion complex of FBX: HP-β-CD::(1:1)M.

5.4.7.2.3 Powder X-Ray Diffraction (XRD) Study

The Powder X-Ray Diffraction (XRD) Study of Plain FBX, pure HP-β-CD, physical mixture, kneaded mixture and freeze dried inclusion complex for FBX: HP-β-CD::(1:1)M was carried out and result had been represented in Fig. 5.24.

XRD study was carried out to investigate the crystalline state of drug which is influencing the dissolution and stability behaviour of compound. The preservation of the crystal structure of the drug in the formulation is crucial for the sustained stability of the drug during its shelf-life. The peak position (diffraction angle) is an identification tool of a crystal structure, whereas the number of peaks is a measure of sample crystallinity in a diffractogram²⁴. The development of an amorphous form confirmed that the drug was dispersed completely in a molecular state with cyclodextrin. It had been investigated by several researchers that the occurrence of a difused diffraction

pattern, appearance of new peaks and elimination of characteristic peaks of the guest/drug molecule, evident for the formation of an inclusion complex of drug with cyclodextrins²⁵⁻²⁸.

The XRD pattern of pure FBX exhibited various diffraction peaks at 7.2, 12.8, 25.8 and 26.1°2 θ indicating the crystalline nature of drug. No diffraction peaks were observed in the diffractogram of HP- β -CD, showed the amorphous form of HP- β -CD. The XRD patterns of physical mixture and kneaded mixture showed sufficiently visible characteristic peaks of FBX, pointing toward the insufficient inclusion or lack of inclusion of FBX in HP- β -CD. The XRD of freeze dried inclusion complex of FBX: HP- β -CD::(1:1)M showed a halo pattern, with the disappearance of all characteristic peaks of FBX which indicated the complete incorporation of FBX in HP- β -CD cavity and formation of complete and stable inclusion complex. The results obtained from XRD analysis were in good agreement with DSC observations.

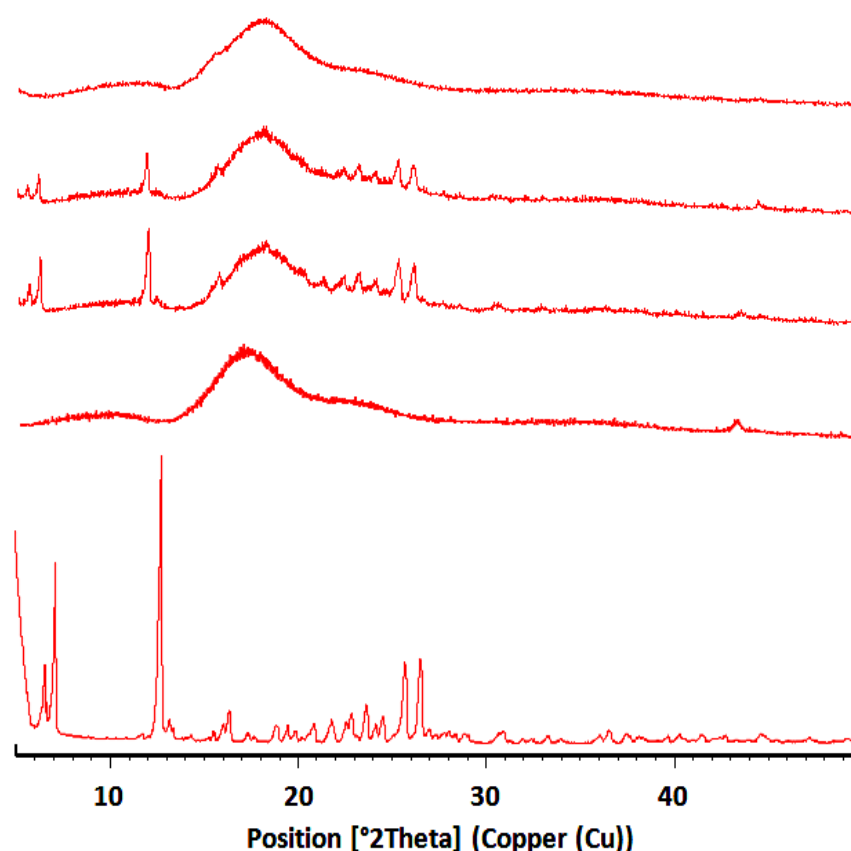


Fig. 5.24 XRD patterns of (A) Plain FBX, (B) HP- β -CD, (C) Physical Mixture for FBX: HP- β -CD::(1:1)M, (D) Kneaded Mixture for FBX: HP- β -CD::(1:1)M and (E) Freeze dried inclusion complex of FBX: HP- β -CD::(1:1)M.

5.4.7.2.4 Percentage FBX content in lyophilized inclusion complex of FBX: HP- β -CD

Percentage FBX content in lyophilized inclusion complex of FBX:HP- β -CD in (1:1) molar ratio was found to be $99.84 \pm 1.28\%$, indicating the suitability of freeze drying method for production of inclusion complex.

5.4.7.2.5 *In vitro* dissolution study

The dissolution profiles for the plain FBX (FBX-P) marketed formulation (FBX-M) and Freeze dried inclusion complex of FBX:HP- β -CD:(1:1)M (FBX-IC) in phosphate buffer pH-6.8 (PB), acetate buffer pH-4.5 (AB), 0.1N HCl and water are presented in Fig. 5.25. The values reported in Table 5.24 and 5.25 are arithmetic means of 3 determinations. It was evident from the data that optimized inclusion complex of FBX-IC served better dissolution profile and drug release than the FBX-P and FBX-M in all the dissolution mediums. The FBX-P and FBX-M did not achieve complete dissolution during 120 min time period and only 9.6-55.4% and 21.6-72.9% of the FBX dissolved over the test period of 120 mins, respectively, in all the dissolution mediums. This may be due to large crystal size of FBX in API and marketed formulation. The FBX-IC showed 46.2-99.9% drug dissolved with significantly enhanced dissolution rate over the time period of 120 mins, in all the selected dissolution mediums. The significant improvement in dissolution characters of inclusion complexes may be due to the formation of readily soluble inclusion complex in the dissolution medium, increased drug particle wettability and reduction of the crystallinity of the drug product.

The Dissolution efficiency (DE), Dissolution percentage at 5 min and 60 min (DP₅ and DP₆₀) and Area under curve (AUC) values were increased in the following order: FBX-P < FBX-M < FBX-IC; while time required to release 50% and 90% of drug (t₅₀ and t₉₀) and mean dissolution time (MDT) were increased in vice versa i.e. FBX-P > FBX-M > FBX-IC. The t₅₀ and t₉₀ for FBX-IC were significantly reduced to 7.9-10.8 mins and 26.6-28.7 mins respectively as compared to FBX-M and FBX-P in phosphate buffer pH-6.8 and water whereas t₅₀ and t₉₀ for FBX-P, FBX-M and FBX-IC were found more than 60 mins in acetate buffer and HCl media (except for FBX-IC in acetate buffer). This may be due to acidic nature of FBX which was completely unionized at this pH.

All the results indicated that the FBX-IC prepared by freeze drying technique was having superior characteristics to plain drug and marketed formulation, indicating a major prospect to enhance the bioavailability of such drugs by inclusion complexation for oral

administration where solubility and dissolution are rate limiting factors in bioavailability in the body. Thus inclusion complexation of poor soluble drug with hydrophilic cyclodextrin is an effective and successful technique in order to improve their biopharmaceutical properties.

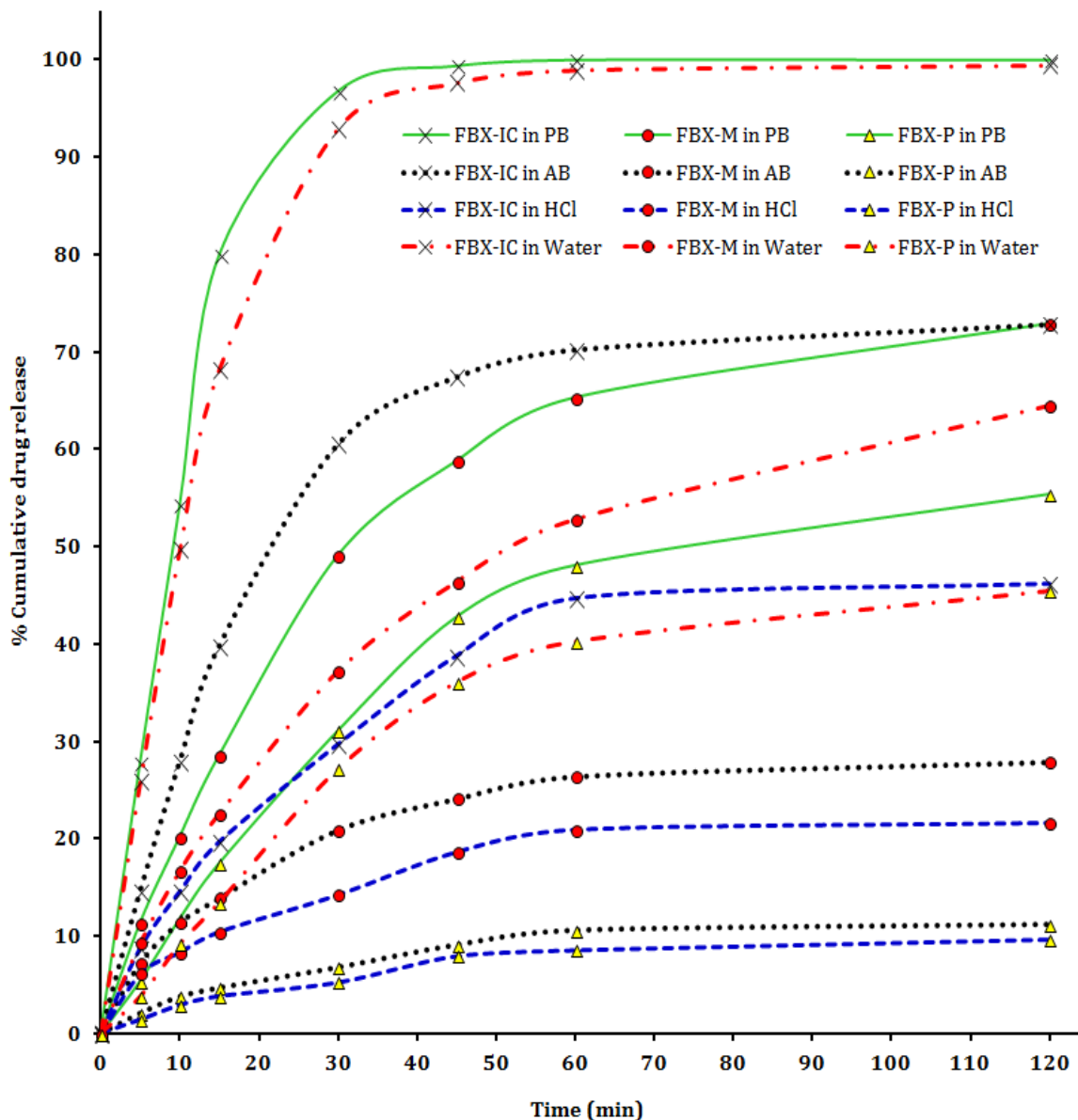


Fig. 5.25 Graphical representation of % Cumulative drug release versus sampling time of FBX-P, FBX-M and Freeze dried FBX-IC in phosphate buffer pH-6.8 (PB), acetate buffer pH-4.5 (AB), 0.1N HCl and water.

Table 5.24 Statistical representation of % Cumulative drug release versus sampling time of FBX-P, FBX-M and Freeze dried FBX-IC in phosphate buffer pH-6.8 (PB), acetate buffer pH-4.5 (AB), 0.1N HCl and water.

Time (min) ⇒	0	5	10	15	30	45	60	120
% Cumulative release from Phosphate Buffer, pH-6.8*								
FBX-IC	0.0	27.8±0.8	54.2±0.3	79.9±0.3	96.7±0.7	99.3±0.4	99.9±0.5	99.9±0.2
FBX-M	0.0	11.4±0.6	20.2±0.4	28.6±0.3	49.1±0.4	58.8±0.2	65.3±0.1	72.9±0.4
FBX-P	0.0	5.4±0.1	11.8±0.2	17.5±0.1	31.1±0.5	42.8±0.4	48.1±0.2	55.4±0.3
% Cumulative release from Acetate Buffer, pH-4.2*								
FBX-IC	0.0	14.6±0.5	27.9±0.2	39.8±0.6	60.5±0.9	67.4±0.4	70.2±0.5	72.8±0.6
FBX-M	0.0	7.2±0.5	11.4±0.7	13.9±0.2	20.9±0.8	24.1±0.5	26.4±0.1	27.9±0.4
FBX-P	0.0	2.1±0.4	3.8±0.2	4.7±0.3	6.8±0.2	9.1±0.6	10.6±0.5	11.2±0.2
% Cumulative release from 0.1N HCl*								
FBX-IC	0.0	8.8±0.3	14.6±0.5	19.7±0.5	29.7±0.6	38.8±0.2	44.7±0.5	46.2±0.5
FBX-M	0.0	6.1±0.2	8.3±0.5	10.4±0.5	14.2±0.4	18.6±0.8	20.9±1.1	21.6±0.7
FBX-P	0.0	1.4±0.5	2.9±0.2	3.8±0.5	5.2±0.4	7.9±0.8	8.5±0.7	9.6±0.5
% Cumulative release from water*								
FBX-IC	0.0	25.9±0.5	49.7±0.5	68.2±0.7	92.9±0.9	97.6±0.4	98.9±0.9	99.4±0.5
FBX-M	0.0	9.3±0.5	16.7±0.4	22.6±0.8	37.2±0.2	46.4±0.3	52.8±0.6	64.5±0.1
FBX-P	0.0	3.8±0.3	9.2±0.2	13.5±0.6	27.2±0.4	36.1±0.4	40.3±0.8	45.5±0.7

* Data are shown as Mean±SD, n=3.

Table 5.25 Comparison of various dissolution parameters of FBX-P, FBX-M and Freeze dried FBX-IC in phosphate buffer (PB), acetate buffer pH-4.5 (AB), 0.1N HCl and water.

	DE	DP ₅	DP ₆₀	t ₅₀	t ₉₀	MDT	AUC
In Phosphate Buffer, pH-6.8*							
FBX-IC	0.91±0.03	27.8±0.5	99.9±0.4	7.9±0.3	26.6±0.5	10.8±0.7	10892±29
FBX-M	0.56±0.07	11.4±0.6	65.3±0.1	37.5±0.7	>60	28.1±0.4	6698±38
FBX-P	0.40±0.02	5.4±0.1	48.1±0.2	>60	>60	32.7±0.3	4835±36
In Acetate Buffer, pH-4.2*							
FBX-IC	0.61±0.09	14.6±0.7	70.2±0.5	27.4±0.4	>60	19.1±0.9	7345±39
FBX-M	0.23±0.01	7.2±0.5	26.4±0.1	>60	>60	22.0±0.3	2734±27
FBX-P	0.09±0.03	2.1±0.4	10.6±0.5	>60	>60	26.4±0.1	1048±31
In 0.1N HCl*							
FBX-IC	0.37±0.04	8.8±0.6	38.8±0.2	>60	>60	22.8±1.0	4404±23
FBX-M	0.17±0.04	6.1±0.2	20.9±1.1	>60	>60	22.8±0.6	2099±47
FBX-P	0.07±0.01	1.4±0.5	8.5±0.7	>60	>60	30.1±0.3	862±25
In water*							
FBX-IC	0.88±0.04	25.9±0.5	98.9±0.9	10.8±0.4	28.7±0.7	13.3±0.6	10608±45
FBX-M	0.46±0.03	9.3±0.5	52.8±0.6	55.7±0.9	>60	31.5±0.5	5525±61
FBX-P	0.34±0.05	3.8±0.3	40.3±0.8	>60	>60	34.3±0.3	4025±32

* Data are shown as Mean±SD, n=3. DE: Dissolution efficiency, DP₅: Dissolution percentage at 5 min, DP₆₀: Dissolution percentage at 60 min, t₅₀: time required to release 50% of drug (min), t₉₀: time required to release 90% of drug (min), MDT: Mean dissolution time (min), AUC: Area under curve.

5.4.7.2.6 Stability studies

The stability of FBX-IC was monitored for chemical stability (i.e. percentage drug content). The study was carried out for 6 months at different time intervals (i.e. 1st, 2nd, 3rd and 6th month) stored at 5°C±3°C and at room temperature. It was observed that no significant difference was found between % FBX content of stored formulations from initial % drug content in FBX-IC at both conditions for 6 months (Table 5.26) so it can be concluded that formulation was stable for a period of 6 months and indicating its suitability for storage at both the conditions.

Table 5.26 Chemical stability (i.e. percentage drug content) of Freeze dried FBX-IC at different time intervals stored at 5°C±3°C and room temperature.

Sr. No.	Time	At 5°C±3°C*	At Room Temperature*
		% content of FBX in FBX-IC	% content of FBX in FBX-IC
1	Initial	99.84±1.28	99.84±1.28
2	1 st Month	99.12±0.65	99.31±0.87
3	2 nd Month	99.37±0.48	99.72±0.53
4	3 rd Month	99.61±0.28	99.46±0.89
5	6 th Month	99.49±0.97	99.23±0.75

* Data are shown as Mean±SD, n=3.

5.4.7.3 Cell Line Studies of FBX and it's Inclusion complex with HP-β-CD using Caco-2 cell line model

5.4.7.3.1 *In vitro* Cell Cytotoxicity Studies (MTT Assay)

Cytotoxicity study of Freeze dried inclusion complex of FBX: HP-β-CD::(1:1)M (FBX-IC) and FBX-P was accomplished in Caco2 cells by mitochondrial activity (MTT assay) to assess the safety/tolerability of prepared formulation on viability of cells. As Caco2 cells were used as absorption model, biocompatibility and tolerability of FBX-P and FBX-IC on absorption barrier was necessary. At initial 4 hr and 24 hr, the % cell viability is more than 80% at the 500 µg/ml concentration of FBX-P and FBX-IC. Hence for permeability studies, the drug and formulation concentration was fixed at 250 µg/ml. It can be observed that the FBX-IC showed very less cytotoxicity than the plain FBX upto 48 hours at all the concentrations. (Table 5.27) This confirms the biocompatibility of FBX-IC and explains that composition of inclusion complex did not contribute to toxicity of Caco2 cells^{21,29}. At initial 4 hours, 24 hours and 48 hours, FBX-IC was found to have less cytotoxicity with more than 80% cell viability as compared to FBX-P at all the concentrations in 48 hours condition. This could be attributed to protective action of HP-β-CD due to cavitation of drug molecule in CD. Cytotoxicity graphs at 4 hours, 24

hours and 48 hours were constructed (Fig. 5.26, 5.27 and 5.28) and IC₅₀ values were calculated for FBX-P and FBX-IC (Table 5.28). The higher IC₅₀ values for FBX-IC than FBX-P at all the incubation time conditions concluded to lack of cytotoxicity due to formulation of a bio-tolerable inclusion complex.

Table 5.27 In vitro cytotoxicity studies of FBX-P and FBX-IC in Caco2 cell lines at 4 hours, 24 hours and 48 hours.

Conc. (µg/ml)	%Cell Viability at 4 Hrs.*		%Cell Viability at 24		%Cell Viability at 48 Hrs.*	
	FBX-P	FBX-IC	FBX-P	FBX-IC	FBX-P	FBX-IC
0.1	99.78±0.21	99.95±0.57	98.21±0.54	99.42±0.76	93.42±0.90	95.62±0.84
1	99.12±0.36	99.56±0.82	98.23±0.27	98.75±0.82	92.71±0.61	94.29±0.52
10	98.85±0.74	99.41±0.35	97.96±0.42	98.26±0.39	91.25±0.35	92.52±0.47
100	95.23±0.51	97.35±0.62	93.24±0.42	96.05±0.51	89.56±0.56	91.17±0.29
250	91.42±0.35	95.29±0.69	88.67±0.33	94.85±0.21	83.28±0.82	89.52±0.76
500	88.42±0.72	93.10±0.46	84.23±0.39	91.98±0.74	80.56±0.37	87.98±0.95
1000	85.26±0.63	90.42±0.71	81.69±0.76	89.62±0.65	75.63±0.59	85.32±0.24

* Data are shown as Mean±SD, n=3.

Table 5.28 IC₅₀ values of FBX-P and FBX-IC in Caco2 cell lines at 4 hours, 24 hours and 48 hours.

Conditions	IC ₅₀ Values (µg/ml)*	
	FBX-P	FBX-IC
At 4 hours	3301.52±96.21	5153.89±42.51
At 24 hours	2664.43±25.78	5060.63±68.23
At 48 hours	2359.77±48.63	4863.37±38.53

* Data are shown as Mean±SD, n=3.

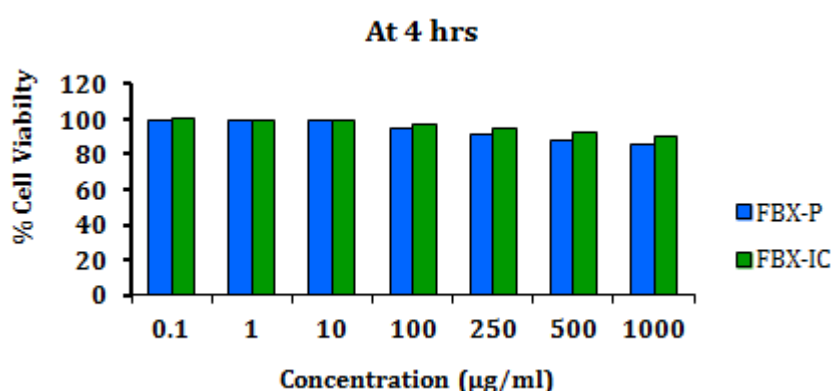


Fig. 5.26 In vitro cytotoxicity studies of FBX-P and FBX-IC in Caco2 cell lines at 4 hours.

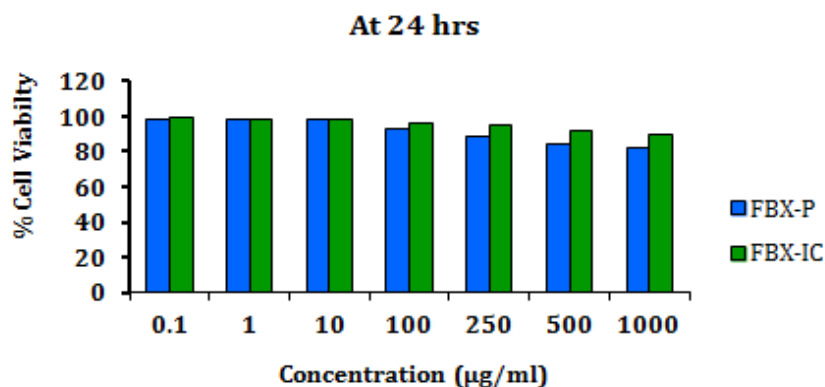


Fig. 5.27 In vitro cytotoxicity studies of FBX-P and FBX-IC in Caco2 cell lines at 24 hours.

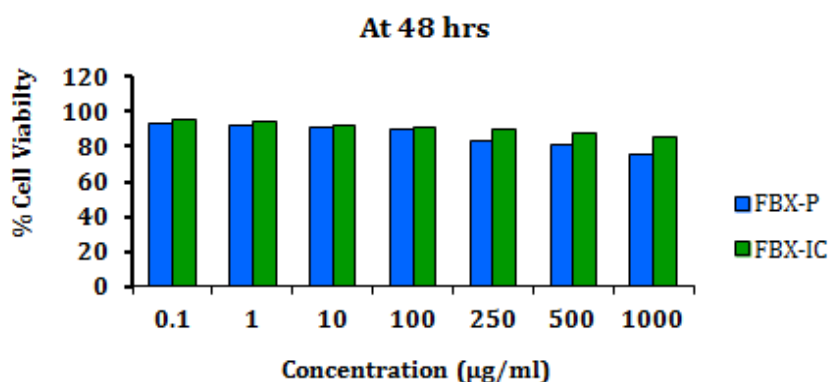


Fig. 5.28 In vitro cytotoxicity studies of FBX-P and FBX-IC in Caco2 cell lines at 48 hours.

5.4.7.3.2 *In vitro* assessment of permeability using Caco-2 cell line model

In this study, *in vitro* permeability assessment of Freeze dried inclusion complex of FBX: HP- β -CD::(1:1)M (FBX-IC), plain FBX (FBX-P) and marketed formulation (FBX-M) was done by calculating apparent permeability coefficient (P_{app}) from apical to basolateral (Table 5.29). Transepithelial permeability of FBX was measured at concentration of 250 μ g/ml, as negligible toxicity towards Caco-2 cells was found at this concentration during MTT assay of the same. The average P_{app} for Lucifer yellow with Caco-2 cells was found $(0.87 \pm 0.07) \times 10^{-6}$ cm/sec, confirmed the integrity of monolayers and suitability of monolayers for further experiment. The P_{app} for FBX-P and FBX-M were calculated and found to be $(10.15 \pm 0.68) \times 10^{-6}$ cm/sec and $(12.19 \pm 0.57) \times 10^{-6}$ cm/sec respectively, while the P_{app} for FBX-IC was observed at $(44.73 \pm 1.25) \times 10^{-6}$ cm/sec which is about 4.41 fold and 3.67 fold higher than the FBX-P and FBX-M, respectively. The found results were very much satisfactory and matching with the aim of the project. It can be

concluded that the higher P_{app} for FBX-IC was because of molecular state of drug and presence of HP- β -CD in the formulation^{30,31}. Whereas the lower permeability coefficient of FBX-P can be attributed to hydrophobicity and low permeation (log P 3.5-3.8) of drug. If the P_{app} value of a compound is less than 1×10^{-6} cm/sec, in between $1-10 \times 10^{-6}$ cm/sec, and more than 10×10^{-6} cm/sec can be classified as poorly (0-20%), moderately (20-70%) and well (70-100%) absorbed compounds, respectively^{32,33}.

Table 5.29 Apparent permeability coefficient (P_{app}) from apical to basolateral for FBX-P, FBX-M and FBX-IC using Caco-2 cells model.

Drug/Formulation	Apparent permeability coefficient (P_{app}) \pm SD (10^{-6} cm/sec)*
FBX-P	10.15 \pm 0.68
FBX-M	12.19 \pm 0.57
FBX-IC	44.73 \pm 1.25

* Data are shown as Mean \pm SD, n=3.

5.4.7.4 Pharmacokinetic evaluation of lyophilized FBX:HP- β -CD inclusion complex using *in vivo* animal model

In vivo animal study was carried out to estimate the oral bioavailability and other pharmacokinetic parameters of prepared Freeze dried inclusion complex of FBX:HP- β -CD::(1:1)M (FBX-IC) with respect to plain drug (FBX-P) and commercial formulation (FBX-M).

The mean drug plasma profile with respect to time is tabulated in Table 5.30, for FBX-P, FBX-M and FBX-IC. Fig. 5.29 represents the same plasma profile graphically. The pharmacokinetic parameters for all the three orally administered forms of FBX were determined using PKsolver add-in in microsoft excel. Non-compartmental analysis of plasma with linear trapezoidal method after extravascular administration in rabbits was performed and obtained parameters are represented in Table 5.31. Plasma FBX concentration profile of FBX-IC showed significant improvement in drug absorption compared to FBX-P and FBX-M. Area under concentration-time curve (AUC_{0-t}) of FBX was found $259.89 \pm 9.42 \mu\text{g} \cdot \text{h}/\text{ml}$ for FBX-IC which was 3.08 fold and 2.29 fold higher with that of FBX-P ($84.30 \pm 1.35 \mu\text{g} \cdot \text{h}/\text{ml}$) and FBX-M ($113.14 \pm 4.12 \mu\text{g} \cdot \text{h}/\text{ml}$), respectively. The area under moment curve ($AUMC_{total}$) showed significantly higher value for FBX-IC ($2383.25 \pm 41.57 \mu\text{g} \cdot \text{h}^2/\text{ml}$), compared to FBX-P ($760.75 \pm 9.24 \mu\text{g} \cdot \text{h}^2/\text{ml}$) and FBX-M ($1076.82 \pm 9.85 \mu\text{g} \cdot \text{h}^2/\text{ml}$). The maximum peak plasma concentration (C_{max}) of FBX-IC was about 2.64 fold and 2.29 fold greater than that of FBX-P and FBX-M, respectively. The enhancement in AUC and C_{max} of FBX-IC compared

to FBX-P and FBX-M could be due to the quick absorption of drug molecule by gastrointestinal wall due to the tremendous increase in solubility and improved dissolution rate of FBX present in form of inclusion complex with HP- β -CD³⁴⁻³⁶. Time to reach maximum plasma concentration (T_{max}) for FBX-IC, FBX-M and FBX-P was found to be 0.75, 1.0 and 1.0 hour, respectively. Mean residence time (MRT) for FBX-IC was decreased by 1.03 and 1.09 fold when compared to FBX-P and FBX-M, respectively. The shortest T_{max} and MRT for FBX-IC may be due to fastest dissolution rate and amorphization of drug due to formation of inclusion complex and the highest T_{max} of FBX-P could be attributed to crystalline nature of drug³⁷.

When half life ($t_{1/2}$) of FBX-IC was compared with FBX-P and FBX-M, the $t_{1/2}$ for FBX-IC (12.04 \pm 0.34 h) was not found much different than that of FBX-P (14.58 \pm 0.29 h) and FBX-M (16.32 \pm 0.18 h). The elimination rate constant ($K_{elimination}$) for FBX-P, FBX-M and FBX-IC were found to be 0.05 \pm 0.01 h⁻¹, 0.04 \pm 0.01 h⁻¹ and 0.06 \pm 0.01 h⁻¹, respectively. No significant difference in $t_{1/2}$ and $K_{elimination}$ of all three was observed which indicated that their elimination was comparable.

Relative bioavailability or bioequivalence is the most important criteria for comparing the bioavailabilities of different formulations of same drug. The relative bioavailability (F) of FBX-IC and FBX-M were found to be 308.29% and 134.21%, respectively, with respect to FBX-P. Thus there was 3.08 fold and 2.29 fold increase in bioavailability of FBX from FBX-IC with respect to FBX-P and FBX-M, respectively. These results could be explained by greater dissolution rate, increased wettability, increased hydrophilicity and reduced crystallinity of FBX in FBX-IC when compared to FBX-P and FBX-M. So it can be observed that enhancement in bioavailability may reduce the daily dose of FBX which will impart physical and economical benefits to patient by means of reduction in dose related side effects of drug when administered in multiple dose regimens.

Table 5.30 Statistical representation of FBX plasma profile for FBX-P, FBX-M and FBX-IC in Albino rabbits following oral administration.

Time (Hour)	FBX mean plasma concentration \pm SD*		
	FBX-P ($\mu\text{g/ml}$)	FBX-M ($\mu\text{g/ml}$)	FBX-IC ($\mu\text{g/ml}$)
0.0	0	0	0
0.5	3.42 \pm 0.11	5.11 \pm 0.17	11.48 \pm 0.26
1.0	6.29 \pm 0.35	9.65 \pm 0.14	32.29 \pm 0.42
1.5	9.54 \pm 0.28	12.51 \pm 0.37	42.98 \pm 0.57
2.0	16.25 \pm 0.51	18.76 \pm 0.25	39.74 \pm 0.72
2.5	14.21 \pm 0.29	16.98 \pm 0.61	35.21 \pm 0.25
3.0	11.54 \pm 0.42	13.42 \pm 0.41	31.63 \pm 0.62
3.5	8.28 \pm 0.24	10.65 \pm 0.48	22.52 \pm 0.48
4.0	6.15 \pm 0.27	8.79 \pm 0.36	16.56 \pm 0.32
4.5	4.16 \pm 0.20	6.39 \pm 0.31	11.89 \pm 0.25
8.0	3.11 \pm 0.18	4.78 \pm 0.46	8.95 \pm 0.29
12.0	0.95 \pm 0.21	1.12 \pm 0.19	5.06 \pm 0.46
24.0	0.62 \pm 0.17	0.81 \pm 0.09	1.89 \pm 0.31
48.0	0.31 \pm 0.12	0.52 \pm 0.13	0.79 \pm 0.08

* Data are shown as Mean \pm SD, n=3, ND: Not detected

Table 5.31 Pharmacokinetic parameters after oral administration of FBX-P, FBX-M and FBX-IC in Albino rabbits.

Pharmacokinetic parameters*	FBX-P	FBX-M	FBX-IC
C _{max} ($\mu\text{g/ml}$)	16.25 \pm 0.51	18.76 \pm 0.25	42.98 \pm 0.95 ^{†#}
T _{max} (h)	1	1	0.75 ^{†#}
AUC _{0-t} ($\mu\text{g}\cdot\text{h/ml}$)	84.30 \pm 1.35	113.14 \pm 4.12	259.89 \pm 9.42 ^{†#}
AUC _{0-∞} ($\mu\text{g}\cdot\text{h/ml}$)	94.37 \pm 2.14	138.02 \pm 6.18	272.51 \pm 12.05 ^{†#}
AUMC _{total} ($\mu\text{g}\cdot\text{h}^2/\text{ml}$)	760.75 \pm 9.24	1076.82 \pm 9.85	2383.25 \pm 41.57 ^{†#}
MRT (h)	9.02 \pm 0.22	9.52 \pm 0.39	8.77 \pm 0.29 ^{†#}
T _{1/2} (h)	14.58 \pm 0.29	16.32 \pm 0.18	12.04 \pm 0.34 ^{†#}
K _{elimination} (h ⁻¹)	0.05 \pm 0.01	0.04 \pm 0.01	0.06 \pm 0.01 ^{†#}
F (%) w.r.t FBX-P	100	134.21	308.29 ^{†#}

* Data are shown as Mean \pm SD, n=3, [†]P<0.05 compared with FBX-P, [#]P<0.05 compared with FBX-M.

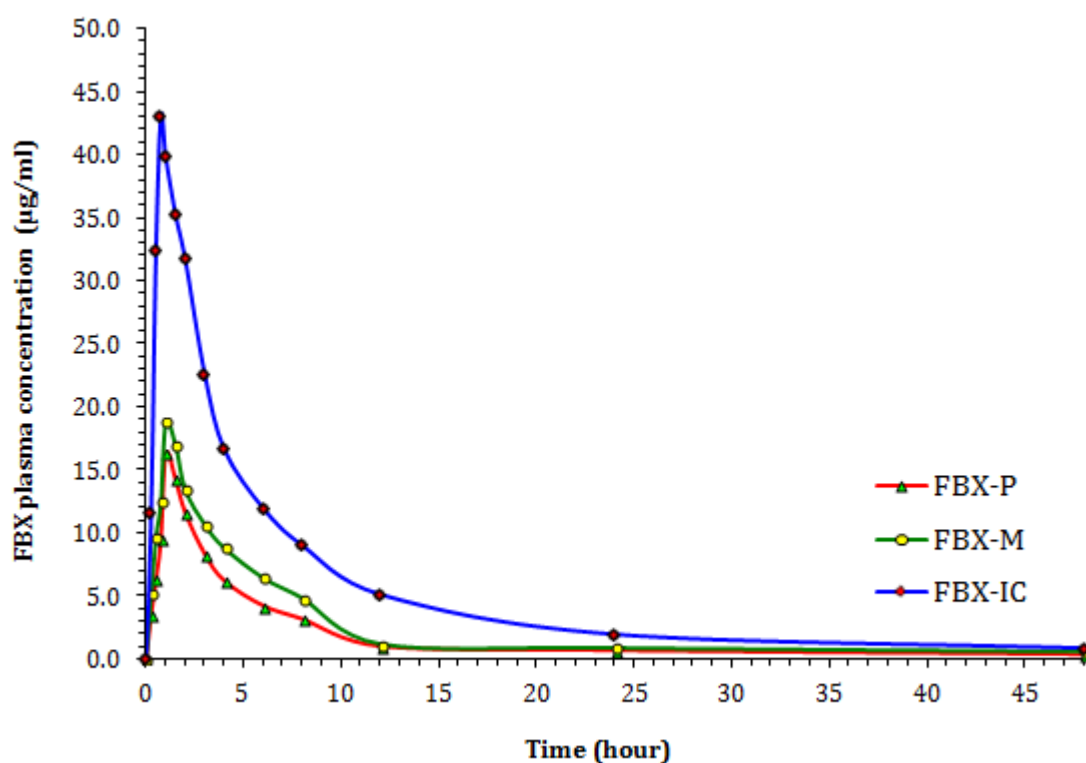


Fig. 5.29 Graphical representation of FBX plasma profile for FBX-P, FBX-M and FBX-IC in Albino rabbits following oral administration.

5.4.8 Conclusion

This study was designed to improve bioavailability of poorly water soluble drug, Febuxostat (FBX) by developing a stable and orally administrable drug:cyclodextrin inclusion complex with better solubility, dissolution and bio-tolerability. FBX:Cyclodextrin inclusion complexes were prepared with β -CD, HP- β -CD, M- β -CD and γ -CD in 1:1, 1:2 and 1:3 molar ratios. The physical mixing, kneading method and freeze drying method were opted for preparation of inclusion complexes. Phase solubility study was carried out in order to characterize the inclusion complexes in liquid state. Phase solubility study provides the stability constant for drug-cyclodextrin inclusion complex as well as it also present the insight into stoichiometry of the complex at equilibrium. The phase solubility studies of FBX with β -CD, HP- β -CD, M- β -CD and γ -CD were studied in water, phosphate buffer pH-6.8 and HCl pH-1.2 according to Higuchi and Connor's method. The FBX:HP- β -CD showed highest stability constant at $736.5 \pm 12.3 \text{ M}^{-1}$, $985.7 \pm 9.2 \text{ M}^{-1}$ and $543.9 \pm 6.5 \text{ M}^{-1}$ in phosphate buffer pH-6.8, water and HCl pH-1.2, respectively. The linear increase in solubility of FBX with increase in CDs concentration, giving rise to A_L -type phase solubility diagram for FBX:HP- β -CD. The R^2

values were also increased in the order of (FBX:HP- β -CD)>(FBX:M- β -CD)>(FBX: β -CD)>(FBX: γ -CD). Additionally, inclusion efficiencies (%IE) were estimated to finalize the best suitable CD and molar ratio. The results clearly showed that the %IE of FBX: HP- β -CD inclusion complex at all the molar ratios were found higher for physical mixture (61.25-63.08%), kneaded mixture (75.69-77.32%) and freeze dried inclusion complex (98.95-99.78%) than the inclusion complexes with other CDs, prepared by respective mode of preparation. It indicated that FBX was uniformly distributed in FBX:HP- β -CD inclusion complex at all molar ratios while others did not show satisfactory drug incorporation. Results also showed that there are minor differences in the inclusion efficiencies of physical mixtures, kneaded mixture and freeze dried inclusion complex of FBX:HP- β -CD at all the three molar ratios, respectively which described that FBX:HP- β -CD in the molar ratio of 1:1 is sufficient to produce an efficient inclusion complex.

The results obtained by FTIR, DSC and XRD studies were in excellent agreement and confirmed the formation of true inclusion complex of FBX with HP- β -CD in 1:1 molar ratio by freeze drying method. The IR spectrum of freeze dried inclusion complex of FBX:HP- β -CD::1:1M showed disappearance of all the characteristic peaks of FBX disappeared which indicate a good inclusion and interaction of FBX with HP- β -CD at the selected molar ratio. The DSC thermogram of freeze dried inclusion complex of FBX:HP- β -CD::(1:1)M had shown an endothermic peak for HP- β -CD but the disappearance of characteristic endothermic peak due to FBX with this system, clearly indicated the formation of true inclusion complex. The XRD of freeze dried inclusion complex of FBX:HP- β -CD::(1:1)M showed a halo pattern, with the disappearance of all characteristic peaks of FBX which indicated the complete incorporation of FBX in HP- β -CD cavity and formation of complete and stable inclusion complex. Moreover these studies also proved the efficiency of freeze drying method of preparation.

Percentage FBX content in lyophilized inclusion complex of FBX:HP- β -CD in (1:1) molar ratio was found to be 99.84 \pm 1.28%, indicating the suitability of freeze drying method for production of inclusion complex. Stability studies concluded that inclusion complex of FBX with HP- β -CD in (1:1) molar ratio was stable for a period of 6 months and indicating its suitability for storage at 5 $^{\circ}$ C \pm 3 $^{\circ}$ C and at room temperature. The dissolution of FBX from inclusion complex with HP- β -CD in (1:1) molar ratio prepared by freeze drying method was found higher than the pure FBX and marketed formulation of FBX in phosphate buffer pH-6.8 (PB), acetate buffer pH-4.5 (AB), 0.1N HCl and water.

9.6-55.4% and 21.6-72.9% of the FBX dissolved over the test period of 120 mins, respectively, in all the dissolution mediums. This may be due to large crystal size of FBX in API and marketed formulation. Whereas, lyophilized inclusion complex of FBX showed 46.2-99.9% drug dissolved over the time period of 120 mins, in all the selected dissolution mediums with significantly enhanced and highest dissolution rate in phosphate buffer pH-6.8.

Cytotoxicity study of Freeze dried inclusion complex of FBX: HP- β -CD::(1:1)M and plain FBX was accomplished in Caco2 cells by mitochondrial activity (MTT assay) to assess the safety/tolerability of prepared formulation on viability of cells. The higher IC₅₀ values for freeze dried inclusion complex than plain FBX at all the incubation time conditions concluded to lack of cytotoxicity due to formulation of a bio-tolerable inclusion complex.

In-vitro permeability assessment of freeze dried inclusion complex of FBX:HP- β -CD::(1:1)M, plain FBX and marketed formulation was done by calculating apparent permeability coefficient (P_{app}) from apical to basolateral. The P_{app} for Freeze dried inclusion complex was observed at $(44.73 \pm 1.25) \times 10^{-6}$ cm/sec which is about 4.41 fold and 3.67 fold higher than the plain FBX and marketed formulation, respectively. The found results were very much satisfactory and matching with the aim of the project.

In vivo assessment demonstrated that freeze dried inclusion complex of FBX:HP- β -CD::(1:1)M exhibited better pharmacokinetic properties compared to plain FBX and commercial formulation. The relative oral bioavailability of FBX in Albino rabbits resulted from Freeze dried inclusion complex was found 3.08 fold and 2.29 fold greater than plain FBX and marketed formulation, respectively.

The obtained results justified the selection of cyclodextrin, molar ratio and method of preparation for the formulation of efficient and stable inclusion complex of FBX with cyclodextrin. The outcome was supported by FTIR, DSC and XRD studies which further lead to enhanced dissolution properties, low cytotoxicity and improved bioavailability of FBX in inclusion complex with HP- β -CD.

7.11 References

- 1 Patel, S. G. & Rajput, S. J. Enhancement of Oral Bioavailability of Cilostazol by Forming its Inclusion Complexes. *AAPS PharmSciTech* **10**, 660-669 (2009).
- 2 Sinha, V., Anitha, R., Ghosh, S., Nanda, A. & Kumria, R. Complexation of celecoxib with β -cyclodextrin: Characterization of the interaction in solution and in solid state. *J Pharm Sci* **94**, 676-687 (2005).
- 3 Zhang, Y. *et al.* DDSolver: An Add-In Program for Modeling and Comparison of Drug Dissolution

- Profiles. *The AAPS Journal* **12**, 263-271.
- 4 Press, B. & Di Grandi, D. Permeability for intestinal absorption: Caco-2 assay and related issues. *Curr Drug Metabol* **9**, 893-900 (2008).
 - 5 Balimane, P. V., Han, Y. H. & Chong, S. Current industrial practices of assessing permeability and P-glycoprotein interaction. *The AAPS journal* **8** (2006).
 - 6 Hidalgo, I. J., Raub, T. J. & Borchardt, R. T. Characterization of the human colon carcinoma cell line (Caco-2) as a model system for intestinal epithelial permeability. *Gastroenterology* **96**, 736-749 (1989).
 - 7 Kratz, J. M., Teixeira, M. R., Koester, L. S. & Simoes, C. M. An HPLC-UV method for the measurement of permeability of marker drugs in the Caco-2 cell assay. *Brazil J Med Bio Res* **44**, 531-537 (2011).
 - 8 Artursson, P. & Karlsson, J. Correlation between oral drug absorption in humans and apparent drug permeability coefficients in human intestinal epithelial (Caco-2) cells. *Biochem Biophys Res Commun* **175**, 880-885 (1991).
 - 9 Elsbey, R., Surry, D. D., Smith, V. N. & Gray, A. J. Validation and application of Caco-2 assays for the in vitro evaluation of development candidate drugs as substrates or inhibitors of P-glycoprotein to support regulatory submissions. *Xenobiotica; the fate of foreign compounds in biological systems* **38**, 1140-1164 (2008).
 - 10 Matsson, P. *et al.* Exploring the role of different drug transport routes in permeability screening. *J Med Chem* **48**, 604-613 (2005).
 - 11 Shin, S.-C., Bum, J.-P. & Choi, J.-S. Enhanced bioavailability by buccal administration of triamcinolone acetonide from the bioadhesive gels in rabbits. *Int J Pharm.* **209**, 37-43 (2000).
 - 12 Zhang, Y., Huo, M., Zhou, J. & Xie, S. PKSolver: An add-in program for pharmacokinetic and pharmacodynamic data analysis in Microsoft Excel. *Comp Meth Prog Biomed* **99**, 306-314, (2010).
 - 13 Liversidge, G. G. & Cundy, K. C. Particle size reduction for improvement of oral bioavailability of hydrophobic drugs: I. Absolute oral bioavailability of nanocrystalline danazol in beagle dogs. *Int J Pharm.* **125**, 91-97 (1995).
 - 14 Center for Drug Evaluation and Research-Center for Biologics Evaluation and Research. (U.S. Food and Drug Administration, Rockville, Maryland, USA 2002).
 - 15 Reagan-Shaw S, Nihal M & Ahmad N. Dose translation from animal to human studies revisited. *The FASEB Journal*Life Sciences Forum* **22**, 659-661 (2007).
 - 16 Sathigari, S. *et al.* Physicochemical Characterization of Efavirenz-Cyclodextrin Inclusion Complexes. *AAPS PharmSciTech* **10**, 81-87 (2009).
 - 17 Mukne, A. P. & Nagarsenker, M. S. Triamterene-beta-cyclodextrin systems: preparation, characterization and in vivo evaluation. *AAPS PharmSciTech* **5**, E19 (2004).
 - 18 Jug, M., Kos, I. & Bećirević-Laćan, M. The pH-dependent complexation between risperidone and hydroxypropyl- β -cyclodextrin. *J Inc Pheno Macro Chem* **64**, 163-171, (2009).
 - 19 Omari, M. M. A., Zughul, M. B., Davies, J. E. D. & Badwan, A. A. Effect of Buffer Species on the Inclusion Complexation of Acidic Drug Celecoxib with Cyclodextrin in Solution. *J Inc Pheno Macro Chem* **55**, 247-254 (2006).
 - 20 Zeng, J., Ren, Y., Zhou, C., Yu, S. & Chen, W.-H. Preparation and physicochemical characteristics of the complex of edaravone with hydroxypropyl- β -cyclodextrin. *Carbo Poly* **83**, 1101-1105 (2011).
 - 21 Kiss, T. *et al.* [Cytotoxic examinations of various cyclodextrin derivatives on Caco-2 cells]. *Acta Pharma Hung* **77**, 150-154 (2007).
 - 22 Kiss, T. *et al.* Evaluation of the cytotoxicity of beta-cyclodextrin derivatives: evidence for the role of cholesterol extraction. *Eur J Pharm Sci* **40**, 376-380 (2010).
 - 23 Kiss, T. *et al.* Cytotoxicity of different types of methylated beta-cyclodextrins and ionic derivatives. *Pharmazie* **62**, 557-558 (2007).
 - 24 Veiga, M. D., Diaz, P. J. & Ahsan, F. Interactions of griseofulvin with cyclodextrins in solid binary systems. *J Pharm Sci* **87**, 891-900 (1998).
 - 25 Nakai, Y., el-Said Aboutaleb, A., Yamamoto, K., Saleh, S. I. & Ahmed, M. O. Study of the interaction of clobazam with cyclodextrins in solution and in the solid state. *Chem Pharm Bull (Tokyo)* **38**, 728-732

- (1990).
- 26 Okawara, M., Tokudome, Y., Todo, H., Sugibayashi, K. & Hashimoto, F. Enhancement of diosgenin distribution in the skin by cyclodextrin complexation following oral administration. *Bio Pharm Bull* **36**, 36-40 (2013).
 - 27 Taupitz, T., Dressman, J. B. & Klein, S. New formulation approaches to improve solubility and drug release from fixed dose combinations: case examples pioglitazone/glimepiride and ezetimibe/simvastatin. *Eur J Pharm Biopharm* **84**, 208-218 (2013).
 - 28 Taupitz, T., Dressman, J. B., Buchanan, C. M. & Klein, S. Cyclodextrin-water soluble polymer ternary complexes enhance the solubility and dissolution behaviour of poorly soluble drugs. Case example: itraconazole. *Eur J Pharm Biopharm* **83**, 378-387 (2013).
 - 29 Codruța M. Șoica¹, C. I. P., Sorina Ciurlea, Rita Ambrus, Cristina Dehelean Physico-chemical and toxicological evaluations of betulin and betulinic acid interactions with hydrophilic cyclodextrins. *FARMACIA* **58(5)** (2010).
 - 30 Shen, Y. *et al.* Effects of hydroxypropyl-beta-cyclodextrin on cell growth, activity, and integrity of steroid-transforming *Arthrobacter simplex* and *Mycobacterium sp.* *App micro biotech* **90**, 1995-2003, (2011).
 - 31 Shen, Y., Liang, J., Li, H. & Wang, M. Hydroxypropyl-beta-cyclodextrin-mediated alterations in cell permeability, lipid and protein profiles of steroid-transforming *Arthrobacter simplex*. *App micro biotech* **99**, 387-397, (2015).
 - 32 Artursson, P. & Karlsson, J. Correlation between oral drug absorption in humans and apparent drug permeability coefficients in human intestinal epithelial (Caco-2) cells. *Biochem Biophys Res Commun.* **175**, 880-885 (1991).
 - 33 Yee, S. In vitro permeability across Caco-2 cells (colonic) can predict in vivo (small intestinal) absorption in man--fact or myth. *Pharm Res* **14**, 763-766 (1997).
 - 34 Lin, S.-Z., Wouessidjewe, D., Poelman, M.-C. & Duchêne, D. Indomethacin and cyclodextrin complexes. *Int J Pharm* **69**, 211-219 (1991).
 - 35 Guyot, M., Fawaz, F., Bildet, J., Bonini, F. & Lagueny, A. M. Physicochemical characterization and dissolution of norfloxacin/cyclodextrin inclusion compounds and PEG solid dispersions. *Int J Pharm* **123**, 53-63, (1995).
 - 36 Soliman, O. A. E. *et al.* Amorphous spironolactone-hydroxypropylated cyclodextrin complexes with superior dissolution and oral bioavailability. *Int J Pharm* **149**, 73-83, (1997).
 - 37 Sigfridsson, K., Forssén, S., Holländer, P., Skantze, U. & de Verdier, J. A formulation comparison, using a solution and different nanosuspensions of a poorly soluble compound. *Eur J Pharm Biopharm.* **67**, 540-547 (2007).